Laser Spectroscopy of Acetylene

by

Trevor Erickson

B.S., University of Utah (2014)

Submitted to the Department of Chemistry in partial fulfillment of the requirements for the degree of

Doctor of Philosophy

at the

MASSACHUSETTS INSTITUTE OF TECHNOLOGY

May 2020

Author .....

Department of Chemistry

May 18, 2020

Certified by .....

Robert W. Field

Haslam and Dewey Professor of Chemistry

Thesis Supervisor

Accepted by .....

Robert W. Field

Chair, Department Committee on Graduate Students

This doctoral thesis has been examined by a Committee of the Department of Chemistry as follows:

Professor Adam P. Willard .....

Chairman, Thesis Committee

Professor Gabriela S. Schlau-Cohen .....

Member, Thesis Committee

Professor Robert W. Field .....

Thesis Supervisor

Haslam and Dewey Professor of Chemistry

Laser Spectroscopy of Acetylene

By

Trevor Erickson

Submitted to the Department of Chemistry
on May 18, 2020 in partial fulfillment of the
requirements for the degree of
Doctor of Philosophy

Abstract

The purpose of this thesis is to explore recent advances in the spectroscopy of acetylene. Acetylene is among the most-studied molecules, and an astoundingly large volume of work has been done on it. Highly excited S_1 acetylene suffers from many effects that complicate a thorough understanding of it. For instance, isomerization occurs between *trans*- and *cis*-bent geometries. Any models, including the most successful polyad models that have been used to study S_1 acetylene for many years, that are based on the more stable *trans*-bent structure are doomed to failure at the energy of isomerization is approached.

A further problem is experimental, rather than theoretical. The "interesting" region of S_1 dynamics, namely the energy region in the vicinity of the isomerization barrier, is dissociative. Near the *cis-trans* barrier, the electronic surface interacts with a nearby dissociative curve, and molecules tunnel through the barrier and dissociate.

The lifetime constraints are addressed with a detection technique that, to a certain point, is insensitive to predissociative lifetimes, Photofragment Fluorescence Action Spectroscopy (PFAS). PFAS detection involves the photofragmentation of excited acetylene, at a faster rate than the molecules dissociate. The excited photofragments themselves fluoresce, and this fluorescence is collected as the signal.

Using PFAS, the most detailed spectra of high-energy S_1 ever have been collected. The additional insight into the structure and dynamics of acetylene, both that have already been analyzed and that require further work, are discussed in this thesis.

Thesis Supervisor: Robert W. Field
Title: Haslam and Dewey Professor of Chemistry

Acknowledgements

Of all the people who have helped me on this journey, I'll thank Bob first. Bob has an infectious level of enthusiasm. Meetings with Bob without exception increased my energy and my drive to work hard, and become a better scientist. Even in periods of difficulty in the course of my graduate work, Bob could always be counted on to be a positive influence on me, personally and scientifically.

Since I've started with Bob, it seems appropriate to talk about the other scientific associations I've had. My interest in quantum mechanics and spectroscopy started in Michael Morse's class and lab, and he has a scientific enthusiasm on par with Bob's. Adam Willard offered me a lot of advice, in particular about how to be both a scientist and a father. Steve Coy has been a constant presence in the Field group, and he has provided knowledge and expertise to improve my graduate school experience that wasn't available to me from any other source.

I'm grateful to all the people I've worked with in Bob's lab, from people I only had a few months to learn from such as Carrie Womack and Barratt Park, to those that I spent some time working more closely with, such as Clare Keenan, Catherine Saladrigas, and Piyush Mishra, up to those with whom I spent a lot more time.

I joined the Field Group at the same time as Alex Hull, and have had many profitable and useful conversations with him through the years. I always expected that I'd be the last graduate student of Bob's, but the Covid-19 situation here in early 2020 has changed some plans, and, as he texted me a few days ago, "then there was one."

David Grimes and I worked on completely separate projects in the Field lab, and he joined several years before I did. However, it didn't take long for me to discover that David had practical knowledge and insights that had great potential to improve my experience in the lab, improve my experiments, and increase my scientific understanding. David has also been a good friend in the years since we worked together.

Elizabeth Foreman and I worked closely together for a time. Liz is a great scientist, and a great person. She managed to be involved in my projects, along with multiple other projects across several research groups, and be an expert in all of them.

It's difficult to overstate the effect that the last two group members I've worked with, Jun Jiang and Timothy Barnum, have had on me. These are both brilliant people and great scientists, that's clear. Any time I had questions about theory, experiments, quantum mechanics, statistics, data analysis, anything, these two were the first people I went to, and I nearly always got a satisfactory response or at least a direction to look from the first one I talked to, whichever that was. Equally valuable, I became close friends with

both Tim and JJ. Watching Tim's bell choir concerts, or having dinner with JJ, Yujia, and Anya, are some of my most precious memories from graduate school.

I was often accompanied in my late-night experiments by the entertainment of Troy Lavallee, Joe O'Brien, Skid Maher, Matthew Capodicasa, Grant Berger, and Ellinor DiLorenzo, who provided hundreds of hours of content, from which I garnered literally thousands of hours of entertainment. Thank you.

I had the support of great friends outside of science during this time. The number of people who offered me help and encouragement is too great to name every one of them, but special mention goes to both the Fallons and the Christensens. I became incredibly close with both of these families, and the amount of emotional burden they had to take from my complaints must have been difficult to deal with and is certainly embarrassing for me to contemplate. Sincerely, thank you for your help and support.

I also need to thank my family. My in-laws, aunts, uncles, cousins, parents, and sister have all been tremendously supportive. In particular, my wife has been an incredible source of inspiration. How she's managed to deal with me for five years I'll never know, but I'm grateful in any case. She's made my life so much easier, and so much more enjoyable, all while pursuing her own doctorate degree at the same time as me. She handles strains that would break me, and typically does it with a smile on her face. She also is responsible for most everything that makes our son so wonderful. The two of them together have made every small, inconvenient, even cramped apartment we've lived in feel like home, and made the challenges of graduate school feel like an adventure.

Contents

List of Figures

List of Tables

Chapter 1

History and Origin of My Interest in S_1 Acetylene

The first excited electronic state of acetylene, the $\tilde{A}^1A_u$ or S_1 state, has many properties that make it a worthy subject for deep study. The work of the Field Group has often been focused on using the S_1 state as an intermediate in a *Stimulated Emission Pumping* (SEP) scheme in order to reach high vibrational levels of the ground electronic S_0 state, but the S_1 state is interesting in its own right.

1.1 A Brief Overview of Some Interesting Properties of S_1 Acetylene

The ν_4 and ν_6 normal modes, the *cis* bend and the out-of-plane torsion, are nearly degenerate (the vibrational fundamentals have been observed to lie at 764.9 and 768.3 cm^{-1}, respectively [9]). These two vibrational modes are mixed by Coriolis and Darling-Dennison resonances, and in levels with as few as two quanta of excitation in the bending motions the normal mode quantum numbers are no longer sufficient to explain the structure, with the result that polyads are formed [5]. The quantum numbers v_4 and v_6 are destroyed by these resonances. Kellman [10] applied the idea of classical action-space to the normal modes. The full details of his publications on this topic are beyond the scope of this work, but if quantum states are envisioned as vectors in an N-dimensional space, with their components being the vibrational quantum numbers v_i, resonances

can be envisioned as occupying subspaces within this space, defined by which vibrational modes they mix. Coriolis and Darling-Dennison resonances in S_1 acetylene exchange one (for Coriolis) and two (for Darling-Dennison) quanta of excitation between ν_4 and ν_6. Expressed as raising and lowering operators, $\mathbf{a}_4^+\mathbf{a}_6$ and $\mathbf{a}_4^+\mathbf{a}_4^+\mathbf{a}_6\mathbf{a}_6$. The resonances define a subspace within the normal mode space in which the normal vibrational quantum numbers are invalid. The crucial conclusion is that one resonance can destroy at most one quantum number, and if a resonance is not linearly independent of the other existing resonances in normal mode space, it doesn't destroy any good quantum numbers. The vectors representing the Coriolis and Darling-Dennison operators are scalar multiples of each other, so while there are two resonances and both v_4 and v_6 are no longer valid quantum numbers, a new quantum number, which we call B, exists, which is perpendicular to the resonance vector in normal mode space, i.e. $B = v_4 + v_6$ These sets of states with new quantum numbers that are combinations of the original normal mode quantum numbers are called polyads, and S_1 acetylene is fruitful ground for a rich study of polyad dynamics. In fact, these two vibrations are so thoroughly mixed that the patterns in the spectrum resemble degenerate vibrations of a linear molecule, and to my knowledge this is the only such case that has been reported [5].

The predissociation threshold and *cis-trans* isomerization barrier of S_1 acetylene occur at similar energies, with the minimum of the *cis* well being $\sim$3000 cm^{-1} above that of the *trans*, the predissociaion barrier $\sim$1000 cm^{-1} above that, and the barrier to isomerization $\sim$1000 cm^{-1} higher still [11]. This coincidence of properties on the energy scale leads to interesting avenues of study - for example, the level-dependent predissociation properties. Quantum number dependence of predissociation rates have been observed before (in experiments stretching back decades [6, 12]). Acetylene offers an even more unusual situation that we are just beginning to explore, one where the vibrational levels not only dictate somewhat of a deviation from a single equilibrium geometry, but multiple distinct minima on the S_1 surface with qualitatively different geometries can be observed in the predissociative regime [7, 11]. In fact, the S_1 state is predicted to have an additional vinylidene minimum [13], which opens even more possibilities for investigation.

The *cis-trans* isomerization of the S_1 electronic state is an incredibly rich system for study. The isomerization mechanism [13, 14], frequency of vibration along the isomerization coordinate [15], and mixing of states between the wells [11] have all been studied.

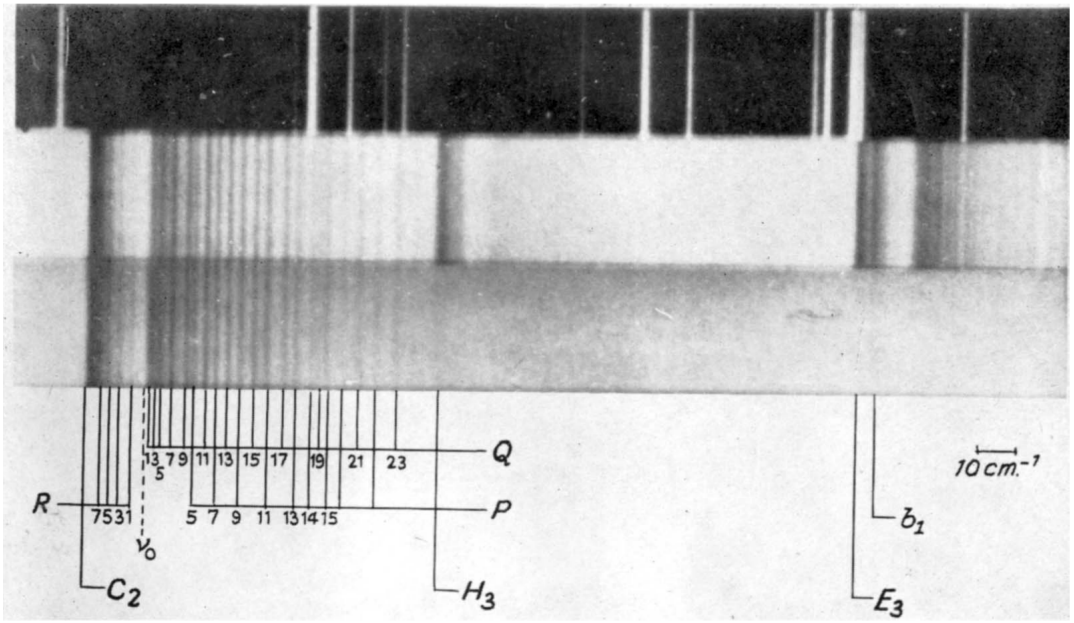

FIGURE 1.1: A small portion of the spectrum taken by Ingold and King. The top portion of the figure is an iron-arc spectrum, used for calibration. The center row is the spectrum taken at room temperature, ∼20 °C. The bottom spectrum is cooled, taken at ∼ -78 °C. Figure reproduced from Reference 1, with permission from from The Royal Society of Chemistry

The primary features explored in this work are related to the various geometries supported by the S_1 surface.

1.2 Determination of the Geometry of the S_1 State

The seminal studies by Ingold and King [1, 16–19] and by Innes [2] demonstrated that the equilibrium structure of the first excited singlet state of Acetylene, the S_1 state, is *trans*-bent, not linear. This was the first molecule shown to belong to a different point group upon electronic excitation [5]. The arguments in support of this structure change made by Ingold and King, and by Innes are instructive.

Ingold and King's analysis was based on absorption data that is of sufficiently high resolution to identify bands and branches, and even some of the more well-separated

rotational lines, far from band-heads. There are several pieces of evidence that combine to indicate a *trans*-bent upper state.

1.2.1 Intensity and Appearance of the Spectrum

First, the general intensity and character of the spectrum presents a problem for a linear-to-linear interpretation. The bands observed contain P, Q, and R branches, and are in general quite weak. As the ground state is a linear Σ state, Q branches cannot appear in the $S_1 \leftarrow S_0$ transition if the upper electronic state is also a Σ state. However, there are not expected to be any states of Π or higher angular momentum character in the energetic region accessed in the spectrum, according to the most up-to-date calculations availible to Ingold and King [20]. The strength of the absorption is also inconsistent with an electronically allowed transition. The spectrum of the S_1 state of acetylene is weak, weak enough that the expected mechanism is a forbidden transition which borrows intensity from a nearby allowed one. Again, the trouble with assuming a linear excited state is that there exists no forbidden transition with a nearby allowed transition from which intensity could be borrowed. However, a large geometry change causes an electronically allowed transition to become weak on the basis of vibrational wavefunction overlap, or Franck-Condon forbidden. In this case, it takes a transition that one might expect to have an oscillator strength in the vicinity of 0.1, and reduces it to 10^{-4} or so.

1.2.2 Vibrational Structure

The second point brought up by Ingold and King that makes the hypothesis of a linear upper state unlikely is related to the vibrational structure of the spectrum. There is only one upper-state vibration that forms a long progression. Such a progression is caused by a significant change in internal coordinates, where a change in vibrational quantum number along a particular direction is accompanied by slow variation in the Franck-Condon overlap of the upper and lower states. If both the upper and lower states are linear, the only motions that could possibly tune a wavefunction into and back out of high overlap with another are the two C-H stretches and the C-C stretch. However, this vibration (with a long Franck-Condon progression) has a harmonic frequency of 1,000 cm^{-1}. C-H stretches occur at energies roughly triple this value, leaving only the C-C stretch as a plausible candidate for this progression. Further investigation makes such a

candidate unlikely, however. The intensities of a progression of bands can be expressed as a function of the displacement between the upper and lower state geometries, first expressed for diatomics by Hutchisson [21] and modified for polyatomics by Craig [22]. Specifically, Craig's work treated groups of atoms vibrating together as a single mass, and assumed that one oscillator was found exclusively in its vibrational ground state, which allowed for a simpler expression. The formulas that Craig derived apply to totally symmetric motions only, and only for electronic transitions that retain the symmetry group of the molecule. In the case of the progression from the ground vibrational state in the ground electronic state to the various vibrationally excited states considered here, both assumptions are reasonable, and the only vibration consistent with a linear-to-linear assumption is the totally symmetric C-C stretch.

Under these conditions, we consider two oscillators whose origins are separated by q, oscillators 1 and 2. We assume a cold initial state. This allows one oscillator to be in its ground state,

$$\Phi_0(\sqrt{\beta_1}x_1) = (\sqrt{\beta_1/\pi})^{1/2}e^{-\beta_1 x_1^2/2}, \tag{1.1}$$

though the other oscillator could be in any harmonic oscillator state, namely

$$\Phi'_n(\sqrt{\beta_2}x_2) = (\sqrt{\beta_2/\pi}/2^n n!)^{1/2}H_n(\sqrt{\beta_2}x_2)e^{-\beta_2 x_2^2/2}, \tag{1.2}$$

where Φ is a harmonic oscillator wavefunction, β is related to the force constant of the oscillator, $\beta = 2\pi/h\sqrt{mk}$, and the H_n are the Hermite polynomials. The overlap integrals between such functions govern the distribution of the intensity of an electronic transition between the various vibrational bands, in accordance with the Franck-Condon principle. The expression for the overlap integral between Φ_0 and Φ'_n, as expressed above, can be shown to be

$$\begin{aligned} \int \Phi_0(\sqrt{\beta_1}x_1)\Phi'_n(\sqrt{\beta_2}x_2)dx = e^{-\beta_1[q^2/2(1+p)]}\times \\ \sum_r \left(\frac{\sqrt{\beta_2}q\rho}{1+\rho}\right)^{n-r}\left[\frac{n!}{r!(n-r)!}\right]^{\frac{1}{2}}\left[\frac{2^{n-r}}{(n-r)!}\right]^{\frac{1}{2}} S_{0r}. \end{aligned} \tag{1.3}$$

Here, $\rho = \frac{\beta_1}{\beta_2}$, and the S_{0r} are overlap integrals between harmonic oscillator wavefunctions with a common origin. These integrals are zero for all odd values of the quantum

number r, and for all even values of r are given by

$$S_{0r} = \frac{1}{(r/2)!}\sqrt{\frac{r!}{2^r}}\left(\frac{2\sqrt{\rho}}{1+\rho}\right)^{\frac{1}{2}}\left(\frac{1-\rho}{1+\rho}\right)^{\frac{r}{2}}. \tag{1.4}$$

For $\rho = 1$, which is to say if the two oscillators share a common potential energy minimum and have the same force constant, the value of the overlap term S_{00} between the two ground vibrational levels is 1 and all other overlap integrals are zero. Recognizing the dependence of line strength on the square of an overlap integral, these expressions give a direct method to calculate the relative strengths of various vibrational bands within an electronic transition as a function of the difference in origin between two bands, q.

Ingold and King use these expressions to test a variety of possible q values, looking for the value that best reproduced the experimental band intensity distribution. The C-C bond length in the ground electronic state is known to be 1.21 Å. Ingold and King found the bond length that best matched the observed intensity distribution to be 1.6 Å. For context, ethane, a molecule with a single C-C bond (compared to ground state acetylene's triple bond) has a bond length of 1.52 Å[23]. It seems unlikely that a single electronic excitation from a molecule with a triple bond would be to a state with a bond longer than the single bond of ethane. This is a problem, but perhaps not a deal-breaker. This same analysis of the bond length, however, will come up again when the rotational structure is analyzed, and will be much more insurmountable then. If, however, we are not constrained to a linear upper state geometry, then vibrational motions other than the C-C stretch become possible candidates for the long vibrational progression in question, and these difficulties disappear for such a hypothesis.

There are additional problems associated with the single long vibrational progression being assigned to the C-C stretch. The hydrogen isotope shift in this progression presents one. In a C-C stretch, minimal independent hydrogen motion is expected. Upon deuteration, one would expect such a vibrational band to change very little. In acetylene, however, the isotope shift in vibrational frequency from acetylene to dideuteroacetylene is very large, around 20%. This indicates that the vibration involves a large amount of hydrogen motion.

Lower state vibrational progressions are also incompatible with the hypothesis of a linear upper state. There is a long progression of hot bands, separated by about 600

cm^{-1}, prominent in the spectrum. The lower-state vibrational structure was sufficiently well known to Ingold and King to make it clear that the only possible vibration that could be responsible for hot bands with this separation is the Π_g symmetry *trans*-bending vibration (the Π_g *cis* bend has a fundamental frequency of $\sim$ 730 cm^{-1}, far enough removed from the observed frequency to be excluded, and the other motions are of much higher frequency). However, in a linear-to-linear transition, the *trans*-bend motion cannot produce a progression, as the equilibrium bond angle of both the upper and lower states must be identical along this degree of freedom, $\theta = 0$. Additionally, levels with odd quanta of the lower state *trans*-bending mode cannot appear in the spectrum due to symmetry restrictions (easily rationalized with even-odd arguments), but several consecutive hot bands are easily recognizable in the acetylene spectrum. Once again, this obstacle immediately becomes a non-issue if the upper state is assumed to be *trans*-bent.

1.2.3 Rotational Structure

As we turn our attention to the rotational structure of the acetylene spectrum, we find more and stronger evidence that S_1 acetylene cannot be linear. While examining the relative intensities of an upper state vibrational progression, we deduced that the length of the upper state C-C bond must be around 1.6 Å if a linear upper state geometry is assumed. If the bond length does indeed increase that much (from 1.2 Å to 1.6 Å), the rotational constant, B", of the lower-state of 1.18 cm^{-1} would be reduced to an upper-state rotational constant, B', of only 0.7 cm^{-1}. Even a small difference between B' and B" causes a band head to appear either to the red or blue side of the band origin in the spectrum. The frequency difference between this band head and the band origin can be calculated on the basis of the values of B' and B". The energy of a level with electronic quantum numbers represented collectively as e, vibrational quantum numbers v, and rotational quantum number J is [24]

$$\begin{aligned} E_{e,v,J} =& H(e) + G(v) + F(J) \\ =& H(e) + G(v) + B_v J(J+1) - D_v (J(J+1))^2 + ... \end{aligned} \tag{1.5}$$

Ignoring centrifugal distortion, we calculate the positions of R branch transitions by

$$\begin{aligned}\nu_R(e', v', J+1 \leftarrow e'', v'', J) &= E_{e',v',J'} - E_{e'',v'',J''} \\ &= H(e') + G(v') + F(J') - \left[H(e'') + G(v'') + F(J'')\right] \\ &= \nu_0 + 2B' + (3B' - B'')J + (B' - B'')J^2 \\ &= \nu_0 + (B' + B'')(J+1) + (B' - B'')(J+1)^2,\end{aligned} \tag{1.6}$$

and P similarly

$$\nu_P = \nu_0 - (B' + B'')J + (B' - B'')J^2, \tag{1.7}$$

where H, G, and F are the electronic, vibrational, and rotational energies, and ν_0 is the band origin. For the common case of a red-degraded band, the band head will occur in the R branch. The transition energy is quadratic in J, so we can find the J at which the band head if formed, J_{turn}, by taking the derivative with respect to J and setting it equal to zero,

$$\frac{d\nu_R}{dJ} = 0 = 3B' - B'' + 2(B' - B'')J_{turn}. \tag{1.8}$$

Rearranging,

$$J_{turn} = \frac{B'' - 3B'}{2(B' - B'')}. \tag{1.9}$$

The distance between the band head and the band origin is the difference between the energy of the transition if $J = J_{turn}$ and the band origin,

$$\nu_R - \nu_0 = 2B' - \frac{(B'' - 3B')^2}{2(B' - B'')} + \frac{(B'' - 3B')^2}{2(B' - B'')}, \tag{1.10}$$

after some algebra, the distance from the band origin to the band head can be expressed by

$$\nu_R - \nu 0 = \frac{-1}{4}\frac{(B' + B'')^2}{B' - B''}. \tag{1.11}$$

For the supposed linear-to-linear transition of acetylene, we calculate a separation of only 2 cm^{-1} between the band origin and the R bandhead. In the spectrum, however, the difference between the Q- and the R-branch heads, which must be close to the difference between the band origin and the R-head, is found to be 17 cm^{-1}, again invalidating the linear hypothesis. In order to achieve a spacing between band head and band origin of this magnitude, the upper state rotational constant, B', must be 1.1 cm^{-1}.

This summarizes the most enlightening and convincing arguments made by Ingold and

King against a linear upper state. Ingold and King chose a planar, *trans*-bent state primarily out of convenience, rather than any specific evidence. Innes refined Ingold and King's arguments in favor specifically of a *trans*-bent state [2].

1.2.4 Clarifications and Fundamental Extensions by Innes

Innes performed further analysis based on both vibrational and rotational structures in the spectrum of S_1 acetylene. It is worth noting that Innes had access to the data used by Ingold and King, as well as to data gathered in an apparatus with roughly triple the path length. Some details, specifically assignment of particular bands as originating from the ground vibrational state on the lower electronic surface, depend on the use of both data sets together.

A non-linear upper state is still likely to be of near-symmetric top character, as the hydrogen atoms are much lighter than the carbon atoms. The rotational constants will be ordered $A >> B \approx C$. For K_a (referred to henceforth as just "K")=0,1,2,... the states are very similar to linear molecule states of characters Σ, Π, Δ,... For a given value of K, there are values $J = K, K+1, K+2$, etc. For a linear-to-linear transition with the transition moment along the molecular b or c axes, which is the case here, $\Delta K = \pm 1$. However, there are weak bands in the spectrum which correspond to changes in K other than ± 1, such as $\Delta - \Sigma$ and $\Delta - \Delta$ transitions. Innes postulated that the most likely scenario for the appearance of such bands is the deviation of the upper electronic state from a true symmetric top. We are now aware of some additional effects that relax the $\Delta K = \pm 1$ selection rule for acetylene, such as axis switching.

Innes introduced some interesting analysis based on the rotational structure of the spectrum as well. Innes' instrument, with increased resolution (compared to that that produced the data used by Ingold and King), was able to resolve rotational lines clearly enough to support additional insights. One detail found was that the value of the rotational constant of the upper state, B', calculated via combination differences using different branches of the same band (i.e., calculated using the Q branch vs. the P or R branch) differed from each other by about 5%. In a linear molecule, such a difference could be explained by the different branches terminating in opposite components of an $L-$ or Λ-type doublet. However, the magnitude of the difference between the calculated B's is about 10 times larger than the doubling in the ground state. The splitting of K

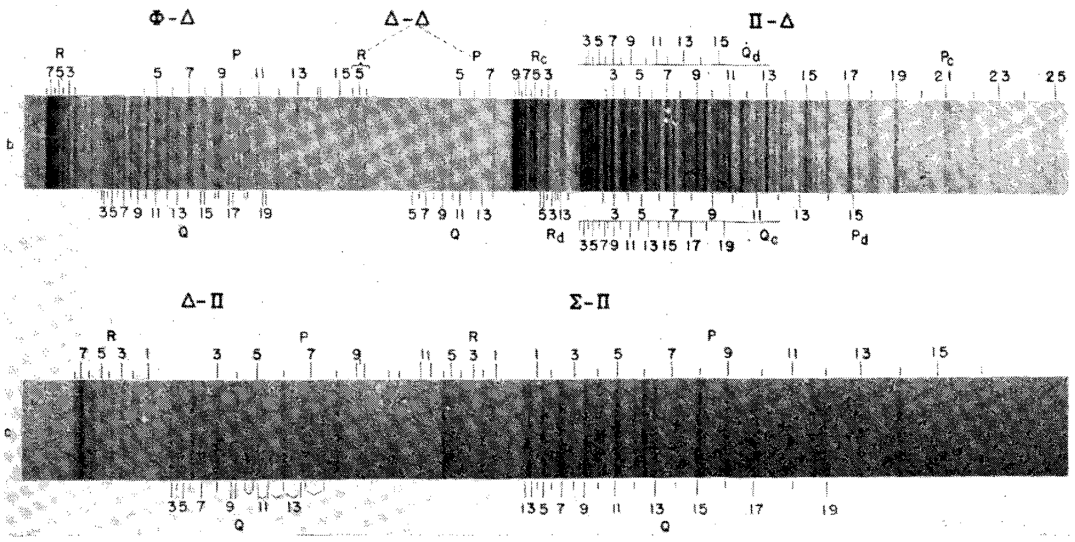

FIGURE 1.2: A portion of the spectrum of acetylene, as recorded by Innes. The pictured portions highlight several different important types of bands. Innes experiment had approximately triple the absorption path of the apparatus used by Ingold and King, along with increased resolving power, so many more details were able to be picked out, and molecular constants derived with greater accuracy. Figure reproduced from Reference 2, with the permission of AIP publishing.

doublets in an asymmetric top reproduce the observed differences in B' values to better than 1 part in 1,000, following the treatment of Wang [25].

After noting, as did Ingold and King, that these observations make a linear upper state impossible, Innes takes the analysis a step farther. Dihedral angles ϕ between 45° and 135° can be eliminated by an analysis of a similar situation in H_2O_2 by Giguère [26]. Upper state acetylene is observed to be quite strongly an asymmetric top, and those angles (from 45 to 135 degrees) turn out to be those for a nearly symmetric top. So, the upper state is at least nearly planar, either near 0° (*cis*) or near 180° (*trans*). The rotational structure of the bands can be analyzed to point toward either a *cis*- or *trans*-bent conformer. As shown by Herzberg and others [27], when the c axis is the symmetry axis, the statistical weights of the rotational levels of the lower set of $K = 1$ levels will be the same as the $K = 0$ levels, whereas if the b axis is the symmetry axis, the $K = 0$ levels' statistical weights will match those of the higher set of $K = 1$ levels. A closer look at this phenomenon occurs later in this chapter, see section 1.3.4. The spectra show the c axis to be the symmetry axis, and therefore a *trans*-like structure is the correct one. In addition, the moment of inertia sum rule for molecules that are planar at equilibrium, $I_c^e = I_b^e + I_a^e$, is very nearly satisfied for the S_1 state of acetylene. The vibrational states of acetylene, even the ground vibrational state, are of course not strictly planar due to

zero-point vibrations, but for ground state vibrational coordinates $v_i = 0$, the variation from the planar sum rule $I_c^{[v_i=0]} - I_a^{[v_i=0]} - I_b^{[v_i=0]}$ is slightly positive, and if several values of the vibrational coordinates are plotted and the value of the sum rule defect is extrapolated back to estimate the value at equilibrium, it is very nearly zero, pointing toward a planar structure.

1.3 Selection Rules of the $\tilde{A}$-$\tilde{X}$ Transition of Acetylene

In order to understand the features in the spectrum of the $\tilde{A}$-$\tilde{X}$ acetylene band system in a more comprehensive way, we shall now consider the transition selection rules of acetylene, focusing on the geometries relevant to this electronic transition. An important realization is that, in situations such as this where multiple geometries are relevant, traditional rigid molecule group theoretical analysis is less useful than in transitions where there is no change in the rigid molecular point group. A different type of group theory is required, which takes into account only symmetry operations that commute with the Hamiltonian of the molecule.

1.3.1 Discussion of the Symmetry Operations of Acetylene

The rotations and reflections normally associated with the phrase "symmetry operation" are supplanted in the case of the $\tilde{A}$-$\tilde{X}$ transition in acetylene by other, more rigorous symmetries. These operations are generally applicable and independent of both the instantaneous and equilibrium arrangement of particles in space, which means that they will be appropriate for any geometry, even geometries that don't have an obvious point of spatial symmetry (such as the $\tilde{C}^1B_2$ state of SO_2, which has unequal bond lengths [28]). For our purposes, the useful operations of this group are (1) the exchange of identical nuclei, and (2) the inversion of the space-fixed axis system. These symmetries are evident from simple physical arguments - identical nuclei are indistinguishable, and thus the energy levels of the Hamiltonian cannot change when any two identical atoms are permuted. The spherical symmetry of electromagnetic forces leads to the validity of the inversion operation [29]. Other operations exist to which the molecular Hamiltonian is invariant, for example translation or rotation of the molecule in space, but these other operations will be less useful for our purposes here than the two listed above.

$\mathbf{G_8}$	E	$(ab)(12)$	E^*	$(ab)(12)^*$	(12)	(ab)	$(12)^*$	$(ab)^*$
$Ss+$	1	1	1	1	1	1	1	1
$Ss-$	1	1	-1	-1	1	1	-1	-1
$As-$	1	-1	-1	1	1	-1	-1	1
$As+$	1	-1	1	-1	1	-1	1	-1
$Aa+$	1	1	1	1	-1	-1	-1	-1
$Aa-$	1	1	-1	-1	-1	-1	1	1
$Sa-$	1	-1	-1	1	-1	1	1	-1
$Sa+$	1	-1	1	-1	-1	1	-1	1

TABLE 1.1: The G_8 symmetry group character table, which is relevant to acetylene. This full group must be used when there is sufficient internal energy that bonds can break and reform in the molecule.

The complete set of all operations that involve the exchange of identical nuclei and inversion of the space-fixed axis system, along with all unique combinations of these operations, is called the Complete Nuclear Permutation/Inversion (CNPI) group. The CNPI symmetry treatment was pioneered by Hougen [30] and Longuet-Higgins [31]. I will follow the notation and logic of Lundberg [32], with important clarifications and expansions from Bunker and Jensen [29], in the discussion of the operations of this group.

I begin by defining the operations of the group, specifically for acetylene. Acetylene is composed of two carbon atoms and two hydrogen atoms. We will label the two carbon atoms a and b, and the two hydrogen atoms 1 and 2. To indicate a permutation of identical carbon nuclei, the notation (ab) will be used, and similarly permutations of hydrogen nuclei will be denoted (12). The identity operator, which leaves the molecule unchanged, will be represented by E, and the operator that inverts the laboratory-fixed axes, E^*, will be called the parity operator. These operations and all distinct combinations of them form the CNPI group for acetylene. The complete set of operations includes E, E^*, (ab), $(ab)^*$, (12), (12)*, $(ab)(12)$, and $(ab)(12)^*$. The group that these operations together form is called G_8. The entire character table is presented in Table 1.1.

We shall consider the effects of performing these operations on a complete molecular wavefunction, Ψ_n. To illustrate, we will begin by examining the effect of the permutation

operator on the wavefunction of a nondegenerate state. The application of the time-independent Hamiltonian operator to the wavefunction Ψ_n is

$$H\Psi_n = E_n\Psi_n. \tag{1.12}$$

We apply an arbitrary permutation operator P to the wavefunction, and recognize that the Hamiltonian operator commutes with the permutation operator to obtain

$$HP\Psi_n = E_nP\Psi_n. \tag{1.13}$$

Since Ψ_n is, by assumption, nondegenerate, only one eigenfunction can exist that returns the eigenenergy E_n. Then,

$$P\Psi_n = c_n\Psi_n \tag{1.14}$$

where c_n is a constant. Considering that any permutation operator, no matter how complex, can be expressed as a series of simple two-particle permutations, we will now assume P to be such an operation, e.g. (12). We lose no generality here, as the following treatment could be adapted to include more complicated operations. We apply the two-particle permuter, P, to both sides of the previous equation to obtain

$$P^2\Psi_n = Pc_n\Psi n. \tag{1.15}$$

P^2 is the identity operator, and the constant c_n commutes with the permutation operator P, so this can be rewritten as

$$\Psi_n = c_nP\Psi_n = c_n^2\Psi_n. \tag{1.16}$$

It's clear, then, that $c_n = \pm 1$. The same arguments can be applied to the parity operator, and wavefunctions that transform into themselves or into their negatives are referred to as having + or - parity, respectively. The utility of the transformation of the wavefunction due to permutation is somewhat more subtle. The transformation properties of the total wavefunction of a molecule under particle permutations are unambiguous. All wavefunctions are required to be symmetric with respect to the exchange of bosons, and antisymmetric with respect to the exchange of fermions [33]. All states must follow these rules, and therefore it would seem that permutation symmetries do not help to classify molecular states. However, inasmuch as parts of the molecular wavefunction Ψ_n

can be separated, for example into electronic, vibrational, rotational, nuclear spin, and electron spin parts, the symmetries of each of thse parts can be examined and useful properties recognized.

1.3.2 Symmetry Properties of Acetylene

As described above, the molecular Hamiltonian commutes with the inversion of the lab-fixed reference frame, which leads to the quantum number "parity", denoted as $+/-$. Additionally, the properties of a molecule are independent of the orientation of the molecule in space. The symmetry group related to arbitrary rotations of the space-fixed axes is called $\mathbf{K}(spatial)$. We will not examine the properties of this group here, but the manner in which the molecular wavefunction transforms under the operations of $\mathbf{K}(spatial)$ determines the values of the quantum numbers corresponding to total angular momentum and its projection on the space-fixed $\mathcal{Z}$ axis, J and M_J.

In acetylene, the rigorously good quantum numbers we will use are J, parity, and nuclear permutation symmetry for pairs of identical particles. We will denote the permutation symmetry as (Ss/Aa), where symmetry or antisymmetry with respect to permutation of the carbon atoms is indicated by the uppercase letters, and with respect to the hydrogen atoms by the lowercase letters. Along with these rigorously good quantum numbers, we will use the label K_a, which in a near-prolate top such as acetylene is a useful tool for organizing the energy levels, and will have some propensity rules for transitions associated with it. *Trans*-bent acetylene is not a prolate symmetric top, K_a is not a strictly good quantum number and does not induce a rigorous selection rule). The labels we will use to distinguish states are $|J, K_a, Ss/Aa, +/-\rangle$.

The full CNPI group of a molecule can be incredibly cumbersome. In the case of acetylene, there are only 8 independent symmetry operations, and the group is called G_8. However, for molecules with more identical atoms, there are more allowed operations, and for relatively simple molecules the order of the group can quickly become extremely large. For example, considering ethene instead of acetylene, a simple addition of 2 hydrogen atoms, increases the dimension of the group from 8 operations to 96. Moreover benzene, C_6H_6, has well over one million operations. All of the CNPI operations (when performed on an equilibrium structure) can be considered to transfer the molecule to an identical minimum on a potential energy surface. In some cases, the new minimum

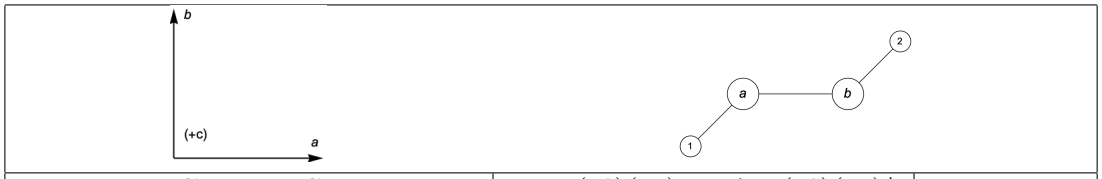

CNPI-MS						E	$(ab)(12)$	E^*	$(ab)(12)^*$			
Equivalent Rotation						R_0	R_c^π	R_c^π	R_0			
$D_{\infty h}$	G_8		C_{2h}	CNPI		E	C_2^c	σ_{ab}	i			
Σ_g^+	A_1'	A_1''	A_g	$Ss+$	$Aa+$	1	1	1	1		J_c	
Σ_u^-	A_2'	A_2''	A_u	$Ss-$	$Aa-$	1	1	-1	-1	Γ^*	c	
Σ_g^-	B_1'	B_1''	B_g	$Sa-$	$As-$	1	-1	-1	1		J_a	J_b
Σ_u^+	B_2'	B_2''	B_u	$Sa+$	$As+$	1	-1	1	-1	a	b	

TABLE 1.2: The Molecular Symmetry subgroup of the full CNPI group G_8 (CNPI-MS) for the *trans*-bent configuration of acetylene, which consists of only the feasible operations (operations that do not break C-H bonds). The first three columns correspond to labels of rigid point groups. The fourth column contains the true symmetry labels. As the molecule approaches energies where the breaking and reforming of bonds becomes feasible, these two states will begin to form tunneling doublets. Both the CNPI operations and the equivalent point group operations (rotations, reflections, etc.) are included in the table. The symmetry properties of the electric dipole operator, Γ^*, are worth noting.

may be separated from the original one by such a large energy barrier that the energy splitting between them cannot be resolved by experiment. In such a case, the CNPI operation that transfers the molecule between the two minima need not be considered. In the case of a rigid molecule, any operation that changes the connectivity of the atoms is excluded. It's fairly straightforward to list the infeasible operations for linear and *trans*-bent acetylene, though in some cases, particularly cases with a stereocenter, more care must be taken. For the geometries of acetylene I will be considering, the chemically feasible operations are limited to E, E^*, $(ab)(12)$, and $(ab)(12)^*$. This set of symmetry operations is called the "Molecular Symmetry group", or MS group, and is isomorphic to the molecular point group for rigid molecules.

1.3.3 CNPI Symmetry Operations in Space

It's a worthwhile diversion to discuss a few more details of how CNPI operations act on the various coordinates of a molecular wavefunction, as this information will help to establish the classification of the various parts of a wavefunction, understood from the more traditional point group analysis, into CNPI symmetry groups.

Consider the permutation operator (12). When the permutation operator is applied, all coordinates of the particles 1 and 2 are exchanged. As an example, the application of

the (12) permutation operator to a polyatomic molecule may be expressed as

$$\begin{aligned}(12)[X_1, Y_1, Z_1, X_2, Y_2, Z_2, X_3, ...] &= [X_1', Y_1', Z_1', X_2', Y_2', Z_2', X_3, ...] \\ &= [X_2, Y_2, Z_2, X_1, Y_1, Z_1, X_3, ...].\end{aligned} \tag{1.17}$$

We'll consider the coordinates of the particles in two different frames of reference: first, a set of axes (X,Y,Z) which are parallel to the lab-fixed reference frame (X,Y,Z), with the origin fixed at the molecular center of mass. The second is a set of axes (x,y,z), with origin fixed at the nuclear center of mass (not the molecular center of mass), with orientation defined by the Eckart conditions, which minimize the interactions between vibration and rotation [34]. When assigning the orientation of the (x,y,z) axis system, you begin by specifying a convention to unambiguously relate the (x,y,z) axes with the equilibrium configuration inertial axes, a, b, and c. Taking H_2O as an example, one might choose to take the z axis of the equilibrium structure as coincident with the a inertial axis, oriented so that H_2 has a positive z coordinate and H_1 has a negative z coordinate, the x axis oriented so that the oxygen atom has a positive x coordinate, and the y axis oriented to yield a right-handed axis system. The Eckart conditions are then used to determine the orientation of the instantaneous molecular frame axis system. The Eckart conditions could produce axes oriented in several ways - the conditions are designed to minimize rovibrational interactions and several axis systems can achieve this (for example, inverting the direction of all axes maintains the separation of rotation and vibration, but changes the value of all coordinates). Of the possible axes that conform to the Eckart conditions, we choose the system that, if the atoms are smoothly displaced back to the equilibrium structure, reproduces the convention for axis assignment that we chose.

When the permutation operator is applied to a molecule, for example the operation (12), which exchanges identical hydrogen atoms in a water molecule, the coordinates of particles 1 and 2 in space-fixed axis system (X,Y,Z) are interchanged. After the new positions are calculated, molecule-fixed axes (x,y,z) are attached to the equilibrium structure of the molecule, using the same convention chosen earlier for assigning x, y, and z to a, b, and c of the equilibirum structure. The Eckart rules are applied after the symmetry operation to define the instantaneous orientation of the molecule-fixed axes.

We will also consider the effects of the inversion operator, E^*, on the coordinates of

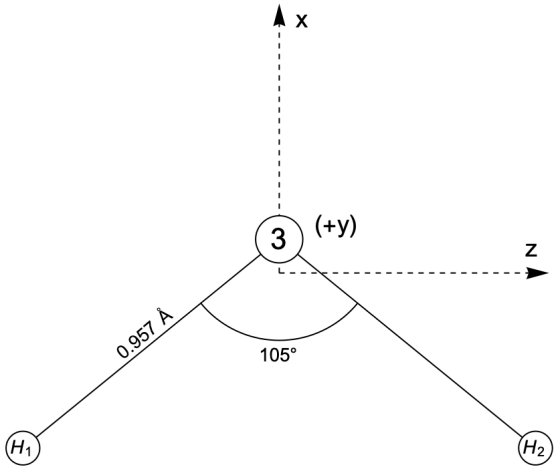

FIGURE 1.3: A water molecule is pictured at its equilibrium structure. The molecule-fixed axes (x, y, z) have been attached according to the conventions chosen in the text. The "$+y$" indicates that the y axis is coming out from the plane of the figure, creating a right-handed axis system.

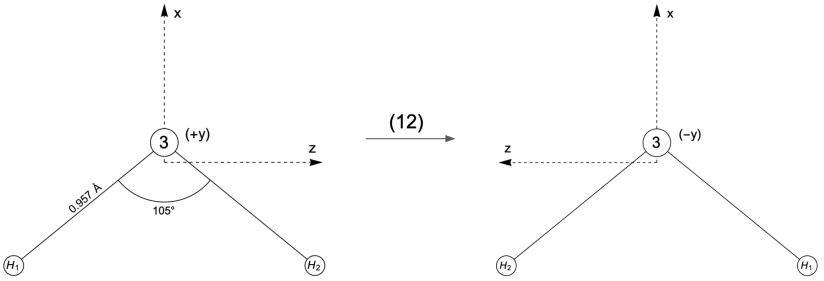

FIGURE 1.4: A demonstration of the effect of the permutation operator (12) on the nuclei of a water molecule in their equilibrium positions. Note that the operation is performed, and then the internal axes (x, y, z) are attached to conform to convention.

the molecule. The inversion operator changes all spatial coordinates of the particles, both nuclei and electrons, to their negatives in the (X,Y,Z) axis system, parallel to the space-fixed (X,Y,Z) system but with origin at the molecular center of mass. Expressed as an equation,

$$\begin{aligned} E^*[X_1, Y_1, Z_1, X_2, Y_2, Z_2, ...] &= [X_1', Y_1', Z_1', X_2', Y_2', Z_2', ...] \\ &= [-X_1, -Y_1, -Z_1, -X_2, -Y_2, -Z_2, ...]. \end{aligned} \tag{1.18}$$

As for the permutation operation, we will first perform the coordinate changes of the particles, and then attach the molecule-frame axes according to the conventions specified earlier. Figure 1.5 demonstrates the effect of the E^* operator on our same example water molecule.

With an understanding of how the CNPI symmetry operations act on the coordinates

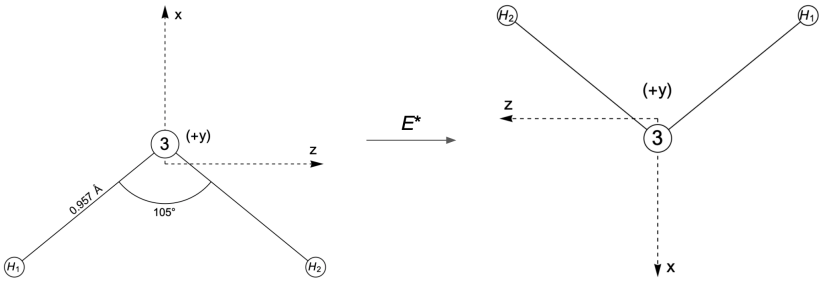

FIGURE 1.5: The effect of the inversion operation, E^*, through the origin of the (X, Y, Z) axis system, with origin molecular center of mass and orientation parallel to the lab-fixed (X,Y,Z) axes. Again, the internal (x, y, z) axes are attached, following the chosen convention, after the symmetry operation is applied.

of a molecule, both in the space- and molecule-fixed frames, we can begin to study each part of the molecular wavefunction to understand the properties of the states of acetylene in the context of its rigorously defined symmetry group.

1.3.4 Nuclear Spin Wavefunction: Statistical Weights

The most common isotopologue of acetylene includes ^{12}C and ^{1}H. The carbon atoms are bosons of nuclear spin 0, and the hydrogen atoms are fermions of nuclear spin $\frac{1}{2}$. $|\Psi_{total}\rangle$ must have permutation symmetries of Sa, with either parity allowed. In order to understand the possible symmetries of the nuclear spin part of the wavefunction, $|\Psi_{ns}\rangle$, we begin by constructing nuclear spin wavefunctions. We will use θ to represent the nuclear spin zero wavefunction, and α and β to represent the $\left|\frac{1}{2}\right\rangle$ spin-up and $\left|-\frac{1}{2}\right\rangle$ spin-down wavefunctions, respectively. The possible functions for the $^{12}C_2{}^1H_2$ isotopologue, then, are

$$\begin{array}{cc} \alpha_1\alpha_2\theta_a\theta_b & \beta_1\alpha_2\theta_a\theta_b \\ \alpha_1\beta_2\theta_a\theta_b & \beta_1\beta_2\theta_a\theta_b \end{array}$$

These basis functions form a reducible representation in the G_8 symmetry group. The procedure to generate this reducible representation is to apply each of the symmetry operations of G_8 to this set of functions, and count how many functions are left unchanged by the operation. Then, that reducible representation can be expressed as a unique combination of irreducible representations. The reducible representation is

G_8	E	$(ab)(12)$	E^*	$(ab)(12)^*$	(12)	(ab)	$(12)^*$	$(ab)^*$
χ^{ns}	4	2	4	2	2	4	2	4

To reduce the reducible representation to a sum of irreducible representations, we need to find the coefficients a_i which make the following true,

$$\Gamma = a_1\Gamma_1 \oplus a_2\Gamma_2 \oplus a_3\Gamma_3 \oplus ... \tag{1.19}$$

where Γ is the reducible representation shown in the table above (for example), and the Γ_n are the irreducible representations of the group. We find the coefficients a_i by recognizing the orthogonality of the irreducible representations. We can treat the action of the reducible representation and those of the irreducible representations under the various symmetry operations as vectors, and essentially take the dot products of these vectors (normalized by dividing by the order of the group) to find the projections of the irreducible representation onto the reducible representations,

$$a_i = \frac{1}{h}\sum_R \chi^{\Gamma}\left[R\right]\chi^{\Gamma_i}\left[R\right]^* . \tag{1.20}$$

where h is the order of the group and R runs over all the elements of the group. Here, h is 8 and R includes each of the operations already discussed. Applying this operation to our reducible representation, we find that this basis of nuclear spin wavefunctions reduces to $\Gamma_{ns} = 3Ss+ \oplus Sa+$. Only nuclear spin wavefunctions of symmetries $Ss+$ and $Sa+$ can exist, with $Ss+$ wavefunctions being three times as prevalent. This will produce clearly discernible patterns in the spectrum, and will restrict the symmetries available to the remainder of the wavefunction. When the symmetry of Γ_{ns} is $Ss+$, the remainder (electronic, electron spin, vibrational, and rotational parts) of the wavefunction can be of either $Sa-$ or $Sa+$ symmetry, because the allowed permutation symmetries of the total wavefunction are constrained by the types of particles being permuted (bosons or fermions). These $Ss+$ levels have statistical weight of three. If Γ_{ns} belongs to the $Sa+$ symmetry, the direct product of the symmetries of the remaining parts of the wavefunction must belong to the symmetry groups $Ss-$ or $Ss+$, and these levels have statistical weight of one. States that have symmetry $Aa+$, $Aa-$, $As+$, and $As-$ after factoring out ψ_{ns} correspond to nuclear spin wavefunctions that have statistical weight of zero, and these states will not exist. The same procedure can be carried out for any isotopologue with pairs of identical carbon and hydrogen atoms, just by adjusting the basis nuclear spin states used to account for the possible spin states of the nuclei. We won't derive the results here, but obtaining them is fairly straightforward, if tedious

for situations with many possible spin states. Lundberg does this analysis for several isotopologues [32].

1.3.5 Vibrational Wavefunctions: Background

The use of CNPI symmetry properties, rather than a rigid point group model, is particularly important when analyzing the vibrational properties of a molecule with multiple minima of distinct geometries supported by its electronic surface. The Franck-Condon Principle [35] defines the vibrational contribution to a transitions's strength in a spectrum, in the case that the wavefunction can be factored. For now, we will proceed under the assumption that that factorization is possible, and discuss it in more detail in Section 1.3.10.

As the Franck-Condon principle specifies, the the strength of a transition is proportional to the square of the matrix element between the vibrational wavefunctions of the initial and final states,

$$S_{\nu'\nu''} \propto \left\langle \Psi'_{\nu} \middle| \Psi''_{\nu} \right\rangle^2 . \tag{1.21}$$

These matrix elements of course can only be evaluated correctly if the wavefuntions are expressed in the same basis set, so we express

$$\Psi''_{\nu} = \sum_i a_i \Psi'_{\nu_i} \tag{1.22}$$

based on the completeness of the eigenfunctions of the Hamiltonian. The product of wavefunctions

$$\Psi'^{*}_{\nu} \Psi''_{\nu} = \Psi_{\nu} \left[\sum_i a_i \Psi'_{\nu_i} \right] \tag{1.23}$$

must belong to the totally symmetric representation for the matrix element to be non-zero. The symmetry and parity, then, of the final and initial vibrational wavefunctions must be identical. The CNPI symmetries, as discussed, are structure-independent and can be used to evaluate the values of these matrix elements when the geometries of the two states differ.

The symmetry properties of the vibrational motions can be determined by examining the effect of the symmetry group operations on the Cartesian displacement coordinates of the atoms in the molecule. Returning to our example of the water molecule, we add

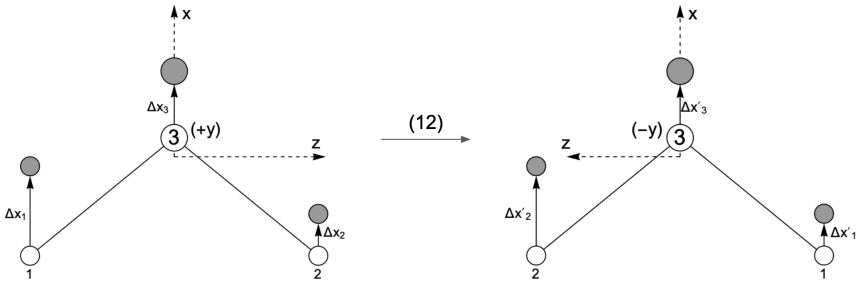

FIGURE 1.6: The effect of the symmetry operation that permutes particles 1 and 2 on their x-coordinate displacements. The values of the displacements after the operation is applied, $\Delta x_i'$, are $\Delta x_1' = \Delta x_2$, $\Delta x_2' = \Delta x_1$, and $\Delta x_3' = \Delta x_3$

to our picture the existence of displacements (in the x direction only, for now) in the molecular coordinates.

The effect of the (12) permutation operation on the x coordinates of the nuclei in this water molecule can be clearly seen in the figure. We can see that

$$\begin{aligned}(12)[\Delta x_1, \Delta x_2, \Delta x_3] &= [\Delta x_1', \Delta x_2', \Delta x_3'] \\ &= [\Delta x_2, \Delta x_1, \Delta x_3]\end{aligned} \tag{1.24}$$

As we know from Figure 1.4, the y and z axes exchange upon application of the permutation operator (12), in addition to the other effects of the permutation. To be clear, this reversal of the molecule-fixed axes results from our prescription for understanding the effects of symmetry operations: First, apply the permutation (or other operation), and then attach axes following the conventions chosen. Based on the new axes, we find

$$\begin{aligned}&(12)[\Delta y_1, \Delta z_1, \Delta y_2, \Delta z_2, \Delta y_3, \Delta z_3] \\ &=[\Delta y_1', \Delta z_1', \Delta y_2', \Delta z_2', \Delta y_3', \Delta z_3'] \\ &=[-\Delta y_2, -\Delta z_2, -\Delta y_1, -\Delta z_1, -\Delta y_3, -\Delta z_3]\end{aligned} \tag{1.25}$$

We find the character of all Cartesian motions under the symmetry operator (12) in the usual way - every coordinate after the permutation that is a scalar multiple of its pre-permutation value, contributes an amount equal to that scalar multiple. In this case, atoms 1 and 2 don't contribute anything (as the displacement of one has been replaced by a multiple of the other), Δx_3 contributes 1, Δy_3 and Δz_3 both contribute -1, to give a total character of

$$\chi[(12)] = -1. \tag{1.26}$$

The same procedure can be applied to all of the symmetry operations of the molecule of interest. The resultant characters for the Cartesian coordinates across all symmetry operations of the group form a reducible representation for the group. This can be reduced in the usual way to a sum of irreducible representations, which is aided by recalling that the Molecular Symmetry subgroup of the full CNPI symmetry group is isomorphic to the molecular point group. In the case of our water molecule example, the total irreducible representation of the transformation of all Cartesian coordinates is

$$\Gamma_{Car} = 3A_1 \oplus A_2 \oplus 2B_1 \oplus 3B_2. \tag{1.27}$$

This representation includes all possible displacements of Cartesian coordinates, which includes not only the vibrational motions we are interested in learning more about, but also translations and rotations. The characters of the various rotations and translations, fortunately, can be easily calculated. They depend upon the transformation properties of the Cartesian displacement coordinates that we already deduced, and in the case of H_2O are, for rotations,

$$\Gamma(R_x, R_y, R_z) = A_2 \oplus B_2 \oplus B_1 \tag{1.28}$$

and, for translations,

$$\Gamma(T_x, T_y, T_z) = A_1 \oplus B_1 \oplus B_2. \tag{1.29}$$

Subtracting the characters of those motions from our set of characters for all Cartesian displacements, we find that the vibrational normal coordinate representation is

$$\Gamma(Q_1, Q_2, Q_3) = 2A_1 \oplus B_2. \tag{1.30}$$

Symmetry species can be assigned to particular vibrations by examining the effect of the vibration under the symmetry operations in the same way that we examined the Cartesian displacements, but it will be even simpler because each normal coordinate belongs to a single symmetry species.

Classifying the symmetry of a vibrational wavefunction depends upon understanding the symmetries of the normal modes themselves. Once that is established, the symmetry of specific wavefunctions $\Psi_{vib,n}$ can be determined.

In the harmonic approximation, the vibrational wavefunction is a product of harmonic

oscillator wavefunctions. The irreducible representation species of the complete wavefunction is a product of the representations of the harmonic oscillator wavefunctions.

The harmonic oscillator wavefunction when the vibrational quantum number v is zero is

$$\Phi_0 = Ne^{-cQ^2} \tag{1.31}$$

where N and c are constants dependent upon the particular oscillator and Q is the vibrational displacement of the mode. The harmonic oscillator potential energy function is proportional to Q^2, and must be totally symmetric in the Molecular Symmetry group because the Molecular Symmetry group is a symmetry group of the Hamiltonian. Q^2, and Φ_0, then, must also be totally symmetric in the Molecular Symmetry group. Recall that any harmonic oscillator wavefunction can be expressed by applying the raising operator a^+ to the lowest harmonic oscillator eigenfunction Φ_0 v times,

$$\Phi_v = N_v(a^+)^v\Phi_0. \tag{1.32}$$

In our formulation, the raising operator a^+ is a function of Q, and transforms like the coordinate Q under symmetry operations. If the totally symmetric representation is given by Γ^{sym} and the representation under which Q transforms is Γ^i, then the total wavefunction will transform as a product of the symmetries of the ground vibrational level and of Q, which is the symmetry of the vibrational motion discussed above, repeated v times, $\Gamma^{sym} \otimes \Gamma^i \otimes \Gamma^i \otimes ...$ which for a nondegenerate vibration will be Γ^{sym} if v is even and Γ^i if v is odd.

The situation is more complicated in the case of degenerate vibrations, but not so complicated as to be unmanageable. Consider a two-dimensional degenerate vibration, with normal coordinates Q_a and Q_b. As is the case with non-degenerate vibrations, we can express the wavefunction as a product of the one-dimensional harmonic oscillator wavefunctions for each motion, with quantum number v_i for each. In the case of a degenerate vibration, however, it proves useful to perform a coordinate change which is analogous to the coordinate change from Cartesian to polar coordinates. We define two new coordinates, Q and α, such that

$$Q_a = Q\cos\alpha, \tag{1.33}$$

$$Q_b = Q \sin \alpha, \tag{1.34}$$

$$Q = \sqrt{Q_a^2 + Q_b^2}, \tag{1.35}$$

and

$$\alpha = \arctan\left(\frac{Q_b}{Q_a}\right). \tag{1.36}$$

The energy of the wavefunction, is expressed in the familiar way using only one quantum number v,

$$E(v) = \hbar\omega\,(v+1)\,, \tag{1.37}$$

and another new quantum number, l, called the vibrational angular momentum quantum number, reflects the possibility of a two-fold degenerate vibration contributing angular momentum to the molecule (note that the energy depends on the vibrational quantum number plus one, not 1/2, which is a result of considering two vibrations). The wavefunctions of the degenerate vibrations can again be expressed using raising and lowering operators. In the Q_a, Q_b formulation, the raising and lowering operators appear familiar, with a raising and lowering operator for each vibration. In the Q, α formulation, there are again four ladder operators, expressed as $R^{+(+)}$, $R^{+(-)}$, $R^{-(+)}$, and $R^{-(-)}$. These operators act such that

$R^{+(+)}$	increases v by one and increases l by one
$R^{+(-)}$	increases v by one and decreases l by one
$R^{-(+)}$	decreases v by one and increases l by one
$R^{-(-)}$	decreases v by one and decreases l by one

The ground state of this oscillator has $v = l = 0$, and these ladder operators don't allow completely independent adjustment of the two quantum numbers, so the possible values of l are restricted to $l = v, v-2, v-4, ...-v$. In parallel with the nondegenerate case, the ground vibrational wavefunction is totally symmetric, and the raising and lowering operators transform in the same way as the vibrational coordinate describing the motion. The application of v ladder operators to the zero-point wavefunction can generate any allowed wavefunction with vibrational quantum number v, so the total symmetry representation of the motion is $\Gamma^{sym} \otimes \left[\Gamma^i\right]^v$, where Γ^i is the irreducible representation by which the vibration transforms. In general, these direct products will not form a single irreducible representation, but rather a direct sum of irreducible

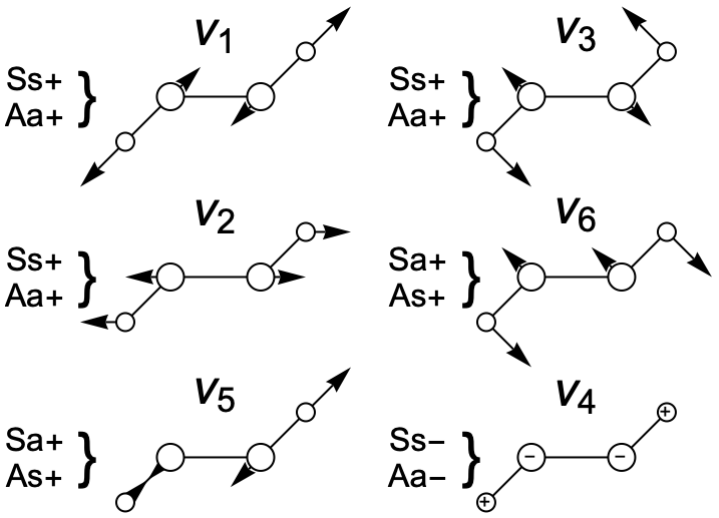

FIGURE 1.7: Cartoon representations of the normal mode vibrations of acetylene in its *trans* configuration. Each motion is labelled by the traditional numbering, with the true CNPI symmetry symmetries of each vibration indicated.

representations. Each of the $v+1$ wavefunctions with different values of l all transform in the same way.

1.3.6 Vibrational Wavefunctions of Acetylene

As linear molecules introduce some extra complications, particularly in their vibrational structure, we'll begin by looking at *trans*-bent acetylene. The vibrational motions of *trans*-bent acetylene are shown in Figure 1.7. If the point-group symmetries of the vibrations and the correlations between point-group symmetries and the true CNPI symmetries are known, the CNPI symmetry labels can be immediately applied. If this information is not known, it can be deduced by examining the diagrams of the vibrational normal modes.

The feasible CNPI symmetry operations have point-group equivalents that produce equivalent results for a rigid structure. Labelling the atoms in a cartoon picture and performing the CNPI symmetry operation, then looking for the point-group operations that move the atoms in the same way, suffices to find the correlation. We find that the feasible operations $(ab)(12)$, for example, permutes both the hydrogens and the carbons in *trans*-bent acetylene, but leaves any axes perpendicular to the plane of the molecule unchanged, which correlates to a C_2 rotation about the c axis. These equivalencies will

be useful in determining the characters of the motions under the CNPI symmetry operations. It should be clear from the diagrams that vibrations ν_1, ν_2, ν_3, and ν_4 transfrom as (1) under a rotation $C_2{}^c$, and therefore under the CNPI operation $(ab)(12)$, while the other vibrations have character (-1) under this operation. In order for a function to have character (1) under $(ab)(12)$, it must have the same transformation properties under the G_8 (ab) and (12) operations. Looking at the G_8 character table (Table 1.1, on page 28), we see that $Ss+$, $Aa+$, $Ss-$, and $Aa-$ transform in this way.

Examining instead the E^* operation, we discover that an inversion of coordinates in the laboratory frame does not alter the placement of the molecule-fixed axis system, but will switch displacements out of the plane of the molecule from being in the positive direction to the negative direction. This correlates to the point-group operation of reflection in the plane of the molecule, and the only vibration of *trans*-bent acetylene that has nonzero character under this operation other than (1) is ν_4, the out-of-plane bend, with character (-1). We now have enough information to label all of the vibrations of *trans*-bent acetylene with their true symmetry labels, and can also understand the correlations between the true symmetry labels and the more commonly used point-group labels, based on knowledge of the point-group character of these vibrations.

We now turn attention to another isomeric form of acetylene which has not yet been discussed, *cis*-bent acetylene. For now, we'll proceed without justification, but it will become clear why the *cis*-conformer is worth discussing later in this thesis (see Section 1.5). As is also the case for *trans*-acetylene, only vibrational motions that have components perpendicular to the plane of the molecule can have negative parity. Only one normal mode has such motion, ν_4. As seen in Table 1.4, the $(ab)(12)$ operation is equivalent to the point group operation C_2^b. From pictures of the nuclear displacements of the *cis*-vibrations, it can be deduced which normal modes are symmetric under this operation.

We turn our attention to the symmetry of the vibrations of linear acetylene. The vibrational structure is more subtle and difficult to classify for the linear arrangement. Once again, the parity operation, E^*, corresponds to a reflection in the $D_{\infty h}$ point group, meaning that once again only vibrations with motions perpendicular to this plane can have negative parity. However, unlike with the other geometries, in linear acetylene the b and c axes are equivalent, meaning that any motion perpendicular to the a axis *could*

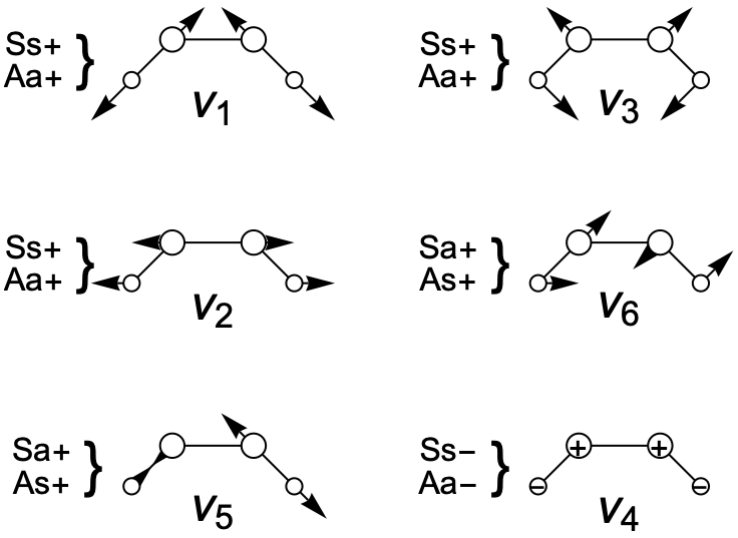

FIGURE 1.8: Pictures of displacements and the CNPI true symmetry labels of the vibrational normal modes in *cis*-bent C_{2v} acetylene.

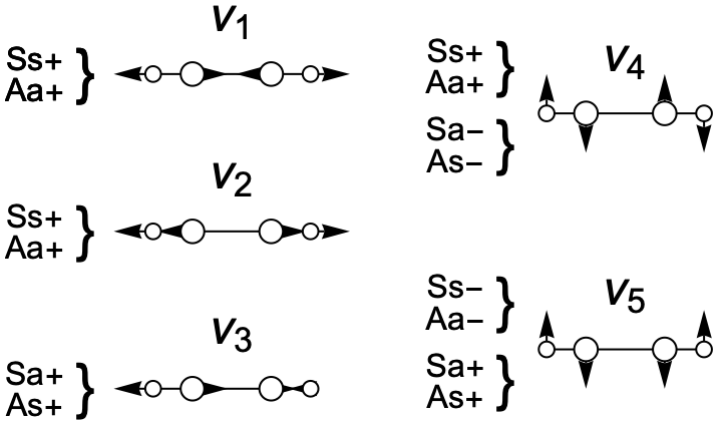

FIGURE 1.9: Pictures of the nuclear displacements in the vibrational normal modes of linear acetylene. The bends have perpendicular components of different true symmetries.

be out of the ab plane, or might not be. The equivalence of the b and c axes is the primary source of the difficulties in understanding linear molecules. Both the *cis* bend and the *trans* bend have one component with positive and one component with negative parity.

As previously, the other symmetry components of the normal modes can be deduced from pictures of the displacements, shown in Figure 1.9. Using the properties of $(ab)(12)^*$, and visualizing the point group equivalent operation i (see table 1.5), allows assignment of the remaining symmetry components.

The symmetry assignments we've discussed so far will assist in identifying transitions

and interactions that are allowed or forbidden, but they will not provide information about vibrational propensity rules. Strict selection rules and propensity rules will both play a particularly important role in double resonance schemes that involve large geometry changes. Our research group, for example, has used *trans*-bent acetylene as an intermediate in a Stimulated Emission Pumping (SEP) scheme to reach highly excited vibrational bands of electronic ground state acetylene, S_0 acetylene. Vibrational factors of the transition matrix elements are the most important consideration in determining the specific intermediate states that can be best used to access the desired final state in such a scheme. An examination of the differences in equilibrium geometry and the normal mode motions that would cause such a displacement can very easily produce predictions of which modes will be Franck-Condon active.

1.3.7 Electronic Wavefunction Symmetry

The electronic wavefunction of a molecule can be approximated as a product of individual orbital wavefunctions,

$$\psi_e = \phi_1\phi_2\phi_3\phi_4... \tag{1.38}$$

The symmetry of the electronic wave function is a direct product of the symmetries of one-electron wavefunctions,

$$\Gamma_e(\psi_e) = \prod_n (\Gamma_n(\phi_n)) \,. \tag{1.39}$$

Walsh diagrams are qualitative pictures that show the energies and symmetries of molecular orbitals as a function of some internal coordinate, usually the angle of a bend [36]. The diagrams are built using qualitative arguments based on how atomic orbital overlap is either optimized or strained based on the locations of the atoms and which types of molecular orbitals are involved in the bonding. Buenker and Peyerimhoff ([3]) performed an *ab initio* study of Walsh's rules, including H_2A_2 molecules. Figure 1.10 is a qualitative simplification of a Walsh diagram published in that study, with the addition of the true symmetry CNPI labels applying to each molecular orbital in the *cis*- and *trans*-bent configurations. The two lowest-energy inner-shell orbitals are not shown in the diagram, so linear acetylene is treated as having filled orbitals up through the $1\pi_u$ orbitals shown. The symmetry elements of the one electron wavefunctions ϕ_i multiply very simply, $A \otimes A = S \otimes S = S$, $A \otimes S = A$, and $(+) \otimes (+) = (-) \otimes (-) = (+)$,

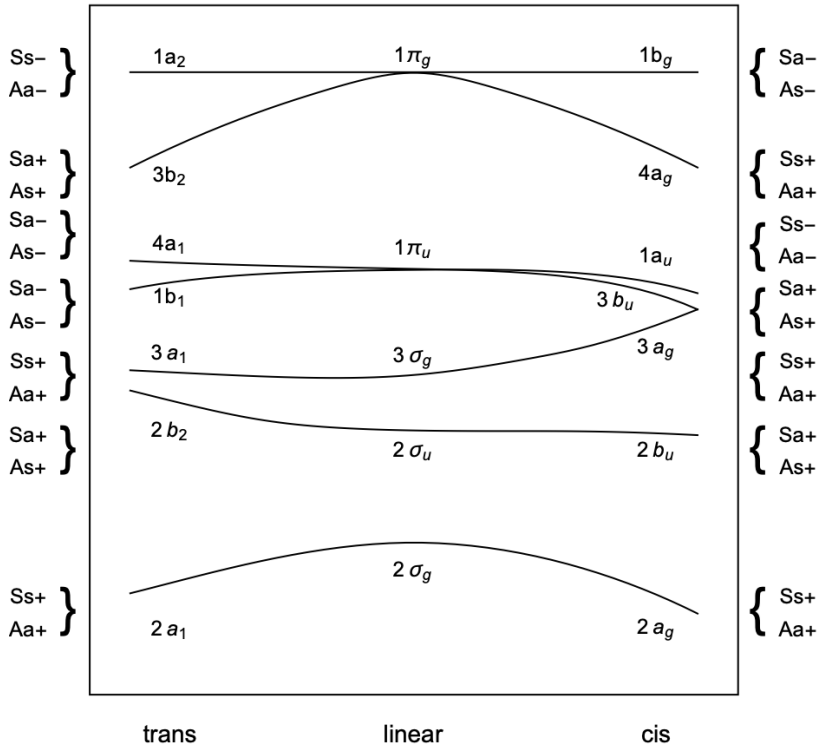

FIGURE 1.10: The Walsh diagram connecting linear acetylene with *cis*- and *trans*-bent acetylene. This is a qualitative diagram, based on a similar picture published by Buenker and Peyerimhoff [3]. The y-axis in this diagram is the orbital binding energy, which can assist in reasoning out why a particular electronic state takes on its geometry at equilibrium.

$(-) \otimes (+) = (-)$. So, for example, $Sa+ \otimes Ss- = Sa-$. Any electronic state with known molecular orbital contribution's symmetry can then be easily calculated.

1.3.8 Rotational Wavefunction Symmetry

Near prolate asymmetric tops all share a rotational energy level pattern, with the details being determined by the particular molecular properties. In all such cases, the energy levels arrange themselves in stacks according to the value of K_a. Within the $K_a = 0$ stack, there is one level per J value (where $K_a = 0, K_c = J$). In all other K stacks, there are two rotational levels per J, again with K_a defined by the stack, and K_c equal to $J - K_a$ and $J - K_a + 1$. The level (of the two with the same J, K_a) that has the higher K_c value lies lower in energy.

The rotational wavefunctions are defined in terms of the Euler angles, which relate the laboratory-oriented (X, Y, Z) axis system to the body-fixed (x, y, z) axis system [29]. Symmetry group operations will change the Euler angles of the molecule, and therefore

CNPI-MS					E	$(ab)(12)$	E^*	$(ab)(12)^*$			
Equivalent Rotation					R_0	R_c^π	R_c^π	R_0			
$D_{\infty h}$	G_8		C_{2h}	CNPI	E	C_2^c	σ_{ab}	i			
Σ_g^+	A_1'	A_1''	A_g	$Ss+$ $Aa+$	1	1	1	1		J_c	
Σ_u^-	A_2'	A_2''	A_u	$Ss-$ $Aa-$	1	1	-1	-1	Γ^*	c	
Σ_g^-	B_1'	B_1''	B_g	$Sa-$ $As-$	1	-1	-1	1		J_a	J_b
Σ_u^+	B_2'	B_2''	B_u	$Sa+$ $As+$	1	-1	1	-1	a	b	

TABLE 1.3: The Molecular Symmetry subgroup of the full CNPI group G_8 (CNPI-MS) for the *trans*-bent configuration of acetylene, shown earlier as Table 1.2, is reprinted here for ease of reference. The first three columns correspond to labels of rigid point groups. The fourth column contains the true symmetry labels. The equivalent rotations, relevant to the rotational wavefunctions in particular, which transform the Euler angles in the same way as the associated true symmetry operation, are included.

the rotational wavefunctions. Fortunately, every symmetry operation will produce a change in the Euler angles that is equivalent to a rotation about one of the inertial axes. These "Equivalent Rotations" are included in the Molecular Symmetry group tables we'll see in this section. By examining the effect of an equivalent rotation on the molecule, in particular the even or odd character of the K_α value associated with the axis of equivalent rotation to the symmetry operation in question, the symmetry properties of the rotational wavefunctions can be deduced. If the b axis is the equivalent rotation axis that defines the symmetry properties, just note that the even/odd character of rotation about any inertial axis is the product of the characters of the other two axes, for example if K_a is odd and K_c is odd, the wavefunction will transform in operations with equivalent rotation about the b axis as though K_b were even.

The parity of a wavefunction is defined by its response to the parity operator E^*. In the case of *trans*-bent acetylene, the parity operator has equivalent rotation R_c^π. We can attach the parity label, $(+/-)$, to the wavefunction based on the value of K_c, $(+)$ for even and $(-)$ for odd. As seen in the MS table, there are only two possible permutation symmetries to assign to a level, either Ss and Aa, or Sa and As (recall that the lables we're using are labels from the full G_8 CNPI group, and the MS group has half as many elements, so two labels from the CNPI group apply to every MS symmetry). The equivalent rotation for the operation that permutes the carbons and hydrogens, $(ab)(12)$, is again R_c^π. The symmetry labels for permutation can also be assigned using K_c: Ss

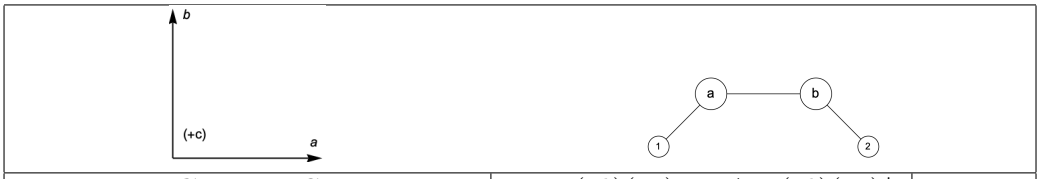

CNPI-MS						E	$(ab)(12)$	E^*	$(ab)(12)^*$		
Equivalent Rotation						R_0	R_b^π	R_c^π	R_a^π		
$D_{\infty h}$	G_8		C_{2v}	CNPI		E	C_2^b	σ_{ab}	σ_{bc}		
Σ_g^+	A_1'	A_1''	A_1	$Ss+$	$Aa+$	1	1	1	1	b	
Σ_u^-	A_2'	A_2''	A_2	$Ss-$	$Aa-$	1	1	-1	-1	Γ^*	J_b
Σ_g^-	B_1'	B_1''	B_1	$Sa-$	$As-$	1	-1	-1	1	c	J_a
Σ_u^+	B_2'	B_2''	B_2	$Sa+$	$As+$	1	-1	1	-1	a	J_c

TABLE 1.4: The Molecular Symmetry subgroup of the full G_8 CNPI symmetry group for *cis*-bent acetylene. The CNPI-MS operations for *cis*- and *trans*-bent acetylene are the same, but the MS groups are different, as the operations correlate to equivalent rotations about different inertial axes.

and Aa for even K_c and Sa and As for odd. Because both symmetry labels are attached using the same equivalent rotation, only 4 of the 8 possible symmetry labels appear in the rotational levels of *trans* acetylene: $Ss-$, $Aa-$, $Sa+$, and $As+$ do not appear.

The *cis*-bent arrangement of acetylene has different rotational symmetry properties than the *trans*-bent. The parity labels are the same as in *trans* acetylene, as the equivalent rotation of the parity operator E^* is once again a rotation around the c inertial axis. The parity labels for *cis* acetylene are then (-) for odd K_c and (+) for even K_c. The $K_a = 0$ stack has alternating parity for alternating values of J, beginning with (+) parity for $J = 0$. The other K stacks all have two levels for each J, K_a pair, with one of the pair having (+) parity and the other (-). The lower level of the lowest J of each K stack (where $J = K_a$) has (-) parity, the higher (+). This pattern alternates with each J in the stack, identically as for the *trans*-bent case.

The permutation operation $(ab)(12)$, however, does not correlate to a rotation around the c inertial axis, but instead around the b axis. The permutation labels of the rotational wavefunctions, then, are assigned according to the even or odd character of K_b, or rather whether K_a and K_c are both even/odd together or opposite. In the K_a-even stacks, the Ss and Aa states are the states of (+) parity. In the K_a-odd stacks, the Ss and Aa states are the states of $(-)$ parity, and the As and Sa states are of (+) parity. When the equivalent rotations of the two relevant symmetry operations are associated with different inertial axes, it means that both combinations of permutation and parity symmetries are present in *cis* acetylene, meaning states of all 8 CNPI symmetries exist.

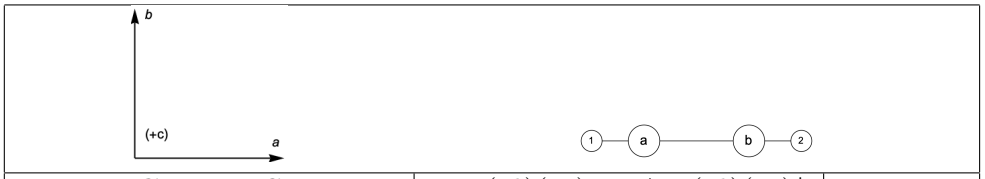

CNPI-MS					E	$(ab)(12)$	E^*	$(ab)(12)^*$	
$D_{\infty h}$	G_8		CNPI		E	C_2	σ_{ab}	i	
Σ_g^+	A_1'	A_1''	$Ss+$	$Aa+$	1	1	1	1	
Σ_u^-	A_2'	A_2''	$Ss-$	$Aa-$	1	1	-1	-1	Γ^*
Σ_g^-	B_1'	B_1''	$Sa-$	$As-$	1	-1	-1	1	J_a
Σ_u^+	B_2'	B_2''	$Sa+$	$As+$	1	-1	1	-1	

TABLE 1.5: The Molecular Symmetry subgroup of the full G_8 CNPI symmetry group for linear acetylene. J_b and J_c belong to the Π_g symmetry group, not shown in the table.

The primary result in the spectrum is essentially the loss of g/u symmetry, which is to say that half the vibrational levels are not inaccessible by one/two photon experiments.

Finally, we consider the rotational symmetry of linear acetylene. Linear acetylene is a more complicated case. The rotational wavefunctions are defined in general in terms of 3 Euler angles, however the orientation of linear molecules is defined by only 2 angles. For a full discussion of how the loss of one Euler angle complicates the analysis of linear molecules' symmetry properties, see the discussion by Bunker and Jensen [29].

Linear molecules are not asymmetric rotors, so our picture of the energy levels will not exactly apply. However, linear molecules can accumulate angular momentum around the a axis, and there will be some properties analogous to a near-prolate rotor. There are two sources of such angular momentum with which we are concerned: vibrational and electronic angular momentum. Degenerate vibrations can accumulate angular momentum about the molecular axis. The angular momentum of vibration ν_i, denoted l_i, can take on values $l_i = v_i, v_i - 2, v_i - 4, \ldots$ 1 or 0. Total vibrational quantum number l is then

$$l = \left| \sum_i (\pm l_i) \right|, \tag{1.40}$$

where the $\pm$ indicates whether the angular momentum associated with different vibrational modes adds constructively (in the same direction along the a axis) or destructively. Linear molecules can also have electronic angular momentum, denoted Λ. This angular momentum originates from the rotation of electrons about the molecular axis. The total vibronic angular momentum

$$K = |\pm\Lambda \pm l| \tag{1.41}$$

is the sum of these two types of momenta, and will form similar patterns to K_a in the asymmetric rotor case. The rotational states of the linear molecule are organized according to K, and states with $K = 0, 1, 2...$ are labeled $\Sigma, \Pi, \Delta, ...$

An important difference between linear molecules organized by value of K and asymmetric rotors is the existence of Σ^+ and Σ^- states, so the $K = 0$ stack can have two different symmetry patterns. Another difference is that, due to the restricted possible values of the l_i, only states of even **or** odd K can appear in a single vibrational state, dependent upon the values of v_i and Λ. For a totally symmetric vibronic state, the rotational levels are organized very much like those of the asymmetric rotor, other than the differences mentioned, including the two levels per J, K set in all levels with $K \neq 0$. In all stacks except the $l = 0$ Σ^+, the lowest energy level is $Sa-/As-$. The symmetry levels then alternate with J in the Σ^- stack with $Ss+/Aa+$, and in the $K \neq 0$ stacks these two symmetry groups exist in each J, K and their energy order alternates with J. In the "extra" Σ^+ stack, the symmetry labels are the opposite of those in the Σ^- stack.

1.3.9 Selection Rules

Now that we've established the symmetry properties of the rovibronic states of acetylene, we can apply those rules (along with others) to obtain selection rules for allowed electric dipole transitions in acetylene.

The rigorous selection rules that apply to rigid rotors will of course still apply to acetylene. For an electric dipole transition, $\Delta J = 0, \pm 1$; $J = 0 \nleftrightarrow J = 0$ (If we are neglecting nuclear spin, otherwise thse selection rules apply to F, not J). The allowed change of projections of J, ΔK_i, are determined by the direction in which the transition dipole is oriented in relation to the inertial axes of the molecule. If the transition dipole is in the a direction, $\Delta K_a = 0, \pm 2, ...$ and $\Delta K_c = \pm 1, \pm 3, ...$ If the transition dipole lies in the b direction, $\Delta K_a = \pm 1, \pm 3, ...$ and $\Delta K_c = \pm 1, \pm 3, ...$ If the transition dipole is in the c direction, $\Delta K_a = \pm 1, \pm 3, ...$ and $\Delta K_c = 0, \pm 2, ...$

Next, we note that the electric dipole operator, Γ^*, belongs in every case to the CNPI symmetry $Ss-$. As the integrand of the transition matrix element $\langle \Psi'_m | \mu | \Psi''_n \rangle$ must be totally symmetric to be non-zero, the initial and final state must be of opposite parity

but identical nuclear permutation symmetry,

$$Ss \leftrightarrow Ss,\ Sa \leftrightarrow Sa,\ Sa \leftrightarrow Sa,\ Aa \leftrightarrow Aa \tag{1.42}$$

and

$$+ \leftrightarrow -. \tag{1.43}$$

Of course, for the case of perturbations, the direct product of the interacting states' symmetries must contain the totally symmetric symmetry, $Ss+$, for the perturbation to be allowed.

1.3.10 Additional Selection Rules Due to Factoring the Wavefunction

Further restrictions on transitions are introduced via approximations. In essence these rules are in fact propensity rules, but may be strong enough, depending on the validity of the approximations used, to make technically allowed transitions weak enough to be unobserved.

The electric dipole operator transforms as the representation of the Molecular Symmetry group that has character +1 under permutations and character -1 under all inversions, including permutation-inversions. This can be seen in the MS group tables, for instance Table 1.2, where the electric dipole operator Γ^* belongs to such a representation. In order to factor the total wavefunction, we express the electric dipole operator expressed in the laboratory frame μ_A as a sum of molecular electric dipole components along the molecule-fixed (x, y, z) axes and a sum of components along the space-fixed (ξ, η, ζ) axes [29]. These two axis systems are rotations of each other, both being centered at the nuclear (not molecular) center of mass. For ease of determining the selection rules that involve angular momenta, rather than using a simple sum of the orthogonal Cartesian coordinates, we will use space-fixed components

$$\begin{aligned} \mu_s^{(1,\pm 1)} &= \frac{\mp\mu_\xi + i\mu_\eta}{\sqrt{2}} \\ \mu_s^{(1,0)} &= \mu_\zeta \end{aligned} \tag{1.44}$$

and molecule-fixed components

$$\begin{aligned}\mu_m^{(1,\pm1)} &= \frac{\mp\mu_x + i\mu_y}{\sqrt{2}} \\ \mu_m^{(1,0)} &= \mu_z.\end{aligned} \tag{1.45}$$

As these two axis systems are simple rotations of each other, they can be inter-converted,

$$\mu_s^{(1,\sigma)} = \sum_{\sigma'=-1}^{1} \left[D_{\sigma\sigma'}^{(1)}(\phi,\theta,\chi)\right]^* \mu_m^{(1,\sigma')}, \tag{1.46}$$

where $D_{\sigma\sigma'}^{(1)}$ is a spherical tensor dependent on the Euler angles ϕ, θ, and χ.

In terms of the space-fixed electric dipole operator μ_A, the line strength is defined as

$$S(f \leftarrow i) = \sum_{\Phi'_{int},\Phi''_{int}} \sum_{A=X,Y,Z} \left| \left\langle \Phi'_{int} \middle| \mu A \middle| \Phi''_{int} \right\rangle \right|^2, \tag{1.47}$$

where the Φ_{int} are the internal wavefunctions of the initial and final states. In terms of our new space-fixed axis system, this becomes

$$S(f \leftarrow i) = \sum_{\Phi'_{int},\Phi''_{int}} \sum_{\sigma=-1}^{1} \left| \left\langle \Phi'_{int} \middle| \mu_s^{(1,\sigma)} \middle| \Phi''_{int} \right\rangle \right|^2. \tag{1.48}$$

The line being examined will only have intensity if the matrix element above is not equal to zero. This rule on the matrix element can be rewritten using separable wavefunctions as

$$\left\langle \Phi'_{nspin}\Phi'_{rot}\Phi'_{vib}\Phi_{elec}^{(e',S',m'_s)} \middle| \mu_s^{(1,\sigma)} \middle| \Phi''_{nspin}\Phi''_{rot}\Phi''_{vib}\Phi_{elec}^{(e'',S'',m''_s)} \right\rangle \neq 0 \tag{1.49}$$

The dipole moment operator does not act on the nuclear spin wavefunctions, so we can separate those parts of the internal wavefunctions

$$\left\langle \Phi'_{nspin} \middle| \Phi''_{nspin} \right\rangle \left\langle \Phi'_{rot}\Phi'_{vib}\Phi_{elec}^{(e',S',m'_s)} \middle| \mu_s^{(1,\sigma)} \middle| \Phi''_{rot}\Phi''_{vib}\Phi_{elec}^{(e'',S'',m''_s)} \right\rangle \neq 0. \tag{1.50}$$

Pulling the first term out from the integral immediately yields an additional selection rule on the transitions,

$$\Delta I = 0. \tag{1.51}$$

We use equation 1.46 to convert the space-fixed matrix element to a body-fixed element. Once again, we separate the parts of the matrix element that don't interact, in this

case the rotational parts of the wavefunction, which depend on the Euler angles, can be separated from the parts that depend on the vibronic coordinates,

$$\begin{aligned}\left\langle \Phi'_{nspin} \middle| \Phi''_{nspin} \right\rangle \sum_{\sigma=-1}^{1} \left\langle \Phi'_{rot} \middle| D^{(1)*}_{\sigma\sigma'} \middle| \Phi''_{rot} \right\rangle \\ \times \left\langle \Phi'_{vib} \Phi^{(e',S',m'_s)}_{elec} \middle| \mu^{(1,\sigma')}_{m} \middle| \Phi''_{vib} \Phi^{(e'',S'',m''_s)}_{elec} \right\rangle \neq 0.\end{aligned} \tag{1.52}$$

The rotational part of this equation can be simplified, by first recognizing that each rotational wavefunction Φ_{rot} is a linear combination of symmetric top wavefunctions,

$$\Phi_{rot} = \sum_{k=-N}^{N} c_k^{(N)} \left| N, k, m \right\rangle, \tag{1.53}$$

and using an expression involving $3j$ symbols, such as those found in Zare [37]. The details of using the $3j$ symbols will be left to the reader, but the rotational wavefunction matrix element will be found to be proportional to a $3j$-symbol which involves the rotational quantum number N, where $N = J - S$, the molecule-fixed projection of N, k, and summed over the coordinates we defined earlier, using index σ,

$$\left\langle \Phi'_{rot} \middle| D^{(1)*}_{\sigma\sigma'} \middle| \Phi''_{rot} \right\rangle \propto \sum_{\sigma'=-1}^{1} \begin{pmatrix} N'' & 1 & N' \\ k'' & \sigma' & -k' \end{pmatrix}. \tag{1.54}$$

From the properties of $3j$-symbols, we can deduce another selection rule enforced on the rotational quantum number N,

$$\Delta N = 0, \pm 1; \;\; N' + N'' \geq 1. \tag{1.55}$$

Only two terms from the original factored wavefunction remain. We factor out the vibrational parts,

$$\left\langle \Phi'_{vib} \Phi^{(e',S',m'_S)}_{elec} \middle| \mu^{(1,\sigma')}_{m} \middle| \Phi''_{vib} \Phi^{(e'',S'',m''_S)}_{elec} \right\rangle = \left\langle \Phi'_{vib} \middle| \mu^{(1,\sigma')}_{m}(e',e'') \middle| \Phi''_{vib} \right\rangle, \tag{1.56}$$

where the inner operator term may be expressed as an integral

$$\mu^{(1,\sigma')}_{m}(e',e'') = \left\langle \Phi^{(e',S',m'_S)}_{elec} \middle| \mu^{(1,\sigma')}_{m} \middle| \Phi^{(e'',S'',m''_S)}_{elec} \right\rangle. \tag{1.57}$$

This inner integral depends upon the nuclear coordinates, so this is not a true separation

of the vibrational and electronic coordinates. From the assumption that the operators $\hat{\boldsymbol{S}}^2$ and $\hat{S}_Z$ commute with the the dipole operator $\mu_m^{(1,\sigma')}$, we obtain another selection rule,

$$\Delta S = 0. \tag{1.58}$$

Examining the vibrational and electronic portion of the wavefunction more closely, we can find a few more rules. It's clear from symmetry rules that

$$\Gamma'_{vib} \otimes \Gamma''_{vib} \otimes \Gamma'_{elec} \otimes \Gamma''_{elec} \supset \Gamma\left(\mu_m^{(1,\sigma')}\right). \tag{1.59}$$

The three operators $\mu_m^{(1,\sigma')}$ do not necessarily transform as irreducible representations of the Molecular Symmetry group, but the three Cartesian components μ_α do. Recognizing that, in the MS group, the μ_α belongs to the same representation as a translation, T_α, we write

$$\Gamma'_{vib} \otimes \Gamma''_{vib} \otimes \Gamma'_{elec} \otimes \Gamma''_{elec} \supset \Gamma(T_\alpha), \tag{1.60}$$

where α is one of the molecule fixed Cartesian coordinates, x, y, z.

Further, we can express the inner integral, $\mu_\alpha(e', e'')$ (the body-fixed axis version of the $\mu_m^{(1,\sigma')}(e, e'')$ above), as a Taylor series expansion in the normal coordinates of one of the two electronic states, with terms

$$\mu_\alpha(e', e'') = \mu_\alpha^{(0)} + \sum_r \mu_\alpha^{(r)}(e', e'')Q_r + ... \tag{1.61}$$

If we truncate this expansion after the first term, the inner integral of the vibrational and electronic matrix elements becomes a constant and can be pulled outside the integral, leaving selection rules

$$\Gamma'_{vib} = \Gamma''_{vib} \tag{1.62}$$

and, in the case of two different electronic states,

$$\Gamma'_{elec} \otimes \Gamma''_{elec} \supset \Gamma(\mu_\alpha) = \Gamma(T_\alpha). \tag{1.63}$$

These are the weakest selection rules we've discussed so far, as they arose from merely using what is usually the most important term in a Taylor expansion, rather than more physical reasoning.

We will now look at some specific cases from the $S_1 \leftarrow S_0$ transition in acetylene. We'll start with the electronic transition: the *trans*-bent S_1 state is formed by promoting one electron from the valence π_u orbital to the higher-lying a_g orbital, leaving an electronic symmetry of $Ss-, Aa-$. The ground linear state of acetylene has all orbitals full, and therefore has symmetry $Ss+, Aa+$. The electric dipole operator belongs to the representation that has character (-1) under the inversion operation, E^*, and character (+1) under permutation. We find

$$[Ss+ \oplus Aa+] \otimes Ss- = [Ss+ \oplus Aa-], \tag{1.64}$$

which indicates that this electronic transition is allowed.

The first excited singlet state of acetylene also supports a cis-bent configuration. In that geometry, the higher lying electron is in a $Ss-, Aa-$, a_2 orbtial, and the electronic state transforms as $Sa-, As-$. We find

$$\Gamma(S_0) \otimes \Gamma(S_{1,cis}) \not\supset \Gamma^*, \tag{1.65}$$

so this electronic transition is forbidden. Certain lines within this electronic state can be weakly observed, either due to the assumptions we made in defining these selection rules being invalid or due to interactions with other states.

1.3.11 Effects that Invalidate Selection Rules

There are some additional effects that we haven't specifically considered which can cause selection rules to be broken. If the equilibrium geometries of the two electronic states involved in the transition, Φ'_{elec} and Φ''_{elec}, are different, then the molecular axes (x, y, z) may be oriented differently in the two states. This is because the Euler angles that describe the orientation of the molecule-fixed axes depend not only on the instantaneous nuclear positions, but also on the equilibrium positions. This effect is called *axis switching* [38]. In essence, we must choose one equilibrium state to apply the Eckart conditions to in order to define a single unifying set of molecular axes (x, y, z). The primary result is that the definition of the quantum or near-quantum numbers K, K_a, and K_c is different for the two states, which relaxes the selection rules on K.

Additionally, Coriolis coupling can mix states of different K. The asymmetric top rotational Hamiltonian can be simplified to

$$H_{rot} = A(J_a - G_a)^2 + B(J_b - G_b)^2 + (J_c - G_c)^2, \tag{1.66}$$

where A, B, and C are the usual rotational constants, J is the total angular momentum, and G is the vibrational angular momentum [5]. Multiplying out the squares,

$$\begin{aligned} H_{rot} =& AJ_a^2 + BJ_b^2 + CJ_c^2 - 2AJ_aG_a \\ & -2BJ_bG_b - 2CJ_cG_c + AG_a^2 + BG_b^2 + CG_c^2, \end{aligned} \tag{1.67}$$

where the Coriolis coupling terms are those that involve the $J_\alpha G_\alpha$ terms. These terms allow mixing of angular momentum due to degenerate vibrational motions with angular momentum from rotation, allowing some bands that are usually considered forbidden to appear in a spectrum, including some $\Sigma - \Sigma$ and $\Pi - \Pi$ bands observed by Ingold, King, and Innes.

The astute reader, or more likely the reader who is familiar with the work of the Field research group, may have noticed the lack of an important isomeric form of acetylene in these discussions, that of the CCH_2 form, vinylidene. This is not the only isomer that has not been discussed, as there are of course non-planar geometries possible (and observed, Reference 39, for instance), but it is an isomer that has received considerable theoretical and experimental attention, particularly in the electronic ground S_0 state of acetylene [40–45].

The excited S_1 state is also predicted to have a minimum in the vinylidene conformation, and in fact this arrangment has been predicted to be the global minimum of the surface [13]. Treating transitions to vinylidene using rigid point groups is even more problematic than other isomeric forms, because the transition to vinylidene involves the breaking and forming of chemical bonds. CNPI symmetry can, of course, be used to understand transitions between vinylidene and other isomeric forms. The analysis is not carried out in this thesis, because the experiments described herein have not observed any evidence of S_1 vinylidene. Lundberg does carry out the CNPI analysis for vinylidene as well as multiple distinct non-planar geometries, and the interested reader is directed to Reference 32.

1.4 Further Advances in the Study of Acetylene, Roughly 1980-2010

After the (significant) diversion into the group theoretical mechanisms required to understand molecules that are not locked to a rigid point group, we return to examining the history of advances in the study of acetylene. Ingold and King, and Innes, presented particularly ground-breaking studies for chemical physics generally. The advances discussed through the rest of the chapter will not be presented in quite the same amount of detail.

1.4.1 Watson's Analyses of the UV Spectrum of Acetylene

The set of papers on the bands of acetylene by Watson and others is a great resource on the vibrational and rotational structure of acetylene [4, 8, 46]. There's a relevant discussion of the energy levels in both the upper and lower electronic states, as well as some very useful information on the dependence of energy levels on J. We have of course already looked at these topics in some detail in this chapter, but for a quick reference and somewhat more accessible take on selection rules in acetylene, these papers are unmatched.

Of particular interest to us are the advances in understanding attributed to this series of papers. The longer-wavelength regions of the $S_1 \leftarrow S_0$ were already quite well understood by the time of these publications. In fact, virtually complete assignments are tabulated up to 45,500 cm^{-1}, with some transitions assigned up to 48,000 cm^{-1}. The origin band is assigned near 42,200 cm^{-1}. A total of well over 200 vibrational bands are assigned in this series, nearly all of which assignments have been verified in the years since.

1.4.2 Advances in the Study of Acetylene, 1990s Through 2000s

In the years following Watson's series of papers, many different research groups contributed various techniques and analyses to the study of S_1 acetylene. Utz and Tobiason performed the first IR-UV double resonance Laser Induced Fluorescence experiments on the S_1 state of acetylene [9]. Using the molecular point group paradigm, both linear S_0

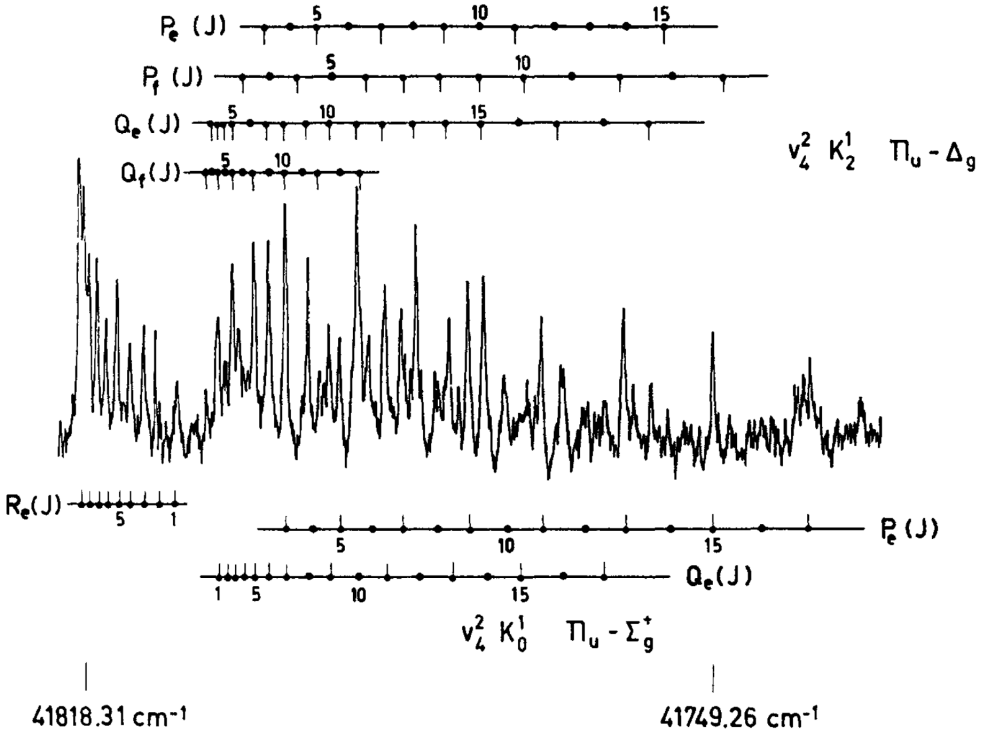

FIGURE 1.11: Branches of two bands in the $S_1 \leftarrow S_0$ transition of acetylene, as recorded by Watson. K in this figure has the meaning that has been used in this thesis, namely angular momentum along the a axis in the upper state, and the quantum number l, the vibrational angular momentum, in the lower electronic state. The notation V refers to the bending vibrations, ν_4 in the lower state and ν_3 in the upper state. Figure reproduced from Reference 4, with permission from Elsevier.

and *trans*-bent S_1 acetylene possess *gerade/ungerade* inversion symmetry. A photon can only connect two states of opposite g/u symmetry (assuming an electric dipole transition). As long as this symmetry is relevant in the upper electronic state, a particular experiment only has hope of accessing half of the vibrational manifold. IR-UV double resonance experiments are now considered to be an essential part of the study of S_1 acetylene, both because of the access to alternate symmetry states, but also because of the ability to tune the Franck-Condon factors to maximize the transition intensity into the desired state.

Utz and Tobiason used the $3\nu_3''$ state as an intermediate in their IR-UV experiments. The ν_3'' vibration is the asymmetric C-H stretch, and is of *ungerade* symmetry. Since the S_1 *trans* well is also of *ungerade* symmetry, vibrational states that are of *ungerade* symmetry are accessible by this method, and transitions to such states are forbidden from the ground state. Utz and Tobiason observed the fundamental levels of both the ν_4' and ν_6' vibrations. Even with only one quantum observed, it was clear that these

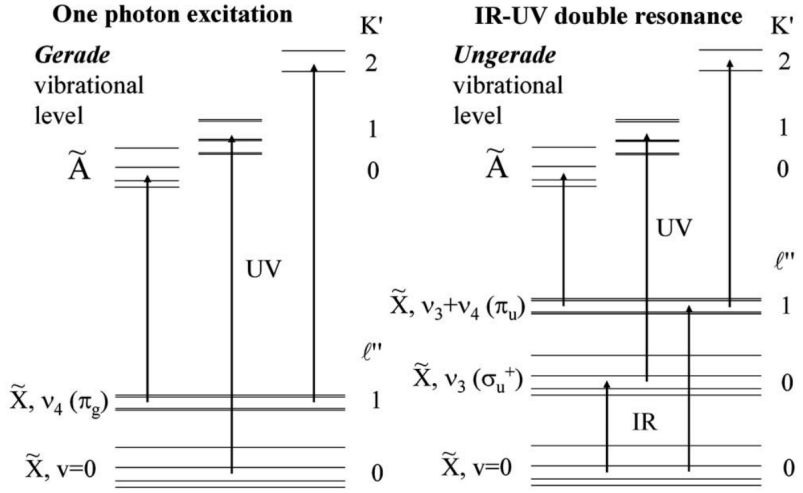

FIGURE 1.12: A cartoon representation of all experiments needed to fully characterize a vibrational level of the acetylene *trans*-bent S_1 electronic state. On the left, examples of the two types of experiments required to characterize *gerade* vibrations upstairs are depicted. In order to fully understand modes 4 and 6, the Darling-Dennison and Coriolis couplings must be separated, so three values of K must be observed. Hot-band transitions from ν_4'' have access to $K = 0, 2$, so between hot and cold band single photon transitions, all *gerade* vibrations can be understood. The situation is similar for *ungerade* vibrations, but an addition photon is needed (no hot bands from *ungerade* vibrational levels downstairs have been observed). Figure reproduced from Reference 5, with permission from AIP.

two modes are heavily mixed. The importance of Coriolis mixing between ν_4 and ν_6 was recognized, and this is still accepted as one of the two most important resonances in the S_1 state of acetylene. The other important resonance, Darling-Dennison, which was recognized some time later by Merer (see Reference 5), mixes states by trading two quanta of energy between modes 4 and 6, so Utz and Tobiason's experiment, which only observed states with one quantum of bend, was blind to this important resonance.

Yamanouchi performed Dispersed Fluorescence (DF) experiments from S_1 acetylene [47]. He observed combination bands that included ν_4' and ν_6', and recognized that such bands could be explained on the basis of the same Coriolis resonance between modes 4 and 6 that Utz and Tobiason described. Yamanouchi was also responsible for the application of polyad analysis to S_1 acetylene, with the only modes involved in important enough resonances to be destroyed being modes 4 and 6, and the new polyad quantum number $B = v_4 + v_6$. The polyad analysis is vital in understanding both S_0 and S_1 acetylene.

1.5 Confirmation of the Existence of *Cis*-bent S_1 Acetylene

The S_1 potential energy surface of acetylene is most commonly observed to exhibit a *trans*-bent geometry. It can be predicted using Walsh's rules that there should also be relatively low-lying cis states on the S_1 surface as well [36]. Calculations of the geometries and energies of several low-lying *cis* states were calculated by So [48]. Some years later, Stanton performed calculations on many properties of the acetylene S_1 state [13]. Not only was it predicted that this electronic state has stable wells at both *cis* and *trans* geometries, but the global minimum is calculated to be of the vinylidene structure, CCH_2.

It wasn't until well over a decade later that definitive experimental evidence of the *cis*-bent structure of S_1 acetylene was observed. The vibrational manifold was essentially completely explained up to energies ~4200 cm^{-1} above the S_1 *trans* zero-point level. However, as Merer and Baraban report, there were a small number of vibrational levels observed that do not fit into the *trans* structure's vibrational states [11]. These states were assigned to *cis*-bent S_1 vibrational states.

Many different evidences combine in the case of the vibrational level that is the main subject of Merer and Baraban's analysis, the level at 46,174 cm^{-1}, as well as several other *cis* states that have also been observed, to demonstrate that they are not localized in the *trans* vibrational well [49].

First among the evidence cited to demonstrate that the 46,174 cm^{-1} level is of *cis* geometry is the isotope shift of the vibrational level upon isotopic substitution. Certain lines of $H^{13}C^{12}CH$ are observable in the spectrum in natural abundance, and the spectrum of $^{13}C_2H_2$ was recorded to determine the mode-dependent isotope shifts [50]. The shifts between ^{12}C, the mixed isotopomer, and ^{13}C variations are found to be ~ -3 and -6 cm^{-1}. Given the energy of the probed state (4000 cm^{-1} above the *trans* zero-point level), no combination of vibration-dependent isotope shifts can be so small for this level. However, the *cis* well is several thousand wavenumbers above the *trans* well, and such small isotope shifts are expected.

Vibrational selection rules also differ between the *cis* and *trans* wells. The easiest way to rationalize this difference is that the *cis* structure does not possess point group

inversion symmetry, and cannot be classed as *gerade* or *ungerade*. The K selection rule ($K' - l'' = \pm 1$) is still good (in the absence of effects that mix K), but the limitation of a particular experiment to only reach vibrations of *gerade gerade* symmetry is no longer valid.

Lifetime studies further confirm the identity of this *cis* vibrational level. The lifetime of most nearby *trans* levels is around 300 ns. The state in question has a lifetime of at least 2 μs. One-photon transitions between the *cis* well and the ground state are electronically forbidden, so the radiative lifetime of *cis* levels is expected to be much longer than *trans*. The possibility exists that the lifetime is extended by interactions with nearby triplet levels, but Zeeman experiments demonstrated no evidence that this is the case.

Progress beyond this point in the study of S_1 acetylene encounters several difficulties that have made securing additional vibrational assignments difficult. There are two problems in particular that have been the most devastating to this effort. The first is theoretical: the model used to understand this electronic state of acetylene is designed to understand the *trans* well, and does not directly account for the presence of *cis*-bent states. This is fine as long as the two wells is a valid picture of the state, but at energies approaching and above the isomerization barrier, this model will not even approximately reproduce the locations of the energy levels. The second problem, and the one that the remainder of this thesis is focused on solving, is predissociation: the lifetime of S_1 states in the vicinity of the isomerization barrier becomes very short, due to tunneling through a barrier onto a dissociative surface [47]. Several techniques have been used to attempt to bypass this limitation, including H-atom REMPI [51, 52], H-atom fluorescence spectroscopy [6], and, the technique that dominates the remainder of this thesis, Photofragment Fluorescence Action Spectroscopy, or PFAS.

Chapter 2

Development and Analysis of Photofragment Fluorescence Action Spectroscopy (PFAS)

The work described in this chapter has been published previously [6, 7]. This chapter emphasizes the work that I did in the initial paper, extensions to the experiment conducted by me after this work was published, and the analysis required to understand the work presented later in this thesis.

2.1 Introduction

As discussed previously in Section 1.2, the first excited singlet state of acetylene, the S_1 state, is *trans*-bent, rather than linear, at equilibrium [1, 16–19]. The S_1 state potential energy surface has a secondary minimum at a *cis*-bent structure (as well as a predicted minimum at the C_2H_2 vinylidene geometry [13]). Group theory arguments indicate, however, that transitions from the ground S_0 state to the *cis*-bent conformer of the S_1 state are electronically forbidden. Levels in the *cis* well can interact with and borrow transition intensity from nearby (in energy) levels in the *trans* well. Our research group (building on the work of others, including Ingold and King) has published essentially complete assignments of all vibrational levels localized in the *trans* well up to an energy of 4500 cm^{-1} above the zero-point level [4, 5, 8, 9, 46, 47, 49, 50, 53–57].

At energies higher than 4500 cm^{-1} above the *trans* zero-point level, we have encountered both difficulty in assigning the spectrum, as well as experimental difficulties in recording spectra. The interactions between the *trans* and *cis* wells distort the pattern of the energy levels in the energetic vicinity of the isomerization transition state. Our fit model, based on polyads [10], is used primarily in the *trans* well and does not explicitly account for the presence of the *cis* well. Levels near and above the barrier to isomerization (calculated to lie at about 5000 cm^{-1} above the *trans* zero-point level) are not accurately predicted by the model.

A major contributor to the difficulties of the experiment, the predissociation threshold of acetylene, lies about 1000 cm^{-1} below the top of the isomerization barrier [58]. The method our group has used to study acetylene has been primarily Laser Induced Fluorescence (LIF). In LIF, the signal is generated by the laser-excited molecules relaxing by fluorescence back down to the S_0 state, releasing photons, which are collected by a photomultiplier tube. The signal collected depends upon the fluorescence quantum yield, $\frac{k_f}{(k_f+k_{nr})}$, where k_f is the radiatiave decay rate and k_{nr} is the non-radiative decay rate. As the energy of the excited state increases, the predissociation rate becomes faster, and fewer molecules survive long enough to relax back down to the ground state. One saving grace of acetylene that has allowed our group to progress to the level that we have is that the predissociation onset is slow, occuring over the span of hundreds of cm^{-1}. As a result, many states above the predissociation threshold are observable via LIF [12]. However, once levels above 5000 cm^{-1} are reached, only about half of the predicted levels are observable by LIF. The combination of the low fluoresence quantum yield and the incomplete nature of our polyad model in the near-barrier region has made finding secure assignments for levels in this energy region challenging.

This chapter focuses on a new detection technique that bypasses the fast predissociation rate that plagues LIF measurements, or at least to extend the frequency range in which useful experimental results can be obtained. This method is called Photofragment Fluorescence Action Spectroscopy (PFAS), offers a higher signal-to-noise ratio than traditional LIF, and is not appreciably more difficult to implement, as it requires only one tunable laser, unlike other strategies such as H-atom fluorescence [6] or Resonance Enhanced Multi-Photon Ionization (REMPI) [52] that could also be used to collect signal from predissociated levels of acetylene. More complicated experimental setups are not incompatible with PFAS, however, and in fact we performed IR-UV double resonance

with the PFAS detection technique, but unlike the other techniques listed here, the use of a probe laser is not required.

2.2 Experimental Details

Several different experiments will be described in this section. First, a few different methods of performing PFAS spectroscopy will be discussed. In order to better understand the fluorescence signal, our research group performed experiments focused on studying the photofragment fluorescence itself. Dispersed fluorescence spectroscopy was performed on the radiation emitted from the acetylene photofragments, using a room temperature flowing gas cell of acetylene. Additional experiments were also done in a cold molecular beam, which complemented the dispersed fluorescence studies in gaining an understanding of the PFAS detection process. The experiments related to both efforts are also described in this section.

2.2.1 PFAS Experiments

The PFAS experiment is conducted in a high-vacuum chamber, pumped by a diffusion pump (Varian, VHS-6), which reaches an ultimate pressure without gas load of 10^{-6} torr, increasing to 5×10^{-5} under gas load. An unskimmed molecular beam of neat acetylene is expanded through a pulsed valve (General Valve, Series 9, orifice diameter=1.0 mm) with 1 atm of backing pressure.

The laser beams used in the initial IR-UV double resonance PFAS experiments were produced by two tunable dye lasers, a Lambda Physik FL3002E and a Lambda Physik FL2002. These lasers were pumped by the third and second harmonics of a Q-switched, injection-seeded Nd:YAG laser (Spectra Physics, Pro-270) operating at 20 Hz. Nonlinear processes, dependent upon the required wavelength, are applied to the output of the dye laser, as described below.

The PFAS technique is based on single-color, multi-photon photodissociaton of acetylene. This photodissociation is resonance-enhanced at the 1-photon level by a rotationally resolved $\tilde{A}$-$\tilde{X}$ transition. In order to facilitate the multi-photon dissociation, the UV excitaiton beam is focused (f=70 cm) before entering the experimental apparatus.

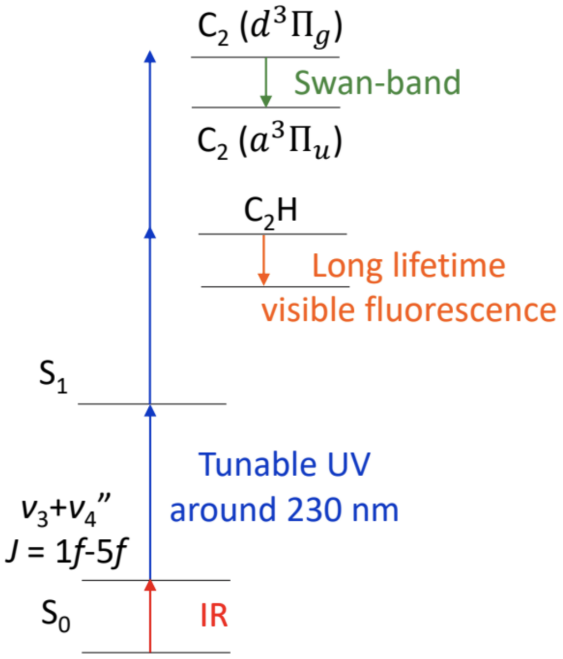

FIGURE 2.1: Level Diagram (energy axis is not drawn to scale) for the photofragment fluorescence detection scheme. The IR laser simultaneously excited the $J = 1 - 5$ f-symmetry rotational levels of the ground vibrational state to S_0 $\nu_3'' + \nu_4''$ combination level's rotational states via Q-branch pumping. The UV laser excites to a single rotational level of the S_1 state, and the same UV laser supplies additional photons to form fluorescent C_2 and C_2H fragments, which provide the observed PFAS signal. The details of this process will be examined in greater detail later in this chapter. The (relatively) long-lived fluorescence is collected by a PMT. Reproduced from Reference 6 with the permission of the AIP.

The lens is situated so the beam waist is a few centimeters away from the molecular beam, to reduce the occurrence of unwanted multi-photon excitations into high-lying Rydberg states of acetylene. This UV beam is produced by the FL3002E laser in the initial experiments, using Coumarin 460 dye. The dye laser output is frequency doubled in a β-barium borate (BBO) crystal, with a small portion of the fundamental output of the dye laser split off and passed through a cell containing heated $^{130}Te_2$ vapor for calibration. An intracavity etalon reduces the spectral width of the dye laser output to 0.04 cm^{-1}, with a power of approximately 350 μJ/pulse.

The IR laser beam used in the IR-UV double resonance PFAS experiments is produced by the FL2002 dye laser. It is generated by difference frequency mixing in a $LiNbO_3$ crystal using the fundamental of the injection-seeded Nd:YAG laser (1064 nm) and the near IR (740-750 nm) output of the dye laser (LDS 751 dye). The IR radiation has an energy of approximately 1.5 mJ/pulse, a spectral width (grating limited) of 0.1 cm^{-1}, and is focused (f=40 cm) to a diameter that matches the diameter of the UV beam in the active

volume of the experimental apparatus. The IR laser is tuned to simultaneously excite acetylene into $J = 1 - 5$ f-symmetry rotational levels of the S_0 $\nu_3 + \nu_4''$ via Q-branch pumping. The laser beams intersect the molecular beam about 1.5 cm downstream from the general valve orifice. Scattered light is minimized in the chamber via Brewster windows and two pairs of irises, which act as baffles (SM1 components, Thorlabs). The UV beam excites the vibrationally hot molecules into selected rovibrational states in the S_1 state. The same UV beam then causes photodissociation, and the resulting fluorescence from excited C_2 via the Swan band and from excited C_2H are detected by a PMT (Hamamatsu R375) at right angles to both the molecular beam path and the path of the lasers (the IR and UV lasers are aligned as counter-propagating beams). The signal recorded has a fluorescence lifetime of approximately 2 μs, and passes through a longpass filter before reaching the PMT to minimize scattered UV light. The PMT signal is passed through a voltage amplifier (Femto DHPVA-200, run at 30 dB or 20 dB amplification, depending on conditions) and monitored on a digital oscilloscope (LeCroy, 9360). The signal is then passed to a computer for processing.

Later PFAS experiments utilized a very similar experimental setup, with the differences all related to the dye laser radiation. In these experiments, the FL3002E etalon narrowed dye laser was replaced with a Sirah Cobra-Stretch dual-grating dye laser, also with a spectral width of approximately 0.04 cm^{-1}, and also pumped using the third harmonic of a Spectra Physics Pro-270 Nd:YAG laser.

In the PFAS experimental setup, there is a valid concern to avoid excitation via a 2-photon resonance up to highly excited Rydberg states of acetylene. Fortunately, the linewidths of such transitions into Rydberg states are expected to be significantly broader than those of interest to this study, due to rapid predissociation of the Rydberg states in this energy regime [59–67]. In the experiment, the UV beam is not focused to the minimum possible diameter, and the active volume lies a few centimeters from the beam waist, in order to optimize the selection of one-photon-resonance-enhanced process, rather than multi-photon dissociation. No such transitions into Rydberg states have been observed in our experiments.

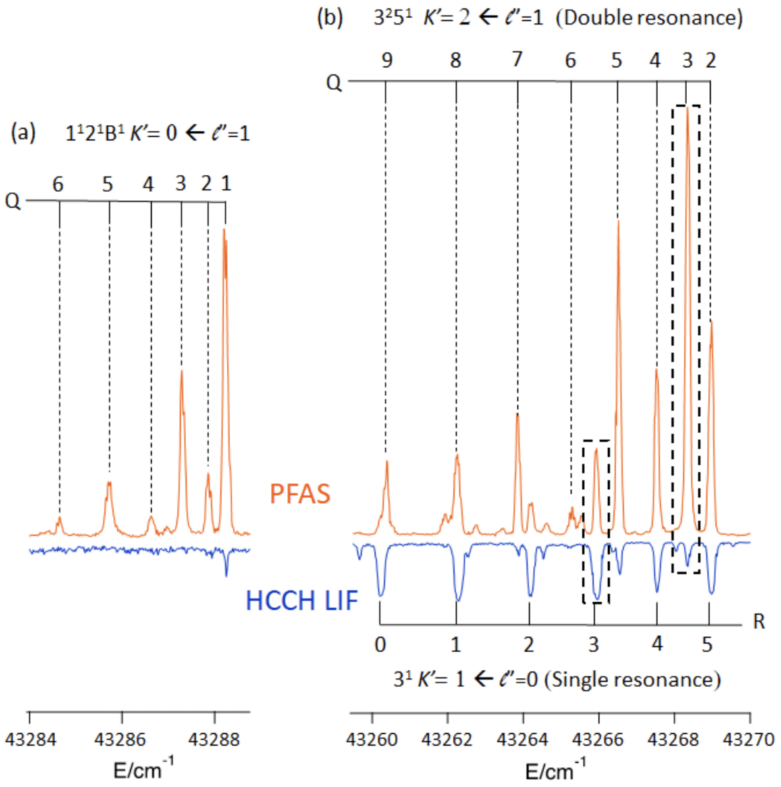

FIGURE 2.2: Spectra recorded by PFAS (plotted with the peaks pointing upward, pictured in orange) and LIF (plotted with the peaks pointing downward, pictured in blue) detection schemes. Horizontal axes represent the energy of the UV photon used in the IR-UV double resonance experiment. The comb lines indicate rotational assignments. (a) IR-UV double-resonance excitation spectrum of the $1^1 2^1 B^1$ $K' = 0$ band. In the S_1 state of acetylene, the vibrational fundamentals ν_4 and ν_6 are of very nearly the same frequency and are strongly mixed, and their distinct identities are destroyed. Instead of attempting to separate these motions, the notation B denotes the nominal value of $v_4 + v_6$. (b) IR-UV double-resonance spetrum of the $3^2 5^1$ $K' = 2$ band. This Q-branch accidentally overlaps with the R-branch of the single resonance 3^1 $K' = 1$ band. An energy diagram is presented in Figure 2.3. The transitions attributed to single resonance terminate on levels with a significantly lower term energy. These lines are of comparable intensity in the two pictured detection schemes. However, the double resonance lines appear with much greater intensity in the PFAS signal, due to its relative insensitivity to predissociation. Two particularly striking examples are highlighted by the dashed boxes. Reproduced from Reference 6 with permission of the AIP.

2.2.2 Photofragment Fluorescence Characterization Experiments

Two different types of experiments were performed to better understand the photofragmentation process. The first is Dispersed Fluorescence (DF). The $K = 1$, $J = 6$, e-symmetry levels of S_1 *trans* 3^4, *trans* 3^5, and *cis* $3^1 6^1$ states were studied.

A UV excitation beam was focused through a room temperature flowing gas cell, which was maintained at 1 Torr. A constant flow of acetylene (BOC, atomic absorption grade

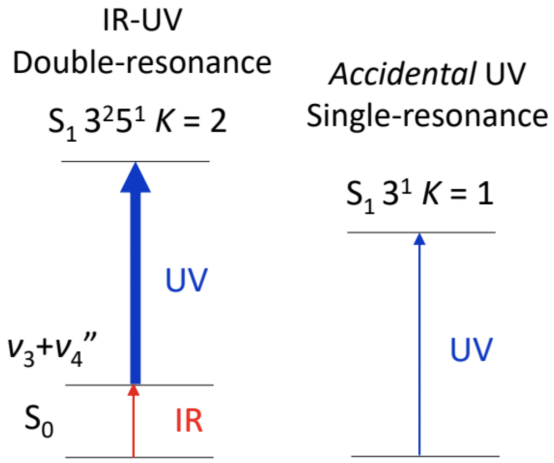

FIGURE 2.3: Level diagram of the IR-UV double-resonance transitions into S_1 $3^2 5^1$, $K' = 2$, and the single-resonance transitions into S_1 3^1, $K' = 1$ levels. Note that the UV photon is of the same energy in both schemes. The spectrum of this overlapped region is depicted in Figure 2.2. Reproduced from Reference 6 with the permission of the AIP.

2.6, 99.6% purity) was input to the cell, pumped by a rotary-vane pump (Edwards, E2M1.5). The acetylene flow rate was controlled by a needle valve.

The fluorescence was collected and imaged on the entrance slit of a monochromator (Spex 750 M, 3/4 meter) by a two-lens system ($f/6$). The monochromator is equipped with a 2400 grooves/mm grating blazed at 400 nm. In all experiments using the monochromator, the first order dispersed light is used. The entrance and exit slits of the monochromator were fixed at 1 mm, which corresponds to approximately 0.4 nm spectral resolution at 600 nm. The grating was scanned during the experiment, the dispersed fluorescence at each step collected by a photomultiplier tube (Hamamatsu, R928). The output signal from the PMT is monitored on a digital oscilloscope (LeCroy 9310) and the data transferred to a computer for storage and processing. The fluorescence time trace at each grating position was integrated to form the DF spectrum. The monochromator was calibrated by an iron-neon hollow cathode lamp (Starna Cells) to an accuracy of ± 0.02 nm. A 400 nm longpass filter (Thorlabs) was placed at the entrance slit of the monochromator to prevent the UV LIF fluorescence (in second-order from the grating) from interfering with the first-order PFAS fluorescence. The UV beam was produced using the output of a dye laser (Sirah, Cobra-Stretch), pumped by the third harmonic of a Q-switched, injection seeded Nd:YAG laser (Spectra Physics, PRO-270, ~100 mJ/pulse). The dye laser output was frequency doubled in a β-barium borate crystal (BBO) to produce the UV radiation with pulse energy of approximately 200 μJ.

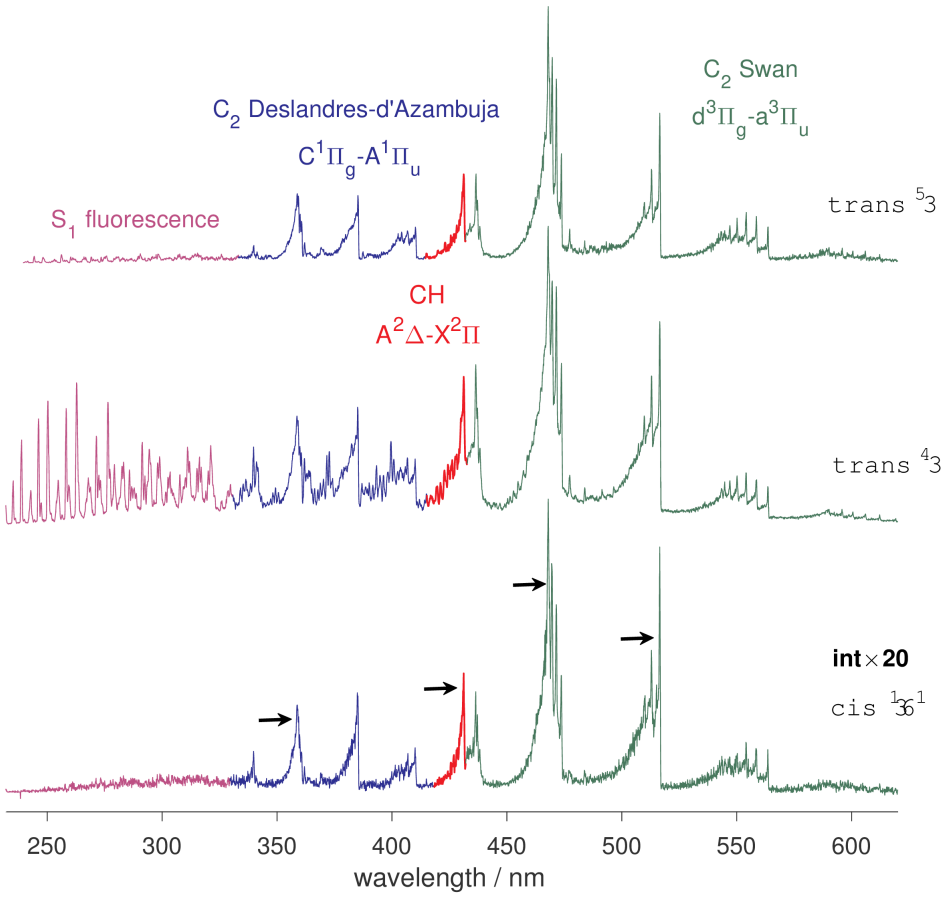

FIGURE 2.4: Dispersed fluorescence spectra of photodissociation products from the $K' = 1$, $J' = 6$, e-symmetry levels of S_1 *trans* 3^5 (top trace), 3^4 (middle trace), and *cis* $3^1 6^1$ (bottom trace, intensity pictured is multiplied by a factor of twenty) vibrational bands. The signal intensities are scaled to account for the wavelength-dependent sensitivity of the PMT used in the experiment. In the supersonic jet experiment (not pictured here), four different bandpass filters are used to approximate integrating a portion of the dispersed fluorescence at a particular wavelength range. The arrows in the bottom panel point to four peaks that correspond to the wavelengths of the filters chosen, which are centered at 360 nm, 430 nm, 470 nm, and 514.5 nm. Reproduced from Reference 7, with the permission of Elsevier.

The photofragment fluorescence was also studied under cold molecular beam conditions. The $K = 1$, $J = 2$, e-symmetry levels of the *trans* 3^4 and *cis* $3^1 6^1$ vibrational states were studied. Guided by results from the DF experiments, 4 different bandpass filters (FWHM=10 nm) (Thorlabs) were used in order to isolate particular portions of the DF spectrum. The filters allow observations near 360, 430, 470, and 514 nm. A 400 nm longpass filter was also used to collect all fluorescence with $\lambda > 400$ nm. Acetylene LIF signals were also collected, through a UG-5 filter. The experimental apparatus is identical to that used for the PFAS experiments described previously, using the Lambda-Physik FL3002E dye laser to produce the UV radiation.

The results of all of these types of experiments are relevant in understanding the work presented in this thesis, and parts of the analysis of each experiment will be included in the following sections.

2.3 Results

2.3.1 PFAS Spectroscopy Results

The IR-UV double-resonance spectra provide valuable information about certain S_1 vibrational levels. The selection rules and important resonances of the $\tilde{A}$-$\tilde{X}$ transition of acetylene create a situation where four separate experiments are required to have access to a sufficient set of rovibrational states of the S_1 surface to extract assignments. Several values of K' need to be observed, meaning lower states with different values of vibrational angular momentum must be utilized. Linear and *trans*-bent acetylene both possess *gerade/ungerade* symmetry, so experiments with access to both these manifolds are also required. Double-resonance experiments such as this allow access to vibrationally ungerade states with $K' = 0, 2$.

The PFAS experiments yield high resolution spectra of these levels in the 46,700-47,300 cm^{-1} region, which is 600-1200 cm^{-1} above the dissociation limit. Some of these states are much more easily observed in PFAS spectra than in traditional LIF spectra. Figure 2.2 shows a comparison for the $1^1 2^1 B^1$ band (B^1 notation is used here because the vibrational modes ν_4 and ν_6 are very thoroughly mixed, so levels with $v_4 + v_6 = i$ are labelled B^i). Many lines are much more prominent in the PFAS spectrum, and in fact nearly the entire Q-branch is unobservably weak in the LIF spectrum, but clearly visible up to $Q(6)$ via PFAS.

In these experiments, PFAS signals are also detected below the dissociation threshold. In the vicinity of the energy of the UV beam, there are both double resonance transitions originating in the $\nu_3'' + \nu_4''$ level and single resonance transitions originating from the ground vibrational state of the S_0 surface. Level diagrams for both the double- and single-resonance type transitions are shown in Figure 2.3. In some cases, single-resonance and double-resonance transitions occur in the same spectral region, as is shown in part (b) of Figure 2.2. In the absence of predissociation, Franck-Condon arguments predict

that the double-resonance excitation pictured in the figure should be approximately an order of magnitude stronger than the single-resonance transitions [68, 69]. The PFAS spectrum reflects this prediction, though the intensity ratio is not quite as large as calculated - though due to experimental limitations, the actual ratio of intensities could be higher than pictured (this particular line saturated the oscilliscope). However, the LIF spectrum has the relative intensities reversed from the expected result. This suggests that PFAS signals are not strongly affected by the predissociation that reduces the intensity of acetylene LIF spectra in this energy region. For our experimental conditions, it would seem that the rate of S_1 photodissociation is faster than the predissociation rate, which is estimated to be approximately $\frac{1}{10}$ ns^{-1} based on time-delayed H-atom REMPI experiments [51]. The possibility that levels exist where photodissociation by the second photon is slower than predissociation, and therefore PFAS is ineffective, cannot be discounted, but no evidence for the existence of such states has yet been observed. PFAS is currently our preferred detection scheme for predissociated levels of acetylene, due to the closer correspondence with relative intensity predictions than LIF and the ease of implementation compared to multi-laser H-atom fluorescence experiments of H-atom REMPI experiments.

2.3.2 Photofragment Fluorescence Studies Results

The DF spectra of acetylene photodissociation products from S_1 *trans* 3^4, *trans* 3^5, and *cis* 3^16^1 levels are shown in Figure 2.4. Fluorescence from 4 distinct sources is seen, and are color coded in the figure. The bulk of the emission is centered at 470 nm, and can be assigned to the C_2 Swan-band ($d^3\Pi_g - a^3\Pi_u$). The next strongest feature also results from excited C_2, the Deslandres-d'Azambuja band ($C^1\Pi_g - A^1\Pi_u$), centered around 380 nm. There are two additional features visible, a weak band attributed to CH $A^2\Delta - X^2\Pi$, at approximately 430 nm, and finally, in some cases, there is S_1 LIF fluorescence visible in the UV. The S_1 *trans* 3^4 states are not significantly predissociated, and long-lived fluorescence signals (∼100 ns) are easily detected. The *trans* 3^5 states, however, are strongly predissociated, and only weak LIF fluorescence from this band, with quite short lifetime (∼10 ns) is observed. No LIF signals from the *cis* 3^16^1 states are observed.

The absence of LIF fluorescence from the *cis* $3^1 6^1$ states is likely because the radiative lifetime of these states is long compared to the collisional lifetime in the cell, so the majority of the energy is collisionally quenched before fluorescence occurs. In collision-free conditions, the previously discussed *trans* 3^4 vibrational band has a lifetime of approximately 250 ns. In the flow cell used in the DF experiments, however, the lifetime is closer to 100 ns, leading us to conclude that molecules in the cell have collision-limited lifetimes of ∼100 ns. On top of this, the *trans* conformer of acetylene has no permanent dipole moment, but the *cis*-bent geometry does (calculated to be 2.5 D, communicated to us by Joshua Baraban in a private communication), and because of this large permanent dipole moment is likely to be even more rapidly quenched by collisions. The measured lifetimes of both C_2 species are within 20% of published values [70–72], leading us to believe that C_2 is not significantly collisionally quenched. The CH fluorescence lifetimes are shortened from 500 ns [73] to 150 ns.

To gain a better understanding of the dissociation dynamics than the somewhat inconsistent collisional quenching from the flow-cell DF experiments can provide, these were augmented by experiments in a collision-free environment. Experiments were performed to highlight each of the different photofragment species, i.e. the two bands from C_2 and the band from CH. In these spectra, there is an obvious very long lifetime ($> 3\mu s$) signal in the fluorescence time traces from the *trans* 3^4 and *cis* $3^1 6^1$ levels. Similar signals were also observed in the ungerade vibrational levels probed via double resonance. This signal from a long-lived excited state is not present in the flow cell experiments, likely again due to collisional quenching. In previous VUV photodissociation studies of acetylene [59, 60, 67, 74–79], a similar signal was attributed to fluorescence from excited C_2H fragments, but the electronic assignment for the observed omission is not conclusively established.

To understand the photodissociation process, the relative intensities of the fluorescence from each photofragment species must be determined. The fluorescence time traces of the experiments, performed via the S_1 *trans* 3^4 and *cis* $3^1 6^1$ levels and with bandpass filters chosen to isolate the primary sources of fluorescence, are fit according to

$$\begin{aligned} I(t_{fit}) &= \left[\int_{-\infty}^{t_{fit}} e^{\frac{(t-b)^2}{2c^2}} dt\right] \sum_s A_s e^{\frac{-t_{fit}}{\tau_s}} \\ &= c\sqrt{\frac{\pi}{2}}\left[1 - \mathrm{erf}\left(\frac{b - t_{fit}}{c\sqrt{2}}\right)\right] \sum_s A_s e^{\frac{-t_{fit}}{\tau_s}}, \end{aligned} \tag{2.1}$$

where the sum is over all the excited molecular species responsible for fluorescence, assuming that each species has a single characteristic decay time τ_s. The fluorescence intensity of each species is denoted A_s. The integral term is included to capture the fast turn-on of the signal due to the ns dye laser pulse. The value of this integral is given in the second line, where erf() denotes the error function. This assumes that the laser pulse has a Gaussian profile, centered at $t = b$ with a FWHM controlled by c, FWHM $= 2\sqrt{2\ln 2} \times c \approx 2.36c$. For the long-lived species, fitting the portion of the decay that is temporally overlapped with, and therefore obscured by, the dye laser pulse is unimportant, but for shorter lived species ($\tau \leq 30$ ns), the fraction of the signal that is obscured by the laser pulse is significant.

The signals from each of the four frequency ranges, selected by the four bandpass filters, were fit according to Equation 2.1. The parameter c, which determines the temporal width of the Gaussian laser pulse, is fixed. The parameter b, which is related to the time at which the center of the laser pulse occurs, is allowed to float in the fit to account for timing jitter in the experiment. The time traces are fit using only the time constants for the species expected to be present in the frequency window queried (selected by the bandpass filter). At 514.5 nm, the C_2 Swan band and C_2H emissions are accounted for. At 470 nm, the S_1 LIF fluorescence (the lifetime of which can be determined using a filter that blocks visible light, which in this case was a UG-5 filter) must be accounted for, along with Swan band and C_2H emission. At 360 nm, the ~30 ns decay from the C_2 Deslandres d'Azambuja band is present, and the C_2H signal is absent. At 430 nm, the C_2 Deslandres d'Azambuja, C_2H, and S_1 fluorescence signals from the prepared *trans* 3^4 and *cis* 3^16^1 states are visible, but the CH A-X emission observed in the flow cell is absent in the collision-free tests, indicating that it may be the result of a collisionaly-induced reaction pathway.

The fluorescence time traces and the fit results are shown in Figure 2.5 for each of the four band-pass filters, applied to fluorescence produced by both of the chosen vibrational bands, the S_1 *trans* 3^4 and *cis* 3^16^1 bands. The parameter c is found to be 5.38 ns, coresponding to a Gaussian pulse FWHM of 12.6 ns. The small discrepancy between the measured pulse FWHM and the expected value for a dye laser pumped by a Q-switched injection-seeded Nd:YAG laser (~6 ns) can most likely be attributed to a combination of the averaging of the signal on top of small time jitter (the standard deviation of the parameter b which accounts for time jitter is ~2 ns) and distortions due to the actual

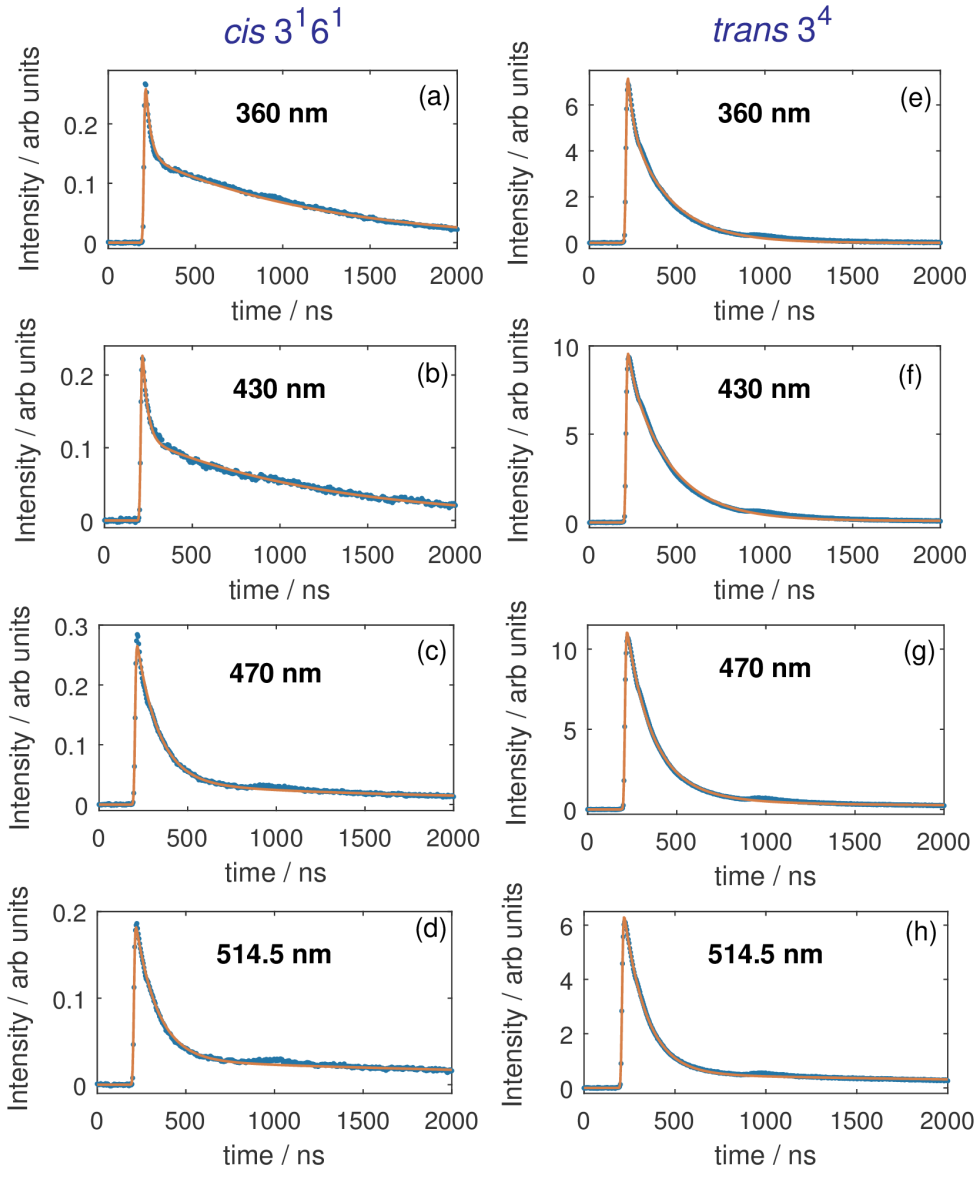

FIGURE 2.5: The fluorescence time traces of the collision-free supersonic jet experiments in the four sampled wavelength regions (360 nm, 430 nm, 470 nm, and 514.5 nm). The filters used to obtain these spectra have approximate FWHM of 10 nm. The time traces on the left result from dissociation via the S_1 *cis* $3^1 6^1$ level, and the traces on the right via the S_1 *trans* 3^4 level. The experimental data are the blue dots, and the time trace fits are in red. The bump in the time trace late in the tail (∼1000 ns) is likely a result of secondary ionization of trace He gas in the PMT. Signals near these bumps ($t = 1000 \pm 200\ ns$) are excluded from the fit. All fits are essentially a sum of exponential decays with different decay times. Each decay rate is indicative of a single fluorescent molecule, and the ratios of the coefficients of the fit exponentials are related to the ratios of excited molecules formed in the experiment, and carry information about the photodissociation pathway. Reproduced from Reference 7, with permission from Elsevier.

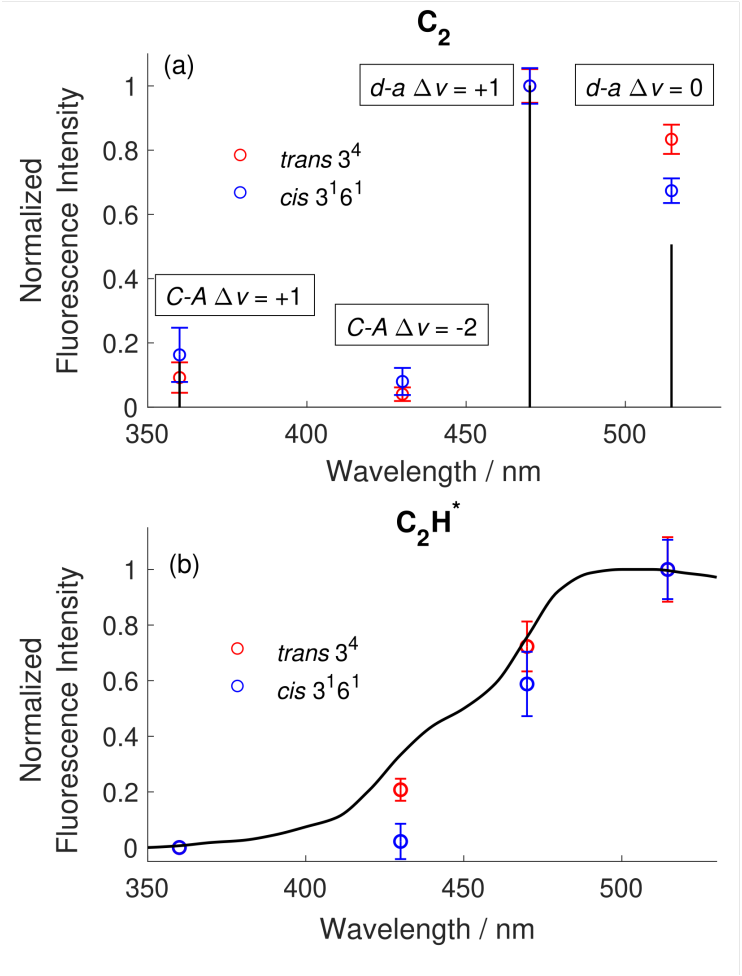

FIGURE 2.6: Fluorescence intensities of (a) C_2 (scaled so the intensity at 470 nm is one) and (b) C_2H^* (similarly normalized to the intensity at 514.5 nm) in the four chosen wavelength regions. In both parts of this figure, the red and blue icons indicate the measured fluorescence intensity collected via the S_1 *trans* 3^4 and *cis* 3^16^1 levels, respectively, with 2σ uncertainties indicated by the error bars. This data was taken under supersonic jet conditions. The black vertical lines and black trace indicate fluorescence collected in a DF experiment, the details of which are explained in the text. The DF signals pictured in panel (a) are scaled by the transmissions of the four bandpass filters utilized in the experiment, as specified by Thor Labs. Reproduced from Reference 7, with permission from Elsevier.

shape of the laser pulse being non-Gaussian. The relative intensities of the fluorescence from the 3 species can be determined in each of the time traces, accounting for the wavelength dependent variation of the quantum yield of the photomultiplier used for detection (Hamamatsu, R375).

Figure 2.6 shows the fluorescence intensities attributed to the various photofragmentation products observed via both intermediate vibrational levels. The black lines in the figure show either our integrated DF experimental intensities, or (in the case of Figure 2.6 b), DF experiments from other research groups [60]. The relatively good agreement

	Our Studies		Our Studies	Literature
trans 3^4	236(2) ns	C_2 $C^1\Pi_g$	29(2) ns	33(1) ns [70]
cis 3^16^1	1.037(16) μs	C_2 $d^3\Pi_g$	125(2) ns	103(6) ns [71, 72]
		C_2H	3.6(6) μs	3-6 μs [77]

TABLE 2.1: Observed lifetimes of the photofragments observed in collision-free studies of the photofragments of acetylene. The literature value for the C_2 C state is an average of the measured lifetimes of $v = 0-4$, and the literature value for the C_2 d state lifetime is an average of measured lifetimes of states with $v = 0-2$. The numbers in parentheses are the 2σ uncertainties in the last digits.

with the DF data for the two C_2 excitations and the C_2H fluorescence indicates that the DF experiments should yield meaningful information regarding the population distribution in C_2, and indicates that the long-lived signal we observe is indeed likely due to C_2H.

The fluorescence lifetimes measured in these experiments are collected in Table 2.1. A few things are worth noting about the values in this table. First, our measured lifetimes for the C_2 d state are quite different from previous studies (about a 20% difference). We believe this can be attributed to the relatively high temperatures of C_2 accessed by our experiment, with J as high as 30 and v as high as 4, with the measured lifetime depending on the lifetimes of all these accessed states. Other studies were performed with significantly cooler samples, particularly rotationally (mostly $J \leq 4$).

2.4 Discussion

Another not yet discussed advantage of PFAS is the large difference between the frequency of the excitation laser(s) and that of the fluorescence that constitutes the PFAS signal. In traditional LIF, the fluorescence and the excitation wavelengths are very similar, and selectively filtering out the scattered light of the excitation laser is nearly impossible. In PFAS, however, the signal is primarily in the visible region of the spectrum, ranging approximately from 400 to 800 nm, while the excitation is in the UV. Readily available longpass filters can be used to significantly reduce the scattered light that obscures the signal, which is a major deficiency in our LIF experiments. This, combined with the ability to isolate the signal via time-gating, makes PFAS a powerful and attractive tool for studies of S_1 acetylene.

2.4.1 Excited C_2H fragment formation

The PFAS signal exhibits a non-linear power dependence (power-index of 1.6, likely due to laser saturation effects). There are two possible pathways to the excited C_2H photofragments; either one photon excites acetylene to the S_1 state, then a second excites to a very high-lying acetylene level. This highly excited molecule then dissociates into excited C_2H and H. The second possible pathway is that the S_1 acetylene dissociates on its own due to predissociation into ground-state C_2H and H, which is then excited by another photon to an excited state. These possibilities are summarized in Equations 2.2 and 2.3.

$$C_2H_2(S_1) + h\nu \rightarrow C_2H_2^* \rightarrow C_2H^* + H \tag{2.2}$$

$$\begin{aligned} C_2H_2(S_1) &\rightarrow C_2H(\tilde{X}^2\Sigma_g^+) + H \\ C_2H(\tilde{X}) + h\nu &\rightarrow C_2H^* \end{aligned} \tag{2.3}$$

Given the evidence, the most likely path for the formation of the excited photofragments begins with the acetylene being excited to a particular rotational level of the S_1 state by the UV laser. The same laser then excites the S_1 molecule again to a highly energized state that quickly dissociates to excited C_2H. Such a fast dissociation to electronically excited C_2H is known to exist [80, 81]. The resulting C_2H fragment molecules are then excited by another photon, as described by Equation 2.2. One substantial reason for this conclusion is the dependence of the second pathway on the predissociation of S_1 acetylene, which in some of the states probed (*trans* 3^4, for example) does not occur.

Both $\tilde{X}$ state C_2H and excited C_2H, which we will now call C_2H^* to distinguish it from ground state C_2H, are long-lived species, and transitions into them are expected to act as transitions between eigenstates in a bound system; in particular there should be specific frequencies at which such transitions can occur. Unless the density of states in C_2H^* is high enough to appear as a continuum (our laser linewidth is roughly 0.04 cm^{-1}, so the density would need to be above 25 levels per cm^{-1} for this to be the case), we would not expect there to be a possibility for a second on-resonance transition at the same frequency as the $S_1 \leftarrow S_0$ transition. However, we see no evidence of this frequency coincidence effect, no unexpectedly missing lines, or transitions that deviate significantly from the expected intensity pattern. This is more evidence that the dominant dissociation pathway is that depicted in Equation 2.2.

It should be mentioned that there are limits to the energetic regions that can be effectively probed by PFAS techniques - at very high S_1 energies ($> 48,500\ cm^{-1}$), the predissociation rate becomes much faster, with lifetimes estimated based on linewidth studies [82] of around 10 ps. The levels studied in this work have lifetimes closer to 10 ns. In our experimental setup, with our laser fluence, the one-photon photodissociation pathway (Equation 2.2) is expected to be reasonably efficient for levels with predissociative lifetimes <1 ns.

2.4.2 Excited C_2 Formation

I have identified the most probable pathway that results in the formation of the fluorescing C_2H^* fragments, and will now discuss the formation of the excited C_2 fragments. As with the C_2H^* formation, there are two possible pathways for the formation of C_2, assuming that the predissociation products of S_1 are not important, as was assumed in the discussion of the formation of C_2H^*. These two processes are depicted as

$$C_2H_2(S_1) + h\nu \rightarrow C_2H_2^* \rightarrow C_2\left(C^1\Pi_g \text{ or } d^3\Pi_g\right) + H_2(X^1\Sigma_g), \tag{2.4}$$

$$\begin{aligned} C_2H_2(S_1) + h\nu &\rightarrow C_2H_2^* \rightarrow C_2H^{*\prime} + H \\ C_2H^{*\prime} + h\nu &\rightarrow C_2H^{**} \rightarrow C_2\left(C^1\Pi_g \text{ or } d^3\Pi_g\right) + H, \end{aligned} \tag{2.5}$$

in which C_2H_2*, C_2H*', and C_2H** are all electronically excited species the identites of which are not well known, and which have not yet been discussed here.

Equations 2.4 and 2.5 begin in the excited S_1 state, so one additional photon is required beyond the number of $h\nu$ symbols shown in the equations. The hydrogen elimination pathway, shown in equation 2.4 requires a total of two photons, and the sequential bond-breaking path shown in equations 2.5 requires three. Hydrogen molecule elimination can also be explained using energetic arguments as a three-photon process, but such a pathway involves a highly excited C_2H_2 species with a very short lifetime and would therefore not be expected to be efficient. I will therefore only consider the two pathways proposed above.

The acetylene S_1 state is a singlet, and the excited C_2H_2* state is also a singlet. This pathway is spin-allowed for the C_2 $C^1\Pi_g$ state, but not for the generation of the $d^3\Pi_g$ state. The sequential photodissociation path, however, is spin-allowed for both singlet

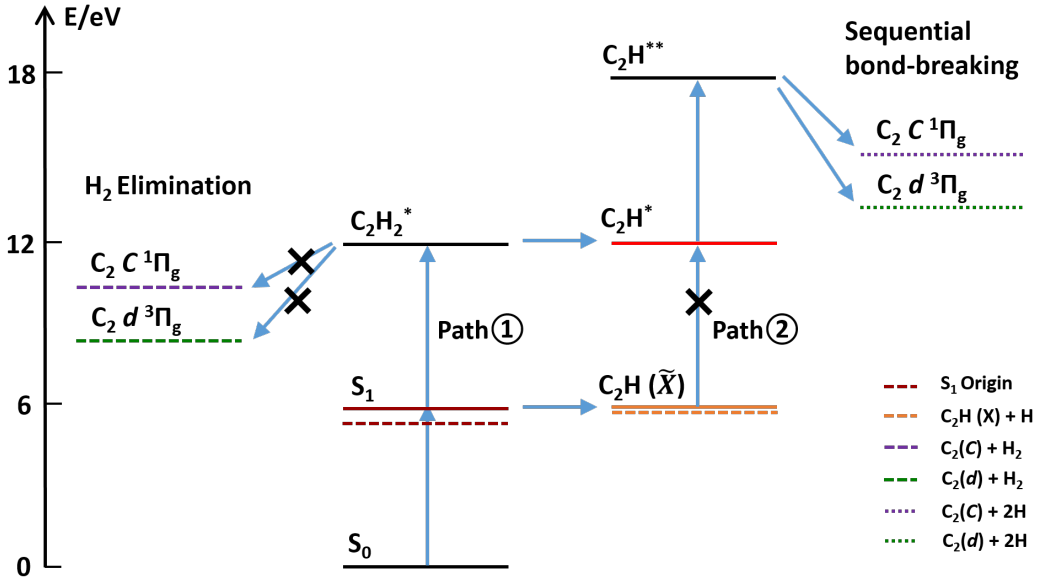

FIGURE 2.7: Mechanisms for one-color, multi-photon dissociation of acetylene. The blue vertical arrows represent the UV laser photon, which has energy ~5.85 eV. The populated S_1 level in the figure is assumed to be predissociated, as predissocated levels have access to more potential dissociation pathways. Hydrogen (molecular and atomic) levels are omitted for clarity. Reproduced from Reference 7, with permission from Elsevier.

and triplet excited C_2 states. In the H_2 elimination pathway, the transition state should have a *cis*-like geometry, which would bring the two H atoms close together to promote bond formation. If this is true, we can expect that the process would be more efficient from a *cis*-bent S_1 level than a *trans*-bent one, due to Franck-Condon overlap integrals. Since the elimination pathway can only lead to the C_2 C state, we would likely see the effect of this Franck-Condon overlap in the ratio between C- and d-state emission from *trans* and *cis* S_1 levels. However, we do not see significantly more C-state emission from the *trans* levels than we do from the *cis*. These arguments suggest that Equations 2.5 account for the majority of the production of both of the fluorescing C_2 species: the $C^1\Pi_g$ and $d^3\Pi_g$ states.

2.4.3 Further Discussion of the Photodissociation Process

The mechanisms for the PFAS photodissociation process that have been discussed in this chapter are summarized in Figure 2.7. The pathways that have been eliminated by our analysis are crossed out. I'll narrate this process for additional clarity. Acetylene molecules are pumped by UV excitation into a specific rotational state of the S_1

electronic state. The same laser beam contributes a second photon to the acetylene, bringing it to a highly excited ($\sim$ 90,000 cm^{-1}) state. The resulting C_2H_2* state rapidly dissociates to C_2H* + H. The C_2H* fragments are then excited by another laser photon of the same frequency to a higher electronic state, C_2H**, which dissociates into the C_2 $C^1\Pi_g$ and $d^3\Pi_g$ states. The C_2H* fragments have a long lifetime and fluoresce in the visible. The C_2 C state fluoresces in the near UV, and the d state in the green region. We estimate in our experiments the relative quantum yields of these three fluorescing species to be C_2H*:$C_2(d)$:$C_2(C)$ = >40 : 4 : 1. The total yield of both C_2 fragments changes by about a factor of two for the *trans* 3^4 vs. the *cis* 3^16^1 species. It's possible that the excited C_2H* fragments created via these two very different vibrational bands have significantly different rovibrational distributions in the excited state, which could could account for the slightly different observed C_2H* fluorescence, and may affect the dissociation into excited C_2.

We have little evidence to identify the C_2H_2* state located at $\sim$90,000 cm^{-1}. A few guiding principles can be proposed - one-photon transitions from both *trans* and *cis* S_1 acetylene must be possible. Based on the fluorescence yields, these transitions must have similar probabilities. Without further information from additional experiments or *ab initio* calculations, the identity of the C_2H_2* state cannot be determined, but any proposed assignment will need to fit these observations.

It's important to note that the PFAS process is not the same as that followed by the often-studied dissociation of acetylene at 193 nm via a ArF laser [73, 83–85]. In those experiments, the S_1 level (or group of levels) has a very short predissociative lifetime, and the fluorescence observed from excited C_2 and C_2H* fragments results from the predissociation of the initially populated S_1 level into C_2H, and then the photodissociation of this product by another 193 nm photon. This follows the proposed (and rejected, for PFAS) pathway depicted in Equation 2.3. In the PFAS pathway, two photons are used to reach an excited state of acetylene C_2H_2*. The PFAS technique is applicable to S_1 vibrational states that are not predissociated, e.g. *trans* 3^4, so, at least for such levels, the 193 nm photodissociation pathway is certainly not relevant.

Molecule	Transition	λ/nm	Detection	λ_{em}/nm
HCP	$\tilde{A}/\tilde{B} \leftarrow \tilde{X}$	240	CP $B \rightarrow X$	~350
CS_2	$\tilde{A} \leftarrow \tilde{X}$	216	CS $A \rightarrow X$	~260
SO_2	$\tilde{C} \leftarrow \tilde{X}$	219	SO $A/B \rightarrow X$	~240/260
NCO	$\tilde{A}/\tilde{B} \leftarrow \tilde{X}$	317	CN $B \rightarrow X$	~390
C_2H_2	$\tilde{A} \leftarrow \tilde{X}$	217	C_2H	>400
H_2CO	$\tilde{A} \leftarrow \tilde{X}$	330	HCO $A \rightarrow X$	>600
HNCO	$\tilde{A} \leftarrow \tilde{X}$	308	NCO $A \rightarrow X$	~440
C_2N_2	$\tilde{A} \leftarrow \tilde{X}$	212	CN $B \rightarrow X$	~390

TABLE 2.2: Some examples are given of molecules that may be suitable for the PFAS detection method. The CS_2 and HNCO $\tilde{A}$ state origins are above the predissociation limit - for these two molecules, the column λ indicates the location of the origin band. For the other six molecules, λ refers to the onset of predissociation, which is above the origin of the listed upper electronic state. λ_{em} is the approximate emission wavelength of the photofragment that makes up the PFAS signal.

2.4.4 PFAS Detection Schemes for Other Molecules

It is tempting to conclude that PFAS detection could be applicable to other C≡C triple-bonded systems, where the hydrogen atoms would be replaced by other molecular fragments. However, as pointed out by Professor Barney Ellison of the University of Colorado Boulder, the C_2 fluorescence detection pathway will likely not be generally applicable, due to competing dissociation pathways that are lower in energy than the production of C_2 [86]. For example, photofragmentation of CH_3CH_2CCH to produce C_2 will be unlikely, as the formation of $HCCCH_2$ and $HCCCHCH_3$ radicals is more energetically favorable, because the lone electron on these species is resonance stabilized.

While the C_2 PFAS detection technique may not work for all molecules with carbon-carbon triple bonds, and in fact may only be applicable to HCCH, similar schemes might be useful in studyies of other molecules. Several potential molecules and their most relevant properties are summarized in Table 2.2. Of the molecules listed, the $\tilde{A} - \tilde{X}$ transition of acetylene, which is described in this chapter, and HNCO have both been observed [52]. All of the schemes listed have properties in common with the acetylene transition described here, namely they are 1+1 photodissociation processes, and the second photon produces fluorescent photofragments from an electronically excited state of the listed molecule.

The PFAS scheme outlined here is different than Photofragment Fluorescence Excitation (PHOFEX) detection. In those experiments, photofragments are probed by an additional laser using LIF detection. PHOFEX detection has been widely used to study

predissociated molecular levels. Examples include the HCO $\tilde{A}$ state [87], H_2CO $\tilde{A}$ state [82], HNCO $\tilde{A}$ state [52, 88], C_2N_2 $\tilde{A}$ state [89], HCP $\tilde{A}$ and $\tilde{B}$ states [61], etc. PHOFEX is likely a more generally applicable detection method than PFAS, but PFAS does have important advantages over other schemes. For example, PFAS requires only a single laser, which significantly simplifies the setup and execution of experiments over PHOFEX detection. The probe laser of PHOFEX detection excites from few (usually one) rotational levels of the probed photofragment. PFAS detects fluorescence from many levels of the excited photofragments. If the dissociated species are produced hot, which is to say distributed over many vibrational and rotational states, the signal from the PHOFEX method could be significantly weaker than a similar dissociation observed by PFAS. On the other hand, PFAS generally involves more free←bound transitions than PHOFEX does, which are generally weaker than bound←bound transitions.

PHOFEX studies are only applicable to predissociated species. PFAS, however, can be applied to non-predissociated species, as well as to predissociated ones, as described here. PFAS efficiency is expected to decrease sharply when the predissociation lifetime is too short (a good metric would be to compare the lifetime to the temporal width of the laser pulse), though the studies of HCNO have detected $\tilde{A}$-state levels with lifetimes as short as 1 ps [88].

As discussed above, when considering the general applicability of C_2 PFAS emission to carbon-carbon triple-bonded systems, larger molecules (more than 4 atoms) will have competing pathways that will make prediction of the existence of fluorescent excited photofragments difficult. However, due to the simplicity in implementing a PFAS detection scheme, and the dependence of the characteristics of the signal on simple filter choices, PFAS is worth considering for larger molecules, especially ones with excited upper states with lifetimes $\geq$ 1 ps. Some possible examples include NCC_2H (cyanoacetylene), C_2HCHO (acrolein), 1,4-$C_4H_4N_2$ (pyrazine), 1,3-$C_4H_4N_2$ (pyrimidine), 1,4-$C_4H_4N_2$ (pyridazine), and C_6H_6 (benzene) [63].

2.5 Conclusion

A new experimental detection scheme, valid for both predissociated and non-predissociated levels of the first excited singlet state, the S_1 state, of acetylene was introduced. Photofragment fluorescence action spectroscopy (PFAS) provides high signal-to-noise ratio, is easy to implement, and can be used to detect states with short predissociation lifetimes - states that are difficult or impossible to study by LIF methods.

An analysis of the photofragments involved in the acetylene PFAS system was also presented. PFAS signal is dominated by fluorescence from the C_2 Swan and Deslandres d'Azambuja bands and from a longer-lived C_2H^* fluorescence band. The relative quantum yields from these three species is estimated to be C_2:$C_2(d)$:$C_2(C)$=>40 : 4 : 1. We determine that both of the electronic states of C_2 observed have high rotational and vibrational temperatures.

The possible mechanisms for photodissociation are discussed. The relative insensitivity of the C_2H fluorescence to the predissociation rate in the S_1 band led us to rule out any mechanism that depends on predissociation at the one-photon level. For the formation of C_2, H_2 elimination is spin-allowed for the C_2 C state, but not for the C_2 d state. We suggest that the excited C_2H^* is formed by the rapid dissociation of a doubly-excited $C_2H_2^*$ species, and that the C_2 excited fluorescent states are formed by the photodissociation of C_2H^*, not by concerted hydrogen elimination.

Chapter 3

Use of PFAS Spectroscopy in the High Frequency Region of Predissociative S_1 Acetylene ($\sim$47,000 cm^{-1})

The Photofragment Fluorescence Action Spectroscopy (PFAS) technique is used in two different experimental schemes to access predissociated rovibrational states on the excited singlet S_1 surface of acetylene. The new information available due to these experiments is outlined, with emphasis on information that leads to a greater understanding of the *cis-trans* isomerization dynamics. Further work required to complete this understanding, as well as further avenues to pursue additional topics of interest, are outlined.

3.1 Introduction

Acetylene has a unique set of properties that combine to make detailed study of it, in particular the ground S_0 and first excited S_1 electronic states, particularly fruitful. It's very simple to conceptualize some of the more basic reasons that C_2H_2 is a useful subject to study. As a four-atom molecule, it's the simplest system (in terms of number of nucleii) that can exhibit non-planar geometries and motions. Neither the ground state

nor the S_1 state are non-planar at their equilibrium geometries, but both exhibit non-planar vibrational motions, and the S_1 surface isomerization involves the analog of the ground state *cis* bend, which is heavily mixed with the torsional (out-of-plane) motion [5]. This vibration is thus vital in understanding the transition state and dynamics of this isomerization.

It's also immediately obvious (from previous chapters in this work, for instance) that the mechanics of the $S_1 \leftarrow S_0$ transition are unusual enough to merit investigation. The qualitative change in geometry between the two equilibrium structures induces interesting spectral patterns, and a thorough understanding of these patterns can yield new models that present particular phenomena as signposts for dynamics such as isomerization (our group, for instance, has studied frequency dip as a marker for isomerization in acetylene and HCN [15], and vibrational level staggering and staggering of the Coriolis-perturbed rotational C_p constant as markers for the double-well potential on the $\tilde{C}^1B_2$ surface of SO_2 [90]). The difference in geometry has another more subtle effect, that many vibrational states are accessible in an electronic transition between the two electronic states, because the Franck-Condon factors can't be assumed to be small for large differences in the vibrational coordinates v_i between the two states.

Additional interest in the acetylene system arises from dynamics within a single electronic state. Both the S_1 and S_0 surfaces of acetylene have multiple minima with distinct geometries [11, 13]. The S_0 surface has a deep well at the well-understood linear geometry, HCCH, and a shallow well at the vinylidene structure, CCH_2. Our group has long been pursuing an effort to understand the acetylene $\leftrightarrow$ vinlyidene isomerization [45]. Many of the most important advances made by our group can either be attributed to this goal, or contributed to it. The global minimum of the S_1 surface has a *trans*-bent geometry, but the surface also supports a *cis*-bent configuration [11]. In fact, calculations indicate that there is also a minimum on this surface at the vinylidene geometry, but we haven't seen any evidence of this [13]. We have, however, seen evidence of and even assigned transitions to rovibrational levels of the *cis*-bent S_1 state. Secure assignments require quite a lot of work, as our model currently only accounts for *trans* vibrational levels of the S_1 state, and levels that belong to the *cis* well can really only be assigned by recognizing levels that don't fit in the *trans* manifold, meaning essentially complete understanding of the *trans* levels is required.

A question worth considering is, if our group has done so much research already on these two electronic states of acetylene, what else can yet be learned here? Here some additional interesting properties of acetylene come in to play. Acetylene has high symmetry, both in a point-group sense and in the more rigorous CNPI framework. This introduces rather restrictive selection rules and propensity rules (compared to some molecules with less symmetry), so it can require some creativity to access all the rovibrational levels of the S_1 surface. In fact, 4 separate sets of experiments need to be performed in order to have a complete picture of the *trans* well of the upper surface.

The resonances on the S_1 surface, in particular the strong Darling-Dennison resonance between ν_4 and ν_6 and strong Coriolis coupling, combine with the result that a full understanding of any particular vibrational band requires observation of $K = 0, 1, 2$ at least. This is because the Coriolis and Darling-Dennison effects perturb the same levels, but have different dependence on K [5]. For an asymmetric top, such as *trans* acetylene, the general rotational Hamiltonian can be simplified to

$$H_{rot} = A\left(J_a - G_a\right)^2 + B\left(J_b - G_b\right)^2 + C\left(J_c - G_c\right)^2, \tag{3.1}$$

where A, B, and C are the normal rotational constants, J is the total angular momentum, G is the vibrational angular momentum, and a, b, and c are the inertial axes with which the rotational constants A, B, and C are associated [91]. Multiplying the squares out, we find the normal rigid rotator Hamiltonian terms (the terms in J_i^2), terms involving the squares of the vibrational angular momenta, and the three first-order Coriolis terms. These terms take the form

$$H_{Cor} = -2AJ_aG_a - 2BJ_bG_b - 2CJ_cG_c. \tag{3.2}$$

The angular momentum components are defined as

$$G_\alpha = \mathbf{Q}^{tr}\boldsymbol{\zeta}^\alpha \boldsymbol{P}, \tag{3.3}$$

where $\mathbf{Q}$ and $\mathbf{P}$ are the vectors of vibrational normal coordinates and their conjugate momenta [92, 93]. $\boldsymbol{\zeta}$ is a skew-symmetric matrix of Coriolis coupling constants. For S_1 acetylene, we are only concerned with the Coriolis couplings between ν_4 and ν_6 and recognize that there is no c-axis Coriolis coupling, so we reject terms in G_c. Multiplying

this matrix equation out, we find the only important terms are

$$G_\alpha = Q_4 \zeta_{46}^\alpha P_6 - Q_6 \zeta_{46}^\alpha P_4, \tag{3.4}$$

where α can only be a or b. The matrix elements of the vibrational angular momenta G_α then follow the matrix elements of the vibrational normal coordinates and momenta Q and P [91]. Each term in G_α has two components, one that raises v_4 and lowers v_6, and one that does the opposite. The matrix elements for the G_α are

$$\begin{aligned} \langle v_4+1, v_6 | G_\alpha | v_4, v_6+1 \rangle &= -i\zeta_{46}^\alpha \hbar\Omega \left[(v_4+1)(v_6+1)\right]^{\frac{1}{2}} \\ \langle v_4, v_6+1 | G_\alpha | v_4+1, v_6 \rangle &= i\zeta_{46}^\alpha \hbar\Omega \left[(v_4+1)(v_6+1)\right]^{\frac{1}{2}}, \end{aligned} \tag{3.5}$$

where Ω is the Mills' abbreviation [94],

$$\Omega = \left(\frac{1}{2}\right)\left[\left(\frac{\nu_4}{\nu_6}\right)^{\frac{1}{2}} + \left(\frac{\nu_6}{\nu_4}\right)^{\frac{1}{2}}\right]. \tag{3.6}$$

The J_α also contribute to the matrix elements of the Hamiltonian. As a near-prolate asymmetric top, the convenient molecule-fixed axis to choose as the quantized axis is a. The terms in J_a, then, are diagonal in the rotational quantum numbers. The two matrix elements of G_b each are associated with J_b, which operator does not commute with the Hamiltonian. However, we can take parallels from the normal x, y, and z analogs to define raising and lowering operators

$$\begin{aligned} J_+^a &= J_b + iJ_c \\ J_-^a &= J_b - iJ_c \end{aligned} \tag{3.7}$$

where $J_\pm^a$ is the operator that raises or lowers the projection of J along the a axis by one. We rearrange to find

$$J_b = \frac{\left(J_+^a + J_-^a\right)}{2}. \tag{3.8}$$

We recall that for general angular momentum raising and lowering operators

$$J_\pm \left|j, m\right\rangle = \hbar\sqrt{j(j+1) - m(m\pm 1)}\left|j, m\pm 1\right\rangle, \tag{3.9}$$

and can easily find the first-order Coriolis matrix elements

$$\langle v_4+1, v_6, J, k|H_{Cor}|v_4, v_6+1, J, k\rangle = 2iA\zeta_{46}^a \Omega k \left[(v_4+1)\,(v_6+1)\right]^{\frac{1}{2}}, \tag{3.10}$$

$$\begin{aligned}\langle v_4+1, v_6, J, k\pm 1 H_{Cor} v_4, v_6+1, J, k \\ = iB\zeta_{46}^b \Omega \left[J(J+1)-k(k\pm 1)\right]^{\frac{1}{2}} \left[(v_4+1)(v_6+1)\right]^{\frac{1}{2}},\end{aligned} \tag{3.11}$$

$$\langle v_4, v_6+1, J, k|H_{Cor}|v_4+1, v_6, J, k\rangle = -2iA\zeta_{46} Z^a \Omega k \left[(v_4+1)(v_6+1)\right]^{\frac{1}{2}}, \tag{3.12}$$

and

$$\begin{aligned}\langle v_4, v_6+1, J, k\pm 1 H_{Cor} v_4+1, v_6, J, k \\ = -iB\zeta_{46}^b \Omega \left[J(J+1)-k(k\pm 1)\right]^{\frac{1}{2}} \left[(v_4+1)(v_6+1)\right]^{\frac{1}{2}}.\end{aligned} \tag{3.13}$$

These matrix elements all depend upon k linearly, in the case of the equations involving the a axis, or nearly depend on k linearly, for the equations involving the b axis.

The Darling-Dennison resonance involves the same two vibrations, ν_4 and ν_6. Lehmann has examined such resonances in some detail [95], and give the matrix element as

$$\langle n_a+2, n_b-2|H_{DD}|n_a n_b\rangle = \frac{1}{4} K_{aabb} \left[(n_a+1)(n_a+2)n_b(n_b-1)\right]^{\frac{1}{2}}, \tag{3.14}$$

where

$$\begin{aligned}K_{aabb} =& \frac{1}{4}\phi_{aabb} + \sum_\alpha -B_\alpha (\zeta_{ab}^\alpha)^2 \frac{(\omega_a+\omega_b)^2}{\omega_a\omega_b} \\ &+ \frac{1}{8}\sum_k \phi_{kaa}\phi_{kbb}\omega_k \left(\frac{1}{4\omega_a^2-\omega_k^2} + \frac{1}{4\omega_b^2-\omega_k^2}\right) \\ &- \frac{1}{2}\sum_k \phi_{kab}^2 \frac{\omega k}{\omega_k^2-(\omega_a-\omega_b)^2}.\end{aligned} \tag{3.15}$$

The Darling-Dennison resonance, then, is independent of the quantum number K. The Coriolis coupling does not perturb levels with $K = 0$, but the Darling-Dennison resonance does, so in order to obtain the most accurate deperturbations, $K = 0$ data is required for all vibrational levels, and two more K stacks are also required to separate the influence of Coriolis and Darling-Dennison resonances, preferably $K = 1, 2$.

There is a strong propensity for acetylene transitions to have $K - l = \pm 1$, as the transition dipole lies (nearly) along the c-axis. Transitions from the ground vibrational

level of the ground electronic state, or any vibrational level that lacks vibrational angular momentum, can only (in the absence of axis switching and Coriolis coupling) connect to levels with $K = 1$. In order to reach all the required K-stacks, experiments that do not begin at the vibrational ground state must be performed.

There is an additional complication in accessing the necessary levels of S_1 acetylene to fully understand the dynamics. For clarity to the reader, we'll use the point-group inversion operation i to explain this complication, but the CNPI inversion operation E* is also applicable. The electric dipole operator is of *ungerade* molecular inversion symmetry. It can only connect states of opposite symmetry, i.e. $g \leftrightarrow u$, $g \nleftrightarrow g$, $u \nleftrightarrow u$. The *trans*-bent S_1 state is of ungerade symmetry, and the linear electronic ground S_0 state is of gerade symmetry. The ground vibrational level is of course also of gerade symmetry. One photon can only connect the ground vibrational level of the ground electronic state to levels of ungerade total symmetry, or levels on the S_1 surface with gerade vibrational symmetry. Experiments that transition to the S_1 state from a state with ungerade vibrational symmetry are required to observe ungerade vibrations upstairs.

Not only are there these complications, with four separate experiments required for every frequency region, but work on S_1 acetylene has been complicated in recent years by predissociation. The predissociation onset in S_1 acetylene is $\sim$1000 cm^{-1} below the bottom of the *cis* well, which is to say $\sim$1000 cm^{-1} below the most interesting dynamics in that electronic state. As high as the energy of the transition state, predissociation is fast enough that traditional detection methods such as Laser Induced Fluorescence (LIF) are untenable. This chapter will delve into my use of PFAS to bypass the short lifetime limitations of states in this energetic region, and my attempt to perform more of the four required experimental evidences to fully understand bands in this regime.

3.2 Experimental Details

Two types of PFAS-detected experiments were performed. The experimental setup shares many features in common with the apparatus used in PFAS experiments on a supersonic jet, described in this work in Chapter 2. This section will summarize the

apparatus and describe in more detail the components unique to the work described in this chapter.

The PFAS experiments were performed in a vacuum chamber, fitted with a diffusion pump (Varian, VHS-6), which achieves an ultimate pressure of 10^{-6} torr. A molecular beam was expanded through a pulsed valve into the vacuum chamber. The nozzle is unusual, and is designed to assist in collecting spectra from hot vibrational levels of the ground electronic state.

The nozzle used in these experiments is based on a nozzle designed by the Ellison research group [96], and is termed a hyperthermal pyrolysis microreactor nozzle. The hyperthermal nozzle consists of a pulsed solenoid valve (General Valve, Series 9, orifice diameter = 1.0 mm), fitted with a SiC tube (1 mm inner-diameter, 2 mm outer-diameter, ~4 cm long). The SiC tube is heated by passing current through it, up to temperatures as high as 1800 K. A constant current source, rather than a constant voltage source, is required as the resistance of SiC has anomalous temperature dependence. The portion of the SiC tube that is heated is separated from the solenoid valve by a baffle, which is water-cooled to protect the valve. Neat acetylene with 1 atm backing pressure is expanded through the pyolysis nozzle. Under gas load, the pressure in the chamber increases to $\sim 5 \times 10^{-5}$ torr.

A single laser beam was used in these PFAS experiments. The laser radiation (Coumarin 440 and Stilbene 420 dyes, 210-220 nm after frequency-doubling) is supplied by a tunable dye laser (dual-grating Sirah Cobra-Stretch), pumped by the third harmonic of a Q-switched, injection-seeded Nd:YAG laser (Spectra Physics, PRO-270), operating at 20 Hz. The output of the dye laser (0.04 cm^{-1} spectral width) is frequency-doubled in a β-barium borate (BBO) crystal, and a small portion of the fundamental output is directed through a cell of $^{130}Te_2$ vapor for calibration. The UV pulse energy is approximately 50 μJ/pulse.

The UV laser intersects the molecular beam approximately 1.5 cm downstream of the exit from the heated SiC tube, with the beam and laser at a right angle. Fluorescence signals are collected by f/1.2 optics and directed to a photomultiplier (PMT) (Hamamatsu, R375), at a right angle to both the UV laser beam and the propagation direction of the moleuclar beam. The fluorescence passes through a 400 nm longpass filter (Thorlabs, FGL400S) before being collected by the PMT to suppress noise from unwanted scattered

laser light. As another measure to prevent excess scattered laser light, the UV laser enters and exits the chamber via Brewster windows, installed at the end of two one-foot-long arms, each of which is equipped with two iris baffles (Thorlabs, SM1 components). The PMT output is sent to a 20 dB amplifier (Femto DHPVA-200), and then monitored on an oscilloscope (LeCroy, 9360). The signal is then transferred to a computer for processing and storage.

Two separate types of experiments were performed, which were designed to observe different states on the S_1 potential energy surface. One was performed with the pyrolysis nozzle off (no current passed through the SiC tube), and was used to target states that have $K = 1$, in *gerade* vibrations. The second set of experiments are performed with the pyrolysis nozzle heated. In these experiments, observation of hot bands originating from S_1 ν_4'' levels into *gerade* vibrational levels on the S_1 surface with $K = 0, 2$ is optimized. The temperature of the nozzle was chosen to maximize the intensity of the signal from the relevant hot bands (the temperature of the nozzle can be chosen to select for several different lower-state vibrational levels [**?**]), and based on estimates of the blackbody radiation emitted by the SiC tube, was ∼500-550 °C.

3.3 Results

Extensive spectra were taken, spanning a very large energy region, in order to have the best chance possible of locating and resolving transitions that are unobservably weak in LIF. Figures 3.1 and 3.2 show the PFAS spectra recorded with the pyrolysis nozzle cold and heated, respectively. The X axes are in wavenumbers, and the Y axes are arbitrary.

The primary purpose of recording this data was, of course, the search for previously unobserved bands. The experimental setup used in the PFAS experiments has somewhat higher rotational temperatures than previous LIF experiments, likely due to less efficient cooling after expansion from the SiC tube. The cooling experienced by a gas in a supersonic expansion depends upon the pressure on both sides of the nozzle the gas is expanded through, as

$$\frac{T_1}{T_0} = \left(\frac{p_1}{p_0}\right)^{(\gamma-1)/\gamma}, \tag{3.16}$$

where T_1 and T_0 are the final and initial temperatures of the gas, p is the pressure of the gas, and γ is the ratio of heat capacities C_p/C_V [97]. In the hot nozzle set up, the seal

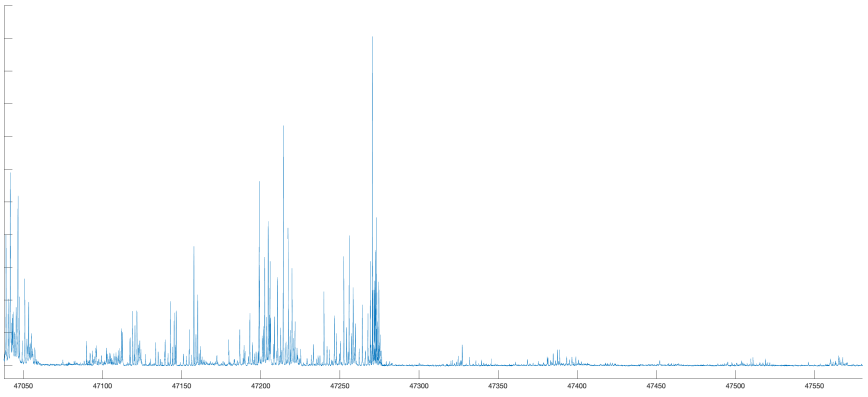

FIGURE 3.1: PFAS spectrum of the $\tilde{A} \leftarrow \tilde{X}$ transition of acetylene. The large features are dominated by bands that have very good Franck-Condon overlap with the ground state, such as transitions to $1^1 3^2$ (two quanta in the *trans*-bend, or "straightening" motion) or 3^5 (five quanta in the straightening motion) vibrational states. These transitions are obvious in LIF, and 5^3 was positively assigned decades ago [8]. More interesting for our purposes are transitions that don't have much intensity, the laser induced fluorescent signal of which would be buried under scattered light from the excitation laser pulse.

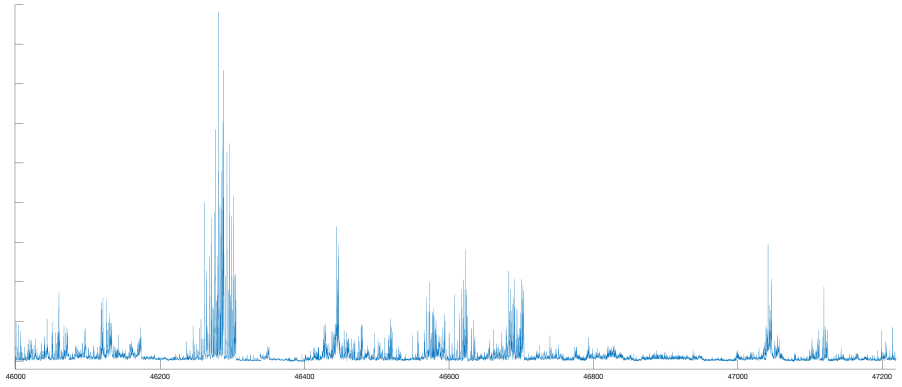

FIGURE 3.2: PFAS spectrum of the $\tilde{A} \leftarrow \tilde{X}$ transition of acetylene, taken with a heated pyrolysis nozzle. This data was taken over a somewhat different energy region than the cold data, in order to see regions of overlapping photon energy and regions of overlapping term energy between states excited from ground vibrational states of the $\tilde{X}$ electronic state and states excited from vibrationally hot levels, with (usually one quantum) energy in ν_4.

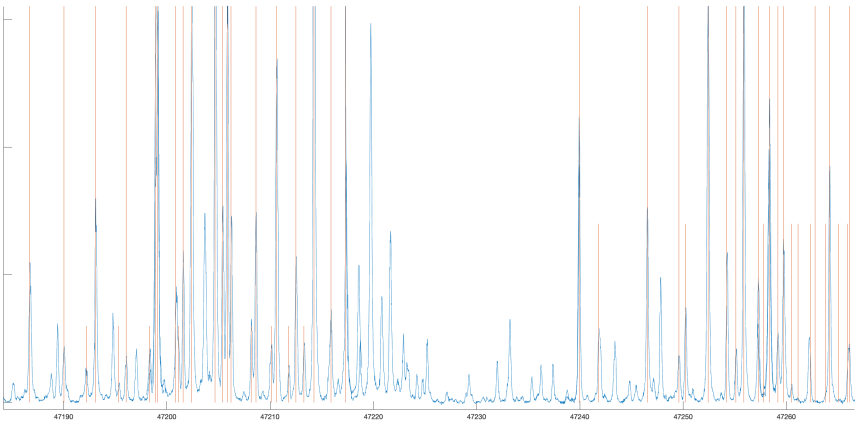

FIGURE 3.3: A particularly striking example of previously unobserved lines being quite clear in the PFAS spectrum. The blue trace is the PFAS spectrum, taken in the cold nozzle experiments, and the orange lines are the locations of all known one-photon transitions in this energy region. There are of course many new lines which can be simply assigned to high-J rotational lines of previously observed bands, but many of these signals, particularly in the region around 47,230 cm^{-1}, seem to belong to new vibrational bands.

between the general valve faceplate and the SiC tube is not perfect, and pressure ratio p_1/p_0 is likely larger in experiments that utilize this nozzle apparatus. This increased temperature leads to many lines that our previous LIF experiments have not shown, but these high-J lines do not really impart much more information about the nature of the S_1 surface and can be mostly ignored. After assigning and removing these lines from consideration, there remain several previously unseen transitions that merit further investigation.

The experiments performed with the cold nozzle are intended to capture *gerade* vibrational levels of the (*ungerade*) S_1 surface, with angular momentum projection quantum number $K = 1$, in particular bands with too low fluorescence quantum yield (due to dissociation) to be observed via LIF. Accompanying these experiments, the data gathered with the nozzle heated are intended to enhance the signal from vibrationally hot lower-state molecules, by increasing the vibrational temperature of the acetylene gas and therefore the number of molecules in excited vibrational states. In particular, the most likely-to-be observed hot bands have lower states with energy in the *trans*-bend, ν_4. The trans bend of the lower S_0 electronic state is a doubly degenerate mode of Π_g symmetry. Excitation in ν_4 contriubtes both vibrational energy and angular momentum about the molecular a axis to the molecule. In the case of the lowest (and therefore

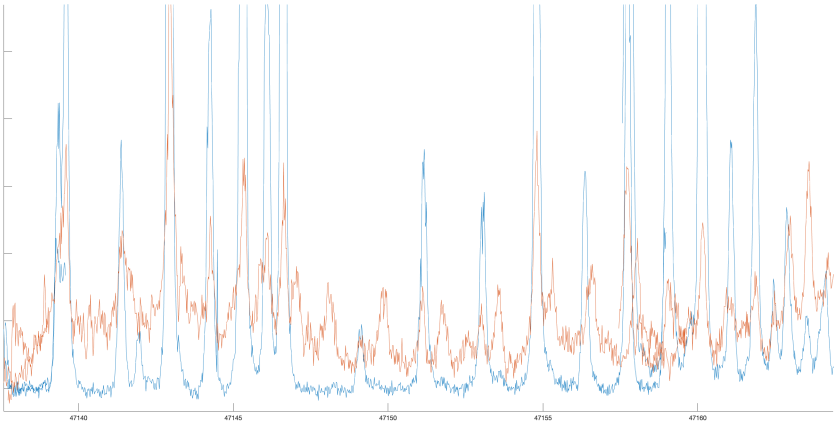

FIGURE 3.4: A portion of the energy region where both cold- and hot-nozzle PFAS spectra were taken. The blue trace is taken with the cold nozzle, and the orange with the hot. The central area of the figure clearly shows several transitions in the hot-nozzle data that are completely invisible in the cold-nozzle analog.

easiest to observe in a pseudo-thermally populated experiment such as this) states with energy in this mode, those belonging to the vibrational state 4^1, there is one quantum of vibrational angular momentum provided by this mode, $l = 1$. The propensity rule $\Delta K = \pm 1$ (this rule is not rigorous due to effects that mix K, such as Coriolis Coupling, and effects that cause the definitions of l and K to be different, such as axis switching) is quite strong, and transitions originating from 4^1 states terminate on states with $K = 0, 1$.

Heating the nozzle indeed allows the observation of transitions that are not visible in the cold nozzle spectrum. The majority of the data taken using the heated nozzle was taken at energies much lower than those used for the cold nozzle data, as the intention is to capture bands of the same vibrational states but different rotational states (different values of K) with the two experiments, so the transition energy need be offset by the energy of the vibration ν_4, $\sim$600 cm^{-1}. However, a small portion of the energy region scanned in both experiments overlaps, and Figure 3.4 shows examples of additional transitions visible in the hot spectrum that are not present in the cold within this small overlapped region.

One of the most interesting results (as yet not completely explained) is related to the behaviour of the PFAS fluorescence decay. Figure 3.5 shows a small portion of the spectrum taken via the heated nozzle experiments, and the fluorescence time traces

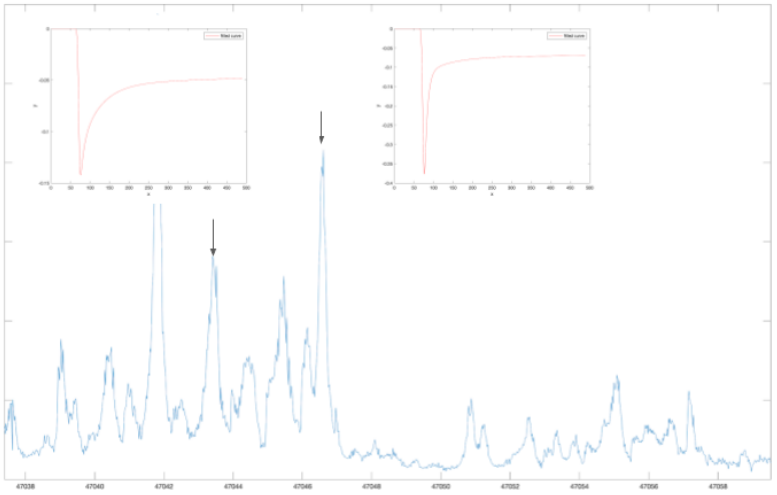

FIGURE 3.5: A portion of the PFAS spectrum taken using the heated pyrolysis nozzle. The insets are the time traces of the decay of the fluorescence due to photofragments, collected via the two acetylene transitions highlighted with arrows (the left trace corresponds to the left arrow). The decay behaviors in PFAS are in general multi-exponential, due to the signal being supplied by a mixture of photofragments with different radiative lifetimes, but the difference in ratios between the coefficients of the various exponential terms is particularly striking between these two large peaks.

collected from the signals of the two transitions marked with arrows. Clearly, the multi-exponential decay terms are qualitatively distinct between the two traces. Obviously different decay patterns have been observed and discussed at length before [7], but this is something of a different case. In the experiments aimed at gaining an understanding of the PFAS process, experimental parameters were intentionally varied in order to highlight particular photofragments with different decay properties. Qualitatively distinct vibrational states (a state localized in the *trans* well and one localized in the *cis* well of the S_1 state) were excited in previous experiments, and different filters were used with the collection optics, chosen specifically to allow signal from only one source to be detected with efficiency. In the case presented here, the same experimental conditions (as far as the collection optics) via the same vibrational state produces vastly different photofragment decay processes.

3.4 Discussion

There are several immediate and obvious advances due to these PFAS spectra. First, these spectra do have the highest signal-to-noise ratio of any single resonance experiments ever performed in this spectral region. In particular, the weaker lines are much clearer in the cold PFAS spectra than in any other experimental scheme ever performed. This includes other detection methods designed to bypass the difficulties of predissociation, such as H-atom REMPI [52] and H-atom Fluorescence Action Spectroscopy, HFAS [6].

The new data has also successfully clarified the details of some perturbations in the spectrum. For example, the 3^4B^2 $K = 1$ level, located at 47206 cm^{-1}, is perturbed at low J by a nearby level, and the magnitude of these perturbations can be accounted for more easily due to the more detailed spectra. A similar clarification occurs for the 3^5 vibrational state, located at 47260 cm^{-1}.

There are also examples of previous assignments being corrected by the new spectra. correction have been made to assignments originating as far back as the analysis by Watson [4]. In particular, the increased sensitivity of the PFAS detection method has detected an R(0) line in what was previously identified as a transition to a level with $K = 2$, which is of course impossible. The new assignment is as a $K = 1$ level, located at 47272 cm^{-1}.

There are many additional lines in the relatively small portion of spectrum where the hot and cold band experiments overlap. This indicates a great deal of enhancement in the hot-band signals. This may be surprising at first, as even at the projected temperatures in the heated nozzle, the population in ν_4'' is less than $\frac{1}{4}$ that in the ground vibrational state, and some cooling is certainly expected to take place in the supersonic expansion. However, the large geometry change between the ground and S_1 electronic states means that, since ν_4'' is the primary Franck-Condon active mode, even as population in excited vibrational states goes down, the transition strength goes up enough to more than make up for the reduced population. It expected that transitions to the ground vibrational state of the S_1 surface gain a factor of as much as ten for each additional quantum of energy in ν_4'' [98]. If one considers that Ingold and King saw hot-band transitions from $5\nu_4''$ in their absorption experiment, which was performed at room temperature, where the

population in that state is ∼0.0001% of the population in the ground vibrational state. In light of this, it is quite reasonable to expect many additional observable transitions in the hot nozzle experiment, even if the relative population in the excited vibrational states is still quite low.

There are quite a few challenges in the way of a thorough understanding of the PFAS spectra. One that perhaps could be corrected with an adjustment of the experimental apparatus is the relatively high rotational temperature observed. This has been somewhat helpful in a small number of cases in understanding interactions between certain states, but in general the additional rotational lines don't really offer any surprising or elucidating information and serve only to clutter the spectrum.

The most unfortunate reality of the PFAS spectra presented in this work is the absence of any new, easily assignable bands. There are quite a few reasons that this may be the case.

The types of transitions to which PFAS is sensitive, but that are invisible to LIF, are in a way quite specific. For LIF to fail, two conditions need to be true; the transition needs to have a lifetime that's comparable to or shorter than the duration of the laser pulse, and the transition must be weak enough that the intensity of the fluorescence doesn't overcome the noise detected by the PMT from scattered laser light. PFAS can detect any transitions that LIF can (or, to be more accurate, there has been no evidence that this isn't the case), and has the additional benefit of being applicable in cases where LIF fails, making PFAS a superior detection method for this region of acetylene. However, in order to actually observe new lines, there must be transitions that are strong enough to be observed in PFAS, not strong enough to overcome scattered light in LIF, and that are to upper states that have lifetimes in a range between "short enough that LIF can't be used," but "long enough that the photodissociation process has time to act before the molecules dissociate on their own." It's possible that no states that our cold band experiment has access to ($K = 1$, *gerade* vibrational symmetry) exist in the probed region. The hot-band spectrum certainly has unassigned bands represented in it, but is crowded and hasn't yielded to attempts of assignment as yet.

Another possibility is that the Franck-Condon factors are very poor in this region. *trans* acetylene is in this energy region nearly energetic enough to isomerize. Vibrational states along the isomerization coordinate are going to have large local motions to account for

the soft potential barrier in the direction of isomerization. In this case, a combination of ν_3 and ν_4 is the required vibrational motion, but ν_6 is thoroughly mixed with ν_4 so in a sense all three of these motions constitute the isomerization coordinate. A naive calculation of vibrational state space (incorporating only states associated with a model based on the *trans* well) gives a value of roughly 1 state per 10 cm^{-1}, with zero states in the vicinity of the isomerization barrier having no excitation in any of the isomerizing modes. Essentially all vibrational states in this region, then, are expected to vary heavily from the range of what we might consider "normal" geometries, and as a result Franck-Condon factors in this energy region may be very small.

Not only is it likely that many transitions in this energy region are quite weak, but the rotational patterns commonly used to recognize and assign vibrational bands may be heavily distorted in this region. It was demonstrated in studies of the predissociation of acetylene that the shape and height of the barrier to dissociation was sensitive to the rotational state that acetylene was in as it approached the barrier, represented by J [12]. If there are similar effects on the isomerization barrier, in this energy region the S_1 states will be very sensitive to it. It's conceivable that, even if there was an isolated and complete vibrational band in the spectrum, the rotational structure would be such that recognizing it as such would be virtually impossible.

Beyond that, even if such a band was found, vibrational assignments will prove troublesome. Our research group has gotten a remarkable amount of mileage out of a simple polyad model, where a few resonances (In this case, just the Coriolis and Darling-Dennison resonances that mix ν_4 and ν_6) are incorporated into our basis states, and all other resonances are treated perturbatively [99]. However, where this model has worked well with some isolated issues (namely, the existence of the *cis* well), near the isomerization barrier the *trans* geometry is no longer a good model for the structure of the molecule, and the polyad model will fail in catastrophic fashion.

Perhaps the most fruitful result from these spectra for future investigation is the unusual time trace behavior in the photofragment fluorescence. This behavior is extremely unusual. Somehow, rotational lines in the same vibrational band are excited to different electronic states of the photofragment C_2 in a non-systematic way. A likely scenario is that the sharp difference in photofragment decay pattern originating from nearby transitions is related to perturbations in the upper levels of these transitions. Accidental

degeneracies could account for the wide variation in decay fragmentation properties. What's interesting about this is the potential for the decay time trace of the PFAS products to be used as a sensitive reporter on the properties of the S_1 state intermediate. What would be particularly valuable is if the accidental degeneracies are with levels localized in the *cis* geometry. As convenient as this would be, it's may not just be wishful thinking. As discussed in chapter 2, many potential pathways to the fluorescent photofragments were considered when the PFAS process was studied. The *cis* geometry would be a more convenient shape from which to perform H_2 elimination, rather than sequential H dissociation. Due to the production of a hydrogen molecule, the energetics of this process are quite different than the accepted sequential mechanism. More work is required in this area, of course, but at this time I am hopeful that the time traces of the PFAS photofragments can be leveraged to report on the properties of the vibrational wavefunction of the probed S_1 state.

3.5 Future Work

The most obvious work still needed is the observation of more vibrational bands. As discussed in this chapter, this is a bit of a daunting process, but some experiments should be fruitful. IR-UV Double resonance experiments will be key to the observation of all vibrational bands. This also gives the advantage of the possibility to craft the intermediate vibrational state in order to maximize Franck-Condon factors with final S_1 states of interest. In addition to filling out the remaining bands in the same energy region observed by this work (recall that several experiments are needed to account for symmetry and K selection rules), bands of higher energy need to be observed. Experimental constraints limited the energies to which I could carry the experiments, but it's not difficult to imagine experiments that bypass the limitations I experienced.

Further work on the properties of the photofragment fluorescence time traces is still needed. The time traces are easily fit according to the process described in understanding the PFAS photofragments dissociation mechanisms [7]. However, at the time of this writing only a small number of lines have been analyzed, and only lines in the hot-band spectrum. There's a rich tapestry of information in these time traces, and the first step in unraveling it is to understand how the photodissociation properties vary among a large number of transitions.

There are several additional experiments that could be performed to provide more information about the photofragmentation process. A few effects could be accounted for if surveys of bands at much lower energy, where the structure of the states is very well understood, are conducted. The opportunity to correlate geometry with time dynamics is fairly obvious in these experiments, and extensions could be made to more isomerization-relevant energies. Less obvious is an investigation into which states exactly the time trace variations are reporting on, which is to say whether the difference in propensity comes in at the one-, two-, or three-photon level. Only changes at the one-photon level will really be relevant in understanding S_1 acetylene, but the other results could contribute to an understanding of the photofragment species.

Another possible experiment involves dispersing fluorescence from the photofragments, and examining it in frequency space. This was of course done during the characterization of the PFAS signal, but from a very select few levels. It's clear from the time traces that different electronic states of the photofragments are excited via different S_1 states, but it's likely also true that the vibrational distributions of the fragments are quite different. The dispersed fluorescence experiment is sensitive to vibrational state, and a study in this area could also contribute to an understanding of what we can learn from the time traces of PFAS.

Perhaps the most important advance that needs to occur is a refinement or replacement of the polyad model by which we understand S_1 acetylene. The usual patterns are broken in S_1 acetylene at very low vibrational energies, but even the patterns defined by our *trans*-centric polyad model are guaranteed to fail above the isomerization barrier. We need to develop a more thorough understanding, perhaps by targeting the *cis* well and using a model for both wells in concert, or investigating higher energies, further removed from the "weirdness" introduced by proximity to the isomerization barrier, and working both down from above and up from below to understand the states in the region of the barrier.

3.6 Conclusion

The advancement of knowledge about acetylene has been a long-lasting effort, with well over a century of work applied to the problem at this point. Many ideas and techniques

which are applicable far beyond the study of acetylene have been produced as a result of these studies. Many obstacles have stood in the way of a comprehensive understanding of acetylene, and many of them have been overcome by clever experiments, technological advancements, and deep knowledge of quantum mechanics.

The current problems standing in the way of a complete understanding of acetylene are daunting. Assigning the transition state in such a system is completely new territory, uncharted waters. The usual patterns broke well below the energies now under consideration, and new patterns designed to understand what caused the normal ones to break are even becoming fairly useless at these energies. This is an intimidating path to consider, truly investigating the unknown, but as my thesis advisor, Bob Field, likes to say, and atom is not a bag of atoms. The complete description of isomerization and transitions states is encoded in the spectrum of acetylene, and with more clever analysis, and the application of quantum mechanical principles, the spectra of S_1 acetylene are knowable and comprehensible.

Bibliography

[1] C. Ingold and G. King. Excited states of acetylene. Part IV. description and analyss of the near-ultra-violet absorption spectra of acetylene and dideuteroacetylene: Nature of the excited state. *Journal of the Chemical Society*, pages 2725–2744, 1953.

[2] K. Innes. Analysis of the near ultraviolet absorption spectrum of acetylene. *The Journal of Chemical Physics*, 22:863–876, 1954.

[3] Robert J. Buenker and Sigrid D. Peyerimhoff. Molecular geometry and the mulliken-walsh molecular orbital model. ab initio study. *Chemical Reviews*, 74:127–188, 1974.

[4] J. K. G. Watson, M. Herman, J. C. Van Craen, and R. Colin. The $\tilde{A} - \tilde{X}$ band system of acetylene: Analysis of long-wavelength bands, and vibration-rotation constants for the levels $n\nu_4''(n = 0 - 4)$, $n\nu_3'(n = 0 - 3)$, and $\nu_2' + n\nu_3'(n = 0 - 2)$. *Journal of Molecular Spectroscopy*, 95:101–132, 1982.

[5] Anthony Merer, Nami Yamakita, Soji Tsuchiya, Adam H. Steeves, Hans A. Bechtel, and Robert W. Field. Darling-Dennison resonance and Coriolis coupling in the bending overtones of the $\tilde{A}^1A_u$ state of acetylene, C_2H_2. *The Journal of Chemical Physics*, 129:054304, 2008.

[6] J. Jiang, C. Saladrigas, and T. Erickson. Probing the predissociated levels of the S_1 state of acetylene via H-atom fluorescence and photofragment fluorescent action spectroscopy. *Journal of Chemical Physics*, 149, 2018.

[7] J. Jiang, A. Muthike, and T. Erickson. One-color (212-220 nm) resonantly-enhanced $(S_1 - S_0)$ multi-photon dissociation of acetylene. *Journal of Molecular Spectroscopy*, 361:24–33, 2019.

[8] J. C. Van Craen, M. Herman, R. Colin, and J. K. G. Watson. The $\grave{A} - \tilde{X}$ band system of acetylene: Analysis of medium-wavelength bands, and vibration-rotation

constants for the levels $n\nu_3'(n = 4-6)$, $\nu_2' + n\nu_3'(n = 3-5)$, and $\nu_1' + n\nu_3'(n = 2, 3)$. *Journal of Molecular Spectroscopy*, 111:185–197, May 1985.

[9] A. L. Utz, J. D. Tobiason, E. Carrasquillo M., L. J. Sanders, and F. F. Crim. The direct observation, assignment, and partial deperturbation of the ν_4 and ν_6 vibrational fundamentals in $\tilde{A}^1A_u$ acetylene (C_2H_2). *The Journal of Chemical Physics*, 98:2742–2753, 1993.

[10] Michael E. Kellman and Gengxin Chen. Approximate constants of motion and energy transfer pathways in highly excited acetylene. *The Journal of Chemical Physics*, 95:8671–8672, 1991.

[11] Anthony J. Merer, Adam H. Steeves, Joshua H. Baraban, Hans a. Bechtel, and Robert W. Field. Cis-trans isomerization in the S_1 state of acetylene: Identification of cis-well vibrational levels. *The Journal of Chemical Physics*, 134(2011), 2011. ISSN 00219606. doi: 10.1063/1.3599091.

[12] Masaaki Fujii, Akimitsu Haijima, and Mitsuo Ito. Predissocation of acetylene in $\tilde{A}^1A_u$ state. *Chemical Physics Letters*, 150(5), 1988.

[13] John F. Stanton, Chang-Ming Huang, and Péter G. Szalay. Stationary points on the S_1 potential energy surface of C_2H_2. *The Journal of Chemical Physics*, 101(1): 356, 1994. ISSN 00219606. doi: 10.1063/1.468142. URL http://scitation.aip.org/content/aip/journal/jcp/101/1/10.1063/1.468142.

[14] Elizete Ventura, Michal Dallos, and Hans Lischka. The valence-excited states T_1-T_4 and S_1-S_2 of acetylene: A high-level MR-CISD and MR-AQCC investigation of stationary points, potential energy surfaces, and surface crossings. *Journal of Chemical Physics*, 118(4):1702–1713, 2003. ISSN 00219606. doi: 10.1063/1.1532312.

[15] Joshua H. Baraban, P. Bryan Changala, GCh Mellau, John F. Stanton, Anthony J. Merer, and Robert W. Field. Spectroscopic characterization of isomerization transition states. *Science*, 350(6266):1338–1342, 2015. ISSN 0036-8075. doi: 10.1126/science.aac9668. URL http://www.ncbi.nlm.nih.gov/pubmed/26659051.

[16] C. Ingold and G. King. Excited states of acetylene. Part I. possibilities of interaction between σ-bond hybridization and π-electron excitation with resulting changes of shape during transitions. *Journal of the Chemical Society*, pages 2702–2704, 1953.

[17] C. Ingold and G. King. Excited states of acetylene. Part II. experimental methods of recording the near-ultra-violet absorption spectra of acetylenes. *Journal of the Chemical Society*, pages 2704–2707, 1953.

[18] C. Ingold and G. King. Excited states of acetylene. Part III. theoretical methods for analysis of near-ultra-violet band-systems of acetylenes. *Journal of the Chemical Society*, pages 2708–2724, 1953.

[19] C. Ingold and G. King. Excited states of acetylene. Part V. measured and calculated frequencies in the near-ultra-violet absorption spectra of acetylene and di-deuteroacetylene: Vibrational and rotational energies of the trans-bent excited state. *Journal of the Chemical Society*, pages 2745–2755, 1953. URL https://doi.org/10.1039/JR9530002725.

[20] I. G. Ross. Calculations of the energy levels of acetylene by the method of antisymmetric molecular orbitals, including σ-π interaction. *Transactions of the Faraday Society*, 48(1951):973–991, 1952. ISSN 00147672. doi: 10.1039/tf9524800973.

[21] Elmer Hutchisson. Band spectra intensities for symmetrical diatomic molecules. *Physical Review*, 36:410, 1930.

[22] D. P. Craig. The franck-condon principle and the size of the excited benzene molecule. *Journal of the Chemical Society*, pages 2146–2151, 1950.

[23] Marlin D. Harmony. The equilibrium carbon-carbon single-bond length in ethane. *The Journal of Chemical Physics*, 93:7522, 1990.

[24] Peter F. Bernath. *Spectra of Atoms and Molecules*. Oxford University Press, 2 edition, 2005.

[25] S. C. Wang. On the asymmetrical top in quantum mechanics. *Physical Review*, 34: 243, July 1929.

[26] Paul A. Giguère. The infra-red spectrum of hydrogen peroxide. *The Journal of Chemical Physics*, 18:88, 1950.

[27] Gerhard Herzberg. *Molecular Spectra and Molecular Structure: II. Infrared and Ramen Spectra of Polyatomic Molecules*. D. Van Nostrand Company, 1945.

[28] G. Barratt Park, Jun Jiang, and Robert W. Field. The origin of unequal bond lengths in the $\tilde{C}^1B_2$ \r\nstate of SO_2: Signatures of high-lying potential energy surface crossings\r\nin the low-lying vibrational structure. *The Journal of Chemical Physics*, 144(14):144313, 2016. ISSN 1089-7690. doi: 10.1063/1.4945622. URL http://scitation.aip.org/content/aip/journal/jcp/144/14/10.1063/1.4945622.

[29] Philip R. Bunker and Per Jensen. *Molecular Symmetry and Spectroscopy*. NRC Research Press, Ottawa, 2 edition, 1998.

[30] Jon T. Hougen. Classification of Rotational Energy Levels II. *The Journal of Chemical Physics*, 39(2):358–365, 1963. ISSN 00219606. doi: 10.1063/1.1733301. URL http://link.aip.org/link/JCPSA6/v37/i7/p1433/s1{&}Agg=doi.

[31] H.C. Longuet-Higgins. The symmetry groups of non-rigid molecules. *Molecular Physics*, 6(5):445–460, 1963. doi: 10.1080/00268976300100501. URL https://doi.org/10.1080/00268976300100501.

[32] James K. Lundberg. The sep spectrum of acetylene: Symmetry properties and isomerization. In Robert W. Field and Hai-Lung Dai, editors, *Molecular Dynamics and Spectroscopy by Stimulated Emission Pumping*. World Scientific, 1995.

[33] W. Pauli. The connection between spin and statistics. *Physical Review*, 58:716–722, 1940.

[34] Carl Eckart. Some studies concerning rotating axes and polyatomic molecules. *Physical Review*, 47:552, 1935.

[35] Edward U. Condon. Nuclear motions associated with electron transitions in diatomic molecules. *Physical Review*, 32:858, December 1928.

[36] A. D. Walsh. The electronic orbitals, shapes, and spectra of polyatomic molecules. part I. AH_2 molecules. *Journal of the Chemical Society*, pages 2260–2266, 1953.

[37] Richard N. Zare. *Angular Momentum*. John Wiley & Sons, 1988.

[38] J. K. G. Watson J. T. Hougen. Anomalous rotational line intensities in electronic transitions of polyatomic molecules: Axis-switching. *Canadian Journal of Physics*, 43:298–320, 1965.

[39] James K. Lundberg, David M. Jonas, Bhavani Rajaram, Yongqin Chen, and Robert W. Field. Rotationally resolved ultraviolet-ultraviolet double resonance study of the nonplanar E state of acetylene. *The Journal of Chemical Physics*, 97 (10):7180–7193, 1992. ISSN 00219606. doi: 10.1063/1.463543.

[40] Yoshihiro Osamura, Henry F. III Schaefer, Stephen K. Gray, and William H. Miller. Vinylidene: a very shallow minimum on the C2H2 potential energy surface. *Journal of the American Chemical Society*, 103(8):1904–1907, 1981. ISSN 0002-7863. doi: 10.1021/ja00398a005. URL http://pubs.acs.org/doi/abs/10.1021/ja00398a005.

[41] Susan M. Burnett, Amy E. Stevens, C. S. Feigerle, and W. C. Lineberger. Observation of X1A1 vinylidene by photoelectron spectroscopy of the C2H2 ion. *Chemical Physics Letters*, 100(2):124–128, 1983. ISSN 00092614. doi: 10.1016/0009-2614(83)80698-8. URL http://www.sciencedirect.com/science/article/pii/0009261483806988.

[42] M. M. Gallo, T. P. Hamilton, and Henry F. III Schaefer. Vinylidene: the Final Chapter? *Journal of the American Chemical Society*, 112(24):8714–8719, 1990. ISSN 0002-7863.

[43] Matthew P. Jacobson, Jonathan P. O'Brien, Robert J. Silbey, and Robert W. Field. Pure bending dynamics in the acetylene X1Σg + state up to 15000 cm-1 of internal energy. *Journal of Chemical Physics*, 109(1):121–133, 1998. ISSN 00219606. doi: 10.1063/1.476529.

[44] Hyunwoo Lee, Joshua H. Baraban, Robert W. Field, and John F. Stanton. High-accuracy estimates for the vinylidene-acetylene isomerization energy and the ground state rotational constants of:C=CH2. *Journal of Physical Chemistry A*, 117(46): 11679–11683, 2013. ISSN 10895639. doi: 10.1021/jp400035a.

[45] Adam H. Steeves, G. Barratt Park, Hans a. Bechtel, Joshua H. Baraban, and Robert W. Field. Communication: Observation of local-bender eigenstates in acetylene. *The Journal of Chemical Physics*, 143(7):071101, 2015. ISSN 0021-9606. doi: 10.1063/1.4928638. URL http://scitation.aip.org/content/aip/journal/jcp/143/7/10.1063/1.4928638.

[46] J. C. Van Craen, M. Herman, R. Colin, and J. K. G. Watson. The $\tilde{A} - \tilde{X}$ band system of acetylene: Bands of the short-wavelength region. *Journal of Molecular Spectroscopy*, 119:137–143, September 1986.

[47] Miwako Mizoguchi, Nami Yamakita, Soji Tsuchiya, Atsushi Iwasaki, Kennosuke Hosina, and Kaoru Yamanouchi. Ir-uv double resonance spectroscopy of acetylene in the $\tilde{A}^1A_u$ $n\nu_3' + \nu_4'$ and $n\nu_3' + \nu_6'$ $(n = 2, 3)$ ungerade vibrational states. *The Journal of Physical Chemistry A*, 104:10212–10219, 2000.

[48] S. P. So, Ross W. Wetmore, and Henry F. Schaefer. Excited singlet electronic states of acetylene: cis and trans structures and energetics. *The Journal of Chemical Physics*, 73(11):5706–5710, 1980. ISSN 00219606. doi: 10.1063/1.440049.

[49] Joshua H. Baraban, P. Bryan Changala, Anthony J. Merer, Adam H. Steeves, Hans A. Bechtel, and Robert W. Field. The $\tilde{A}^1A_u$ state of acetylene: ungerade vibrational levels in the region 45,800-46,550 cm^{-1}. *Molecular Physics*, 110:2707–2723, 2012.

[50] Adam H. Steeves, Hans A. Bechtel, Anthony J. Merer, Nami Yamakita, Soji Tsuchiya, and Robert W. Field. Stretch-bend combination polyads in the $\tilde{A}^1A_u$ state of acetylene, C_2H_2. *Journal of Molecular Spectroscopy*, 256:256–278, 2009.

[51] Toshinori Suzuki and Nobuhisa Hashimoto. Predissocation of acetylene from the $\tilde{A}^1A_u$ state studied by absorption, laser-induced fluorescence, and H-atom action spectroscopies. *The Journal of Chemical Physics*, 110:2042, 1999.

[52] P. Bryan Changala, Joshua H. Baraban, Anthony J. Merer, and Robert W. Field. Probing cis-trans isomerization in the S_1 state of C_2H_2 via H-atom action and hot band-pumped IR-UV double resonance spectroscopies. *The Journal of Chemical Physics*, 143(8):084310, 2015. ISSN 00219606. doi: 10.1063/1.4929588. URL http://dx.doi.org/10.1063/1.4929588.

[53] J. D. Tobiason, A. L. Utz, and F. F. Crim. The direct observation, assignment, and partial deperturbation of ν_5 and $\nu_3 + \nu_4$ in $\tilde{A}^1A_u$ acetylene (C_2H_2). *The Journal of Chemical Physics*, 99:928, 1993.

[54] Anthony J. Merer, Nami Yamakita, Soji Tsuchiya, John F. Stanton, Zicheng Duan, and Robert W. Field. New vibrational assignments in the $\tilde{A}^1A_u - \tilde{X}^1\Sigma_g^+$ electronic

transition of acetylene C_2H_2: the ν_1' frequency. *Molecular Physcs*, 101:663–673, 2009.

[55] Adam H. Steeves, Anthony J. Merer, Hans A. Bechtel, Annelise R. Beck, and Robert W. Field. Direct observation of the symmetric stretching modes of $\tilde{A}^1A_u$ acetylene by pulsed supersonic jet laser induced fluorescence. *Molecular Physics*, 106:1867–1877, 2008.

[56] Anthony J. Merer, Zicheng Duan, Robert W. Field, and James K. G. Watson. Perturbations in the $4\nu_3$ level of the $\tilde{A}^1A_u$ state of acetylene, C_2H_2. *Canadian Journal of Physics*, 87:437–441, 2009.

[57] Jun Jiang, Joshua H. Baraban, G. Barratt Park, Michelle L. Clark, and Robert W. Field. Laser-induced fluorescence study of the S_1 state of doubly-substituted ^{13}C acetylene and harmonic force field determination. *The Journal of Physical Chemistry A*, 117:13696–13703, 2013.

[58] David H. Mordaunt and Michael N. R. Ashfold. Near ultraviolet photolysis of C_2H_2: A precise determination of D_0^0(HCC-H). *The Journal of Chemical Physics*, 101:2630, 1994.

[59] A. Campos, S. Boyé, Ph. Bréchignac, S. Douin, C. Fellows, N. Shafizadeh, and D. Gauyacq. Vacuum-ultraviolet photodissociation of C_2H_2 via Rydberg states: a study of the fluorescent pathways. *Chemical Physics Letters*, 314, 1999.

[60] S. Boyé, A. Campos, S. Douin, C. Fellows, D. Gauyacq, N. Shafizadeh, Ph. Halvick, and M. Bottio-Pasqua. Visible emission from the vibrationally hot C_2H radical following vacuum-ultraviolet photolysis of acetylene: Experiment and theory. *The Journal of Chemical Physics*, 116:8843.

[61] James K. Lundberg, Yongqin Chen, Jean-Paul Pique, and Robert W. Field. Ultraviolet-optical double-resonance study of the predissociated $\tilde{C}^1A_g$ state of acetylene. *Journal of Molecular Spectroscopy*, 156:104–122, 1992.

[62] Jacques Liévin. Ab initio characterization of the $\tilde{C}'^1A_g$ state of the acetylene molecule. *Journal of Molecular Spectroscopy*, 156:123–146, 1992.

[63] Fabrice Laruelle, Séverine Boyé-Péronne, Dolores Gauyacq, and Jacques Liévin. Revisiting Mulliken's concepts about Rydberg states and Rydberg-valence interactions from large-scale ab initio calculations on the acetylene molecule. *The Journal of Physical Chemistry A*, 113(47):13210–13220, 2009. doi: 10.1021/jp903948k. URL https://doi.org/10.1021/jp903948k. PMID: 19639976.

[64] Kazuhide Tsuji, Naoko Arakawa, Akio Kawai, and Kazuhiko Shibuya. Spectroscopy and predissociation of acetylene in the np gerade Rydberg states. *The Journal of Physical Chemistry A*, 106:747–753, 2002.

[65] Kazuhide Tsuji, Kentaro Misawa, Junichi Awamura, Akio Kawai, and Kazuhiko Shibuya. Analysis of low-lying gerade Rydberg states of acetylene using two-photon resonance fluorescence excitation spectroscopy. *The Journal of Physical Chemistry A*, 117:1420–1427, 2013.

[66] M. N. R. Ashfold, B. Tutcher, B. Yang, Z. K. Jin, and S. L. Anderson. Gerade Rydberg states of acetylene studied by multiphoton ionization and photoelectron spectroscopy. *The Journal of Chemical Physics*, 87:5105, 1987.

[67] James K. Lundberg, David M. Jonas, Bhavani Rajaram, Yongqin Chen, and Robert W. Field. Rotationally resolved ultraviolet-ultraviolet double resonance study of the nonplanar $\tilde{E}$ state of acetylene. *The Journal of Chemical Physics*, 97: 7180–7193, 1992.

[68] J. K. G. Watson. Calculated vibrational intensities in the $\tilde{A}-\tilde{X}$ electronic transition of acetylene. *Journal of Molecular Spectroscopy*, 207:276–284, 2001.

[69] G. Barratt Park, Joshua H. Baraban, and Robert W. Field. Full dimensional Franck-Condon factors for the acetylene $\tilde{A}^1A_u - \tilde{X}\Sigma_g^+$ transition. II. Vibrational overlap factors for levels involving excitation in ungerade modes. *The Journal of Chemical Physics*, 141:134305, 2014.

[70] L. Curtis, B. Engman, and P. Erman. High resolution lifetime studies of the $d^3\Pi_g$, $C^1\Pi_g$ and $D^1\Pi_u^+$ states in C_2 with applications to estimates of the solar carbon abundance. *Physica Scripta*, 13(5):270, 1976.

[71] W. Bauer, K. H. Becker, M. Bielefeld, and R. Meuser. Lifetime measurements on electronically excited $C_2(A^1\Pi_u)$ and $C_2(d^3\Pi_g)$ by laser-induced fluorescence. *Chemical Physics Letters*, 123:33–36.

[72] C. Naulin, M. Costes, and G. Dorthe. C_2 radicals in a supersonic molecular beam. Radiative lifetime of the $d^3\Pi_g$ state measured by laser-induced fluorescence. *Chemical Physics Letters*, 143:496–500, 1988.

[73] J. R. McDonald, A. P. Baronavski, and V. M. Donnelly. Multiphoton-vacuum-ultraviolet laser photodissociation of acetylene: Emission from electronically excited fragments. *Chemical Physics*, 33:161–170, 1978.

[74] L. J. Stief, V. J. DeCarlo, and R. J. Mataloni. Vacuum-ultraviolet photolysis of acetylene. *The Journal of Chemical Physics*, 42:3113, 1965.

[75] H. Okabe. Photodissociation of acetylene and bromoacetylene in the vacuum ultraviolet: Production of electronically excited C_2H and C_2. *The Journal of Chemical Physics*, 62(7):2782–2787, 1975. doi: 10.1063/1.430813. URL https://doi.org/10.1063/1.430813.

[76] H. Okabe. Photochemistry of acetylene. *Canadian Journal of Chemistry*, 61(5): 850–855, 1983. doi: 10.1139/v83-153. URL https://doi.org/10.1139/v83-153.

[77] Y. Saito, T. Hikida, T. Ichimura, and Y. Mori. Fluorescence of excited ethynyl radicals produced by pulsed vacuum ultraviolet photolyses of C_2H_2, C_2D_2, and C_2HBr. *The Journal of Chemical Physics*, 80(1):31–35, 1984. doi: 10.1063/1.446448. URL https://doi.org/10.1063/1.446448.

[78] Masako Suto and L. C. Lee. Quantitative photoexcitation and fluorescence studies of C_2H_2 in vacuum ultraviolet. *The Journal of Chemical Physics*, 80(10):4824–4831, 1984. doi: 10.1063/1.446503. URL https://doi.org/10.1063/1.446503.

[79] J. C. Han, Chao Ye, Masako Suto, and L. C. Lee. Fluorescence from photoexcitation of C_2H_2 at 50–106 nm. *The Journal of Chemical Physics*, 90(8):4000–4007, 1989. doi: 10.1063/1.455810. URL https://doi.org/10.1063/1.455810.

[80] A. Tanabashi, T. Hirao, T. Amano, and P. F. Bernath. The Swan system of C_2: A global analysis of Fourier transform emission spectra. *The Astrophysical Journal Supplement Series*, 169(2):472–484, apr 2007. doi: 10.1086/510742. URL https://doi.org/10.1086%2F510742.

[81] G. Herzberg and R. B. Sutton. Tail bands of the Deslandres-d'Azambuja system of the C_2 molecule. *Canadian Journal of Research*, 18a(4):74–82, 1940. doi: 10.1139/cjr40a-005. URL https://doi.org/10.1139/cjr40a-005.

[82] David P. Baldwin, Mark A. Buntine, and David W. Chandler. Photodissociation of acetylene: Determination of D_0^0 (HCC–H) by photofragment imaging. *The Journal of Chemical Physics*, 93(9):6578–6584, 1990. doi: 10.1063/1.458973. URL https://doi.org/10.1063/1.458973.

[83] Hideo Okabe, R.J. Cody, and J.E. Allen. Laser photolysis of C_2H_2 and CF_3C_2H at 193 nm: Production of $C_2(d^3\Pi_g$ and $CH(A^2\Delta)$ and their quenching by Xe. *Chemical Physics*, 92(1):67 – 73, 1985. ISSN 0301-0104. doi: https://doi.org/10.1016/0301-0104(85)80006-9. URL http://www.sciencedirect.com/science/article/pii/0301010485800069.

[84] Alec M. Wodtke and Y. T. Lee. Photodissociation of acetylene at 193.3 nm. *The Journal of Physical Chemistry*, 89(22):4744–4751, 1985. doi: 10.1021/j100268a019. URL https://doi.org/10.1021/j100268a019.

[85] R.S. Urdahl, Yihan Bao, and William M. Jackson. Observation of the LIF spectra of $C_2(a^3\Pi_u)$ and $C_2(A^1\Pi_u)$ from the photolysis of C_2H_2 at 193 nm. *Chemical Physics Letters*, 152(6):485 – 490, 1988. ISSN 0009-2614. doi: https://doi.org/10.1016/0009-2614(88)80446-9. URL http://www.sciencedirect.com/science/article/pii/0009261488804469.

[86] Stephen L Coy, Scott D Halle, James L Kinsey, and Robert W Field. Pressure-induced rotational energy transfer in H_2CO $\tilde{A}^1A_2$ $v_4 = 1$: Dipolar M-dependence with no single-collision elastic contribution. *Journal of Molecular Spectroscopy*, 153(1):340 – 375, 1992. ISSN 0022-2852. doi: https://doi.org/10.1016/0022-2852(92)90482-4. URL http://www.sciencedirect.com/science/article/pii/0022285292904824.

[87] Qiang Cui and Keiji Morokuma. Ab initio MO studies on the photodissociation of C_2H_2 from the $S_1(^1A_u)$ state. II. Mechanism involving triplet states. *Chemical Physics Letters*, 272(5):319 – 327, 1997. ISSN 0009-2614. doi: https://doi.org/10.1016/S0009-2614(97)00530-7. URL http://www.sciencedirect.com/science/article/pii/S0009261497005307.

[88] Whe-Yi Chiang and Yen-Chu Hsu. Fluorescence lifetimes and predissociation processes in the B^2A' state of CCH. *The Journal of Chemical Physics*, 112(17):7394–7399, 2000. doi: 10.1063/1.481339. URL https://doi.org/10.1063/1.481339.

[89] K.-P. Huber and G. Herzberg. *Molecular Spectra and Molecular Structure: IV. Constants of Diatomic Molecules*. Van Nostrand Reinhold Company, 1979.

[90] Jun Jiang, G. Barratt Park, and Robert W. Field. The rotation-vibration structure of the SO_2 $\tilde{C}^1B_2$ state explained by a new internal coordinate force field. *The Journal of Chemical Physics*, 144(14):144312, 2016. ISSN 1089-7690. doi: 10.1063/1.4945621. URL http://scitation.aip.org/content/aip/journal/jcp/144/14/10.1063/1.4945621.

[91] E. B. Wilson, J. C. Decius, and P. C. Cross. *Molecular Vibrations*. McGraw-Hill, New York, 1955.

[92] Takeshi Oka and Yonezo Morino. Calculation of inertia defect: Part I. general formulation. *Journal of Molecular Spectroscopy*, 6:472 – 482, 1961. ISSN 0022-2852. doi: https://doi.org/10.1016/0022-2852(61)90270-3. URL http://www.sciencedirect.com/science/article/pii/0022285261902703.

[93] C. di Lauro and I.M. Mills. Coriolis interactions about X-Y axes in symmetric tops. *Journal of Molecular Spectroscopy*, 21(1):386 – 413, 1966. ISSN 0022-2852. doi: https://doi.org/10.1016/0022-2852(66)90164-0. URL http://www.sciencedirect.com/science/article/pii/0022285266901640.

[94] I. M. Mills. Coriolis interactions, intensity perturbations and potential functions in polyatomic molecules. *Pure and Applied Chemistry*, 11(3-4):325 – 344, 1965. URL https://www.degruyter.com/view/journals/pac/11/3-4/article-p325.xml.

[95] Kevin K. Lehmann. Beyond the x-K relations. *Molecular Physics*, 66(6):1129–1137, 1989. ISSN 07408188. doi: 10.1080/10643389.2012.728825.

[96] Xu Zhang, Anders V. Friderichsen, Sreela Nandi, G. Barney Ellison, Donald E. David, J. Thomas McKinnon, Theodore G. Lindeman, David C. Dayton, and Mark R. Nimlos. Intense, hyperthermal source of organic radicals for matrix-isolation spectroscopy. *Review of Scientific Instruments*, 74(6):3077–3086, 2003. ISSN 00346748. doi: 10.1063/1.1574397.

[97] Michael D. Morse. Supersonic beam sources. *Experimental Methods in the Physical Sciences*, 29:21–47, 1996.

[98] G. Barratt Park. Full dimensional Franck-Condon factors for the acetylene Ã 1A(u)—X Σ(g)+ transition. I. Method for calculating polyatomic linear—bent vibrational intensity factors and evaluation of calculated intensities for the gerade vibrational modes in acetylene. *The Journal of Chemical Physics*, 141(13):134304, 2014. ISSN 1089-7690. doi: 10.1063/1.4896532. URL http://scitation.aip.org/content/aip/journal/jcp/141/13/10.1063/1.4896532.

[99] Robert W. Field, Joshua H. Baraban, Samuel H. Lipoff, and Annelise R. Beck. *Effective Hamiltonians for Electronic Fine Structure and Polyatomic Vibrations*. 2011. ISBN 9780470749593. doi: 10.1002/9780470749593.hrs061. URL http://dx.doi.org/10.1002/9780470749593.hrs061.